RESEARCH REPORT SERIES

Physical oceanography of the Great Australian Bight: the science that underpins

Final Report GABRP Project 1.1

John. F Middleton, David Griffin, John Luick, Mike Herzfeld, Charles James and Peter Oke and John Luick

GABRP Research Report Series Number 20

October 2017

bp
CSIRO
Government of South Australia
Primary Industries and Regions SA
SARDI
SOUTH AUSTRALIAN RESEARCH AND DEVELOPMENT INSTITUTE
THE UNIVERSITY of ADELAIDE
Flinders UNIVERSITY

DISCLAIMER

COPYRIGHT

THIS PUBLICATION MAY BE CITED AS:

Middleton, J.F., Griffin, D., Luick, J., Hertzfeld, M., James, C. and Oke, P. (2017). Physical oceanography of the Great Australian Bight: the science that underpins. Final Report GABRP Project 1.1. Great Australian Bight Research Program, GABRP Research Report Series Number 20, 109pp.

CONTACT

Prof John Middleton
SARDI
e: john.middleton@sa.gov.au

FOR FURTHER INFORMATION

www.misa.net.au/GAB

GREAT AUSTRALIAN BIGHT RESEARCH PROGRAM

The Great Australian Bight Research Program is a collaboration between BP, CSIRO, the South Australian Research and Development Institute (SARDI, the University of Adelaide, and Flinders University. The Program aims to provide a whole-of-system understanding of the environmental, economic and social values of the region; providing an information source for all to use.

CONTENTS

LIST OF FIGURES

LIST OF TABLES

ACKNOWLEDGEMENTS

The authors wish to thank eResearch-SA for access to their supercomputing facilities that were used by SARDI in the modelling studies below. In addition, we thank the NCRIS funded Integrated Marine Observing System for making much of the data used here available and to the IMOS Glider team and Chari Pattiaratchi for running the glider missions for this project. We thank BP for providing the central GAB mooring data and the GAB Research Program for funding and support.

ACRONYMS AND ABREVIATIONS

AVHRR: Advanced Very High Resolution Radiometer

ACCESS-R: Australian Bureau of Meteorology regional weather model.

BRAN 2015: Bluelink Re-Analysis (global re-analysis using OFAM) April 2009-July 2015

CARS: CSIRO Atlas of Regional Seas (Ridgway et al., 2002)

CC: Coastal Current.

CSR: R J. Eanes and Srinivas Bettadpur, 1996: The CSR3.0 global ocean tidal model: diurnal and semi-diurnal ocean tides from TOPEX/Poseidon. Center for Space Research, the University of Texas at Austin, CSR-TM-95-06.

CTD: Device to measure conductivity (salinity), depth and temperature.

ECMWF: European Centre for Medium Range Weather Forecasting weather model

FC: Flinders Current

GAB3: Great Australian Bight grid version 3 (high resolution over shallow water)

JRA-55: Japanese Met Agency 55 km global weather model

LC: Leeuwin Current

NCSS: National Center for Space Science (United States)

NOAA: National Oceans and Atmospheric Administration

OFAM: Ocean Forecasting Australia Model. The Bluelink implementation of MoM.

ROMS: Open Source Regional Ocean Modelling System.

SAC: South Australian Current

SAM: South Australia Model

SHOC CSIRO Sparse Hydrodynamic Ocean Code model

SST: Sea Surface Temperature

TPXO 8.1: Egbert, G.D., and S.Y. Erofeeva, 2002: Efficient inverse modelling of barotropic ocean tides, J. Atmos. Oceanic Technol., 19(2), 183-204.

1. EXECUTIVE SUMMARY

To understand the circulation within the Great Australian Bight (GAB), three distinct hydrodynamic models were used; two shelf-focused models for the four year period 2011 to 2014 (ROMS and SHOC) and one deep-sea focused model (BRAN) for the 23-year period 1994-2016. Good to very good agreement between the shelf model hind-casts and also with data was found for the shelves and at depths less than 200-300 m or so: farther offshore the models were unable to replicate observed features of the meso-scale eddy fields which appear too large and energetic. Discussion of these models therefore focuses on the shelf circulation where hind-cast skill is apparent. These two models reveal details of the shelf circulation as it responds to the strongly seasonal winds of the GAB. The BRAN global model assimilates satellite (and other) observations to constrain it to follow the larger-scale (meso-scale and larger) variability of the ocean.

Mean Winter response: During winter, the average circulation obtained from the models is generally similar to that as understood from previous studies and is largely driven by i) eastward winds, ii) the eastward shelf edge Leeuwin Current (LC) and iii) the 200 - 800 m deep upwelling in the west where the westward deep Flinders Current (FC) is thought to be strongest. In the east, an eastward South Australian Current (SAC) is found that is largest over the shelf break. The SAC acts as an extension of the LC and can have speeds of up to 20 cm/s. Near the coast, the eastward winds drive an eastward Coastal Current (CC). Shelf downwelling is also expected to arise from both bottom transport of the eastward shelf currents as well as from the formation of dense (cold, salty) water in the shallow coastal regions of the GAB where evaporation exceeds precipitation all year round. In qualitative agreement with observations the ROMS model results show the existence of relatively saline bottom water in the shelf and coastal regions of the eastern GAB.

Mean Summer response: The summer-averaged circulation was found to be quite distinct from that obtained in winter and similar in structure to that found in earlier studies. In summer, the winds reverse and are driven by a large high pressure system that leads to periods of alongshore “westward” winds that a) drive coastal upwelling and a westward CC in the central- to eastern GAB and b) lead to a topographic southward Sverdrup transport in the central GAB. The latter is most important as the topographic transport “collides” with the equatorward deep ocean transport leading to a) downwelling all year round at the shelf edge and b) a ridge in sea level that drives a SAC to the east and against the prevailing winds. Deep (500 m to 1000 m) upwelled water is found in the central- to western GAB suggesting the existence of a deep FC.

Nutrient paths: For summer, the upwelling in the eastern GAB is enhanced by the existence of submarine valleys and headlands (de Oliviera and Middleton 2017) which draws nutrient rich water (e.g., nitrates) from depths of 150 m or more along the Bonney Coast and Kangaroo Island regions: this water is transported to the west coast of the Eyre Peninsula. In the far western GAB, SST observations and theory indicate wind-forced upwelling to be largely shut down (Middleton and de Oliviera, 2017). In the central GAB the year-round downwelling would seem likely to preclude upwelling, although other mechanisms such as double diffusion and convective overturning may be important. During winter, atmospheric cooling and evaporation create cold dense water that ultimately is expelled off the shelf and into the 200 - 250 m deep waters of the shelf break. This water may contain high levels of detritus,

sediments and ammonia. In analogy with Spencer Gulf (Middleton et al., 2013) we speculate that ammonia in this detritus might be re-mineralised into atmospheric nitrogen and nitrates.

Field studies: Data from the first-ever deployments of deep-sea gliders in the central GAB were examined. These three missions sampled the continental slope waters to depths of 1000 m, seaward of the 200 m isobaths in September 2014, April 2015 and April 2016. Depression of the isotherms at the shelf edge was observed on most of the glider's visits to the shelf edge, consistent with our picture of the LC. Some evidence in support of the existence of the FC was obtained, although this was overshadowed by the more spatially complex and variable flows associated with both meso-scale and sub-mesoscale eddies, even though these were weak compared with what is seen in most other regions.

Variability: The winter and summer circulation described above is punctuated by the passage of low and high pressure systems that lead to wind-band variability (3 -30 days) of up to 1 m/s in the eastern GAB. All three models provided good hind-casts of much of the observed variability in shelf ocean currents in data obtained from 5 moorings over the 2011-2014 period. The shelf tidal signals were also well reproduced by ROMS and SHOC along with the seasonal variability in monthly averages of shelf currents. Intermittent and strong tidal and inertial band variations were also found in the deep BP mooring data (~ 100 – 1420 m).

The above studies were complemented by an analysis of 23 years of the BRAN global model output to determine the importance of inter-annual variability. The study found that while the LC has a strong seasonal cycle, with a minimum (2 Sv) occurring in early summer (November-January) and a maximum (5.5 Sv) occurring in autumn (May), the inter-annual variation can be just as much on top of that. In some years, the transport exceeded 8 Sv. Conversely, it dropped to near zero in 2015. *RV Investigator* was working in the area in December 2015 (Section 6.4). An equivalent cruise during autumn in a year of strong LC is now needed to see if this is potentially an important factor (*i.e.,* a strong LC is correlated with La Niña years, providing a means of prediction for planning purposes).

Other Themes: Aspects of the model output were provided to other themes of the GAB Research Program to assist in their research. Notably, forward tracking studies and numerical experiments were conducted for the Pelagic Theme 2 to identify pathways of nutrient connectivity to the central GAB, as well as back tracking studies to assist the Petroleum Theme 5 on the initial location of beach stranded tar balls. Information was also provided to the Benthic Theme 3 on bottom stress and locations of deep water animal assemblages, as well as Theme 7 for overall project integration and ecosystem modelling.

2. INTRODUCTION

In this project, we have developed a deep understanding of the oceanography of the Great Australian Bight (GAB); illustrated in Figure 2.1.1; through the development and analysis of high resolution (4 km) hydrodynamic models of the region validated against available data. This project complements and forms a basis for the companion Project 1.2 in the Oceanography Theme which includes a study of the effects of waves on the ocean circulation and develops methods for representing such effects in the hydrodynamic circulation models used in this project.

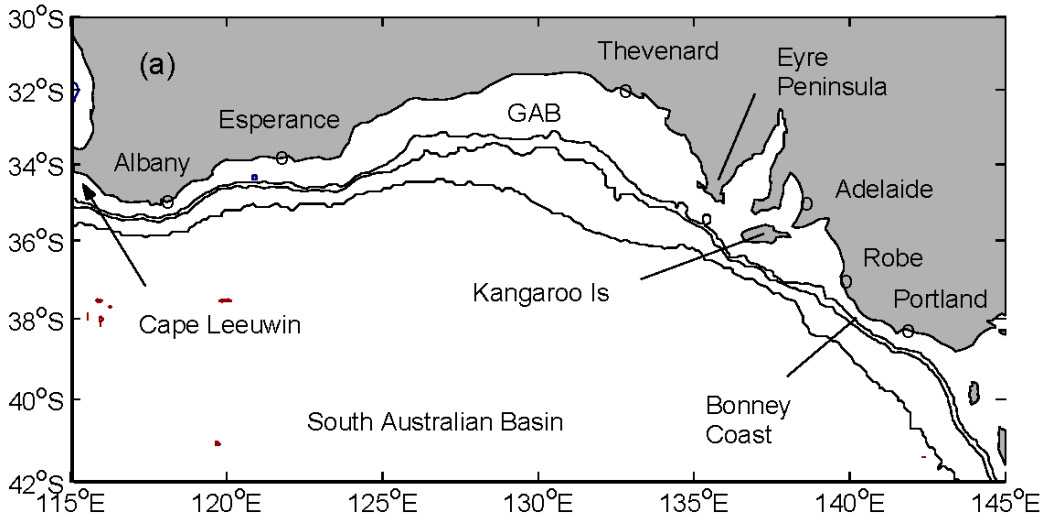

Figure 2.1.1 The Great Australian Bight (GAB) and several notable features. The (black) contours are for the 100 m, 1000 m and 4000 m isobaths.

The broad-scale features of the physical oceanography of the GAB are relatively well-known. However, gaps in our knowledge exist due to the relative paucity of *in-situ* ocean data for the region and lack of focused modelling of the region. High current speeds (>1 m/s) are known to occur near the sea surface as a result of local wind forcing and at depth near the shelf break as a result of unstable eddies. The role of shelf edge eddies and wind-forced currents in mixing, and cross-shelf exchange (upwelling and downwelling) is poorly determined. It has been hypothesised that El Nino events lead to a reduction in winter shelf current speeds and an enhancement of upwelling (Middleton et al., 2007). Evidence for this is limited and further studies are needed to confirm this mechanism and detail its effects on nutrient distributions in the eastern GAB. Correspondingly, the cross-shelf exchange of nutrients driven by wind-forcing appears to be important in determining the shelf distributions of neritic sediments which characterise the benthos of the GAB (Middleton et al., 2014); these carbonate sediments make the southern shelves the largest temperate carbonate factory in the world. However, these inferences regarding the benthos were made using an idealised model of the mean summer circulation of the GAB (Middleton and Platov, 2003) in which the stratification was poorly determined. In addition, the GAB is subject to inflows over the shelf of the warm Leeuwin Current (Cresswell and Griffin, 2004), as well as a

hypothesised shelf-slope Flinders Current (FC); the latter is thought to flow from east to west and provide a deep (400-700 m) conveyor belt for nutrients along the shelf edge (see Middleton and Cirano, 2002; Middleton and Bye, 2007). However, evidence for this current is largely indirect and has been inferred from water mass analyses (Richardson, 2015). There is a need to obtain observational evidence to confirm the existence of the Flinders Current. We did this by deploying gliders as discussed below in Section 5.8 and through an examination of the global BRAN model output.

It is well known that oceanic currents, sea water temperature and nutrient concentrations can have a direct impact on both benthic and pelagic ecosystems. In the latter case, the summer upwelling of nutrients off Kangaroo Island and in the eastern GAB has been shown to be important to the growth of phytoplankton, zooplankton and pelagic fish communities (Ward et al., 2006; Van Ruth et al., 2010 a,b). Such upwelling, in conjunction with alongshore changes in shelf topography, warm inflows and atmospheric heating can also lead to localised eddies and fronts. Fronts and eddies are known to support pelagic communities of tuna (Hobday et al., 2011), as well as prey (e.g. sardines) that feed upon phytoplankton that in turn, can arise from localised upwelling. The depths from which water can be upwelled are unclear, although Kaempf et al., (2004) and Richardson (2015) suggested, from water mass analysis, that these are greater than 350 m. Recent analyses of data (Petroleum Geology and Geochemistry Theme 5) suggest that the asphaltite hydrocarbon balls found along the southern coast may arise from the deep slope of the GAB. This result outlines the need for particle tracking studies of connectivity of the region. The onshore Stokes drift associated with surface waves and swell may also be important to asphaltite ball movement and the coastal settlement of fish larvae spawned offshore as discussed in Project 1.2.

This project (1.1) was designed to provide the physical oceanographic information that is needed to underpin analyses and science that arises in several of the ecological Themes, including the Pelagic Ecosystem and Environmental Drivers, Benthic Biodiversity, Ecology of Iconic Species and Apex Predators and Petroleum Geology and Geochemistry Themes. In each of these themes, there is a need to understand the ecosystems and/or physical environment and the nature and dependency on the ocean physics, such as those outlined above.

A common need of each GAB Research Program theme is for easily accessible (and improved) ocean colour products including chlorophyll-*a* and dissolved organic matter. The improvement of and confidence in these products has been the goal of the Australian Integrated Marine Observing System (IMOS) Bio-Optical Working Group for several years. We have worked with this group and others to provide the basic products to the Themes, and where possible, improvements (or limitations) made using *in situ* data.

A major influence on the circulation of the GAB is forcing from the adjacent regions. Principal among these is the Leeuwin Current (LC), which enters the GAB as a flow along the upper slope and outer shelf, especially during the winter months. The strength of the Leeuwin Current is known to depend on the sea level gradient along the West Australian coast established by the rise and fall of sea level near the equator associated with El Nino. The El Nino/La Nina cycle has a multi-year timescale, so studies of its consequences must span at least a decade or two in order to encompass several cycles, and to be able to distinguish the variability in the GAB that is driven by the inter-annual variability of local meteorological forcing, from that which is driven remotely via the ocean pathways. We have taken

these external influences and longer time scales into account by using the Bluelink 23-year global ocean reanalysis BRAN2016.

2.1 Objectives

The objectives of the project were:

1) To develop high resolution hydrodynamic models of the GAB that will be compared and calibrated with available data.
2) To analyse these models and data to produce the best representation and understanding of the circulation of the GAB.
3) Through particle tracking, determine the ocean flows and pathways that connect the deep, slope regions of oil and gas exploration, to the shelf and coast.
4) Provide the Benthic Biodiversity Theme with maps of bottom currents and stress to qualitatively evaluate ocean current influence on the distribution of benthic sediments.
5) Provide particle tracking information to the Petroleum Geology and Geochemistry Theme, to determine the likely origins of tar balls along the coast of the GAB and southern shelves.
6) In collaboration with the other themes, determine the likely hot-spots of ecosystem activity and physical drivers (e.g. upwelling, downwelling, mixed-layer thickness, temperature and fronts) that may be important to the dynamics of various trophic levels (from pelagic prey species to top-level predators).
7) Where possible improve the ocean colour data and provide easier acquisition as a product deliverable to other Themes.
8) To estimate the heat and volume transport of the Leeuwin Current at the Head of the Bight over a 25-year period.

These objectives have been achieved or largely achieved and directly fill knowledge gaps in the oceanography of the region (Rogers et al., 2013). Results derived for other themes are presented in the relevant Final Theme Report.

3. METHODS

In order to meet the objectives stated above, two distinct, high resolution (~ 4 km grid) hydrodynamic regional models were developed for the region. The model developed by SARDI was a version of the open source Regional Modelling System (ROMS; https://www.myroms.org/). The model has been applied to the Spencer Gulf region (Middleton et al., 2013). CSIRO developed a version based on their in-house model SHOC (Sparse Hydrodynamic Ocean Code; http://www.emg.cmar.csiro.au/www/en/emg/software/EMS/hydrodynamics.html). Both models have been well tested in other projects and the various parameters and numerical schemes (e.g., for mixing) adopted here are detailed in Appendix 2

In each case, the models were embedded in the output of the 10 km grid (global) BRAN 2015 model so as to drive the open boundaries and provide initial conditions for the regional models. BRAN 2015 is a data assimilating model and therefore judged the best available for the GAB and surrounding regions. See http://wp.csiro.au/bluelink/global/bran/ for details. Other forcing data adopted, including those for the tides (TPXO) - http://volkov.oce.orst.edu/tides/global.html are listed in Appendix 1 and 2.

Model runs of ROMS and SHOC were made for 4 years and (2011 to 2014) and the model validation and interpretation was made in several ways. First, (in Section 4), the mean winter and mean summer results were determined and compared to each other through a) plan-view sections and b) cross-shelf sections at 126 ^{o} E, (western GAB), 130.8 ^{o} E (central GAB) and 136 ^{o} E (eastern GAB). Where the ROMS and SHOC results are found to be similar suggests the likelihood of predictive skill (and *vici-versa*). In turn, these model results are, where possible, compared to plan view and sectional data such as *in situ* temperature and salinity, as well as satellite products for sea surface temperature (SST) and sea surface height (SSH). These comparisons allow an overall estimation of model performance, as well as the determination of the large-scale circulation ocean circulation.

Next in Section 5, observations of time series of currents, temperature and salinity were obtained from available mooring data described in Appendix 1. These observations were then compared with the model outputs to examine model validity in the tidal band (1-36 hrs), weather-band (3-30 days) and as monthly averages. The results from 3 glider missions along the deep slope of the GAB were also analysed to examine oceanographic properties of the region including the Flinders Current (FC).

In Section 6, the ROMS model was used to examine likely paths of connectivity and possible origins of (neutrally buoyant) hydrocarbon balls in the GAB. In Section 7, the BRAN2016 model was used to examine the inter-annual variability induced by the Leeuwin Current. In Section 8, research assistance to other themes is summarised.

4. THE LARGE SCALE: HYDRODYNAMIC MODELLING AND OBSERVATIONS.

4.1 Description of the expected large scale seasonal circulation and forcing

To put the new model results in context, a summary of the expected winter and summer circulation features are outlined below.

The wind stress fields used by the ROMS and SHOC model were respectively obtained from the 6-hourly archives of: European Centre for Medium Range Weather Forecasting (ECMWF) and Australian ACCESS model output. These wind stress fields are almost identical. The winter mean winds (Figure 4.1.1) are directed predominantly to the east and increase in magnitude to the south resulting in an equatorward Sverdrup transport in the southern ocean (Middleton and Bye, 2007) as indicated in the schematic of circulation for the GAB (Figure 4.1.2).

The surface Ekman transport associated with the winter winds is also equatorward and acts to raise coastal sea level and drive a (geostrophic) Coastal Current (CC) from Cape Leeuwin in the west to Portland in the South-East (Figure 2.1.1). In addition, the LC brings relatively warm water into the GAB, remains largely trapped along the shelf edge and extends as far as Kangaroo Island (Middleton and Bye 2007) where it is known as the South Australian Current (SAC; Black, 1857). The region is characterised by eastward propagating storms that drive intense alongshore currents of up to 1m/s. A feature of the region is that evaporation exceeds precipitation all year round so that during winter, dense cold, salty water is formed in the shallow coastal regions of the GAB and gulfs. This dense water flows out onto the shelf slope to depths of 250 m or so (Middleton and Bye, 2007). In conjunction with the offshore bottom boundary layer (BBL) of the wind-forced flow, downwelling to depths of 300 m is found all along the continental slope. A deep (400 - 600 m) westward flowing FC has been postulated to exist along the western continental margin (Middleton and Bye, 2007). The FC is a northern boundary current, and in analogy with the great western boundary currents, is driven by an equatorward Sverdrup transport.

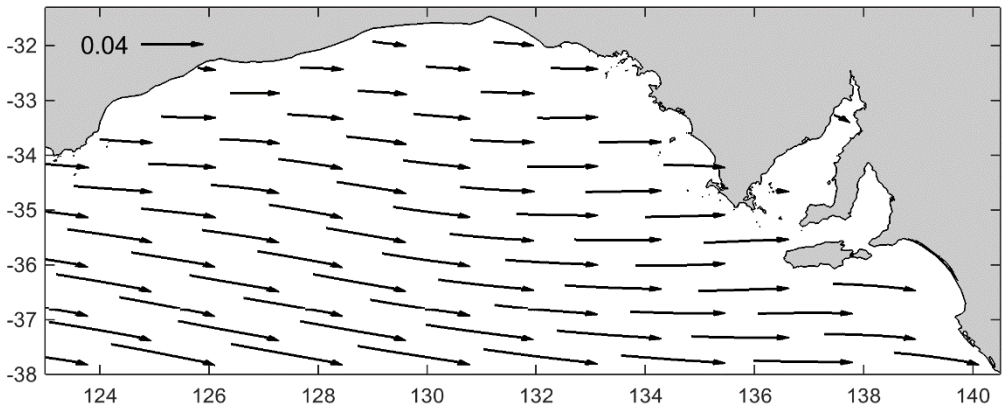

Figure 4.1.1 The 2011-2012 winter averaged surface wind stress for the ROMS model as obtained from the ECMWF data. Units: Pascals and a vector arrow of length 0.04 Pa is shown.

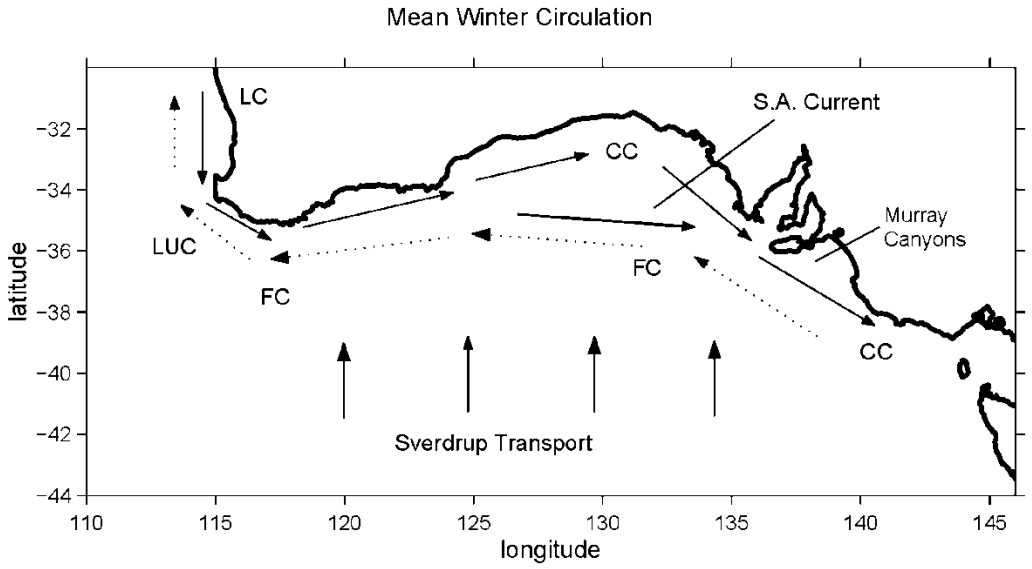

Figure 4.1.2 Schematic of wintertime circulation. The major current features are labelled and include the Coastal Current (CC), Leeuwin Current (LC), Leeuwin Under Current (LUC), Flinders Current (FC) and S.A. Current (SAC).

However, it seems to be very weak to non-existent in the east but largest in the far west (118 ^{o}E) where it is known as the Leeuwin Undercurrent (LUC) with speeds of order 20 cm/s during June 1987 (Cresswell and Peterson, 1993).

During summer, the mean wind fields reverse (Figure 4.1.3) and reflect the dominant presence of an atmospheric high pressure system within the greater Bight region that extends from Albany in the west to Portland in the east (Figure 2.1.1). As shown in the schematic of the mean summer circulation (Figure 4.1.4), a quite different current structure is expected during summer with westward upwelling coastal currents (CC) and a poleward topographic Sverdrup transport over the shelf.

The likely dynamics of these summer features were explained in the modelling studies by Herzfeld and Tomczak (1999) and Middleton and Platov (2003). In summary:

- Near the coast and between the Bonney Coast and central GAB, the coastal currents (CC) are directed to the west in the eastern and central GAB and arise from the lowered coastal sea level due to the offshore Ekman transport due to the wind. This offshore transport can lead to 4 - 5 upwelling events each summer. In the central GAB, shelf edge upwelling is suppressed by the downwelling noted below. In the western GAB, observations show that the upwelling is weak or absent even when winds are alongshore. Middleton and de Oliveira (2017) have shown that this may well result from the relative proximity of Cape Leeuwin which acts as a “geographical origin” for Coastal-Trapped Wave generation and the shut-down of upwelling.
- Within the wide central GAB, a topographic Sverdrup transport arises that redirects the westward CC to the south leading to the formation of an anticyclonic (anticlockwise) gyre. The seaward arm of this gyre is associated with the eastward SAC within the GAB.
- The (summer) SAC again flows to the east as found during winter, but now opposite to that of the winds. The likely explanation for the SAC involves changes in sea level due to density

anomalies. The southward topographic transport within the GAB converges with the northward deep ocean Sverdrup transport along the shelf break (200 m depths) leading to a) sea level being raised over the shelf break and b) downwelling to depths of 300 m or so. The shelf edge downwelling should also result in a light water anomaly (compared to that offshore) that also acts to raise sea level and drive a (geostrophic) SAC to the east and then south east: dense (light) water sits lower (higher) in the water column. Middleton and Platov (2003) also showed that the effect of deep upwelled dense water found below can also lead to a trough in sea level over the shelf slope since dense water sits lower in the water column. The shoreward side of the trough can act to intensify the SAC, while further offshore a westward current can be generated (Figure 4.1.4).

The analyses of Middleton and Cirano (2002) also suggest the deep westward FC should be slightly larger during summer and larger in magnitude in the western GAB with a hydrographic signature of deep upwelling. Finally, we note that water mass analyses of the GAB (Richardson, 2015) also indicate a general deep westward flow from Tasmania to Cape Leeuwin: water masses formed off Tasmania (Tasman Intermediate Water (TIW) and Tasman Antarctic Mode Water (TAMW)), are found at similar depths in the western GAB. These deep water masses (600 – 1000 m) and associated transports are not seasonally dependent.

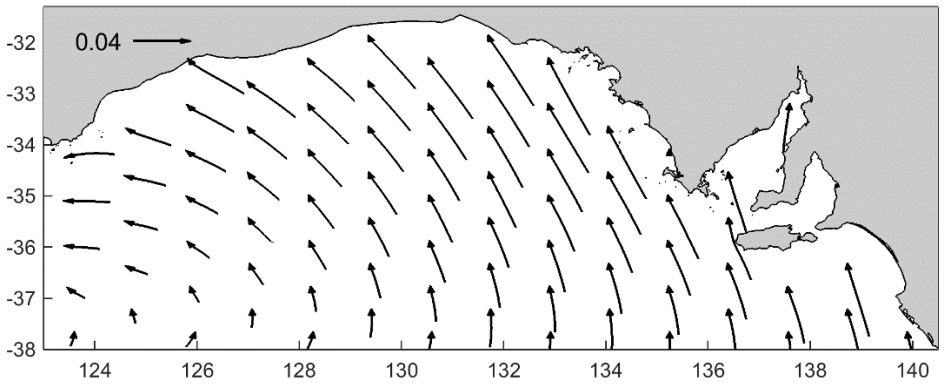

Figure 4.1.3 The 2011-2012 summer averaged surface wind stress for the SHOC model as obtained from the ACCESS data. Units: Pascals and a vector arrow of length 0.04 Pa is shown.

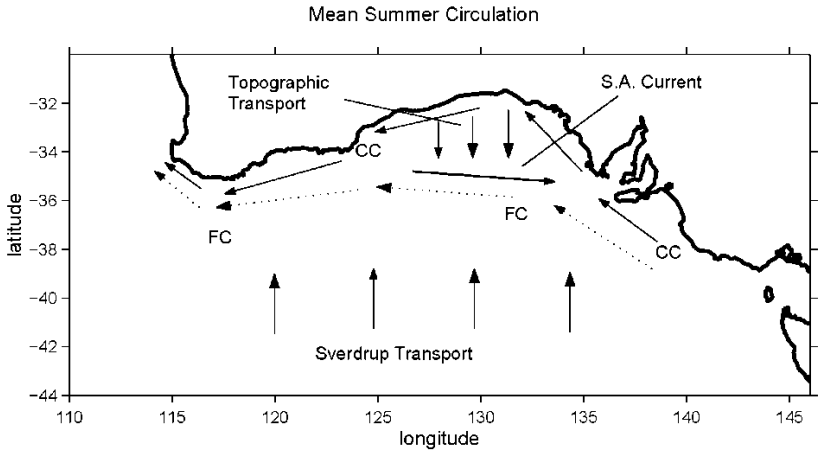

Figure 4.1.4 Schematic of summertime circulation. The major current features are labelled and include the Coastal Current (CC), Leeuwin Current (LC), Leeuwin Under Current (LUC), Flinders Current (FC) and S.A. Current (SAC).

4.2 Winter model/data comparison.

Two versions of both the ROMS and SHOC models were developed as part of this project. The first versions (V1) were initially developed and through extensive model/data comparisons, improved through a number of modifications resulting in a second version (V2). The model parameters adopted for each version are summarised in Appendix 2.

For ROMS, the changes made to V1 were (i) doubling the number of vertical levels from 15 to 30 (to improve accuracy in the vertical), (ii) less smoothing of the topography, (iii) stronger relaxation to observed SST (to improve model estimates), and (iv) use of different open boundary condition algorithms to eliminate artificial flow features along the open boundaries.

For SHOC, the changes to V1 included (i) adoption of a more rectangular model grid, (ii) use of the BRAN2015 global model outputs, and (iii) increase in the background diffusivity of momentum to K = 150 m^2/s.

For ROMS, the changes led to a marginal improvement in the eddy field but unrealistic eddies were found near the open boundaries. The increase in topographic and vertical resolution improved evident correlations with key time series of currents particularly near the topographically complex Eyre Peninsula- Kangaroo Island region.

For SHOC, the changes went some way towards reducing the magnitude of the deep water eddy fields in V1, which were too energetic when the viscosity was insufficient to suppress the numerical instabilities.

However, the shelf circulation for depths less than 300 m for each model were found to be similar but improved in the V2 model case: all results presented here are from the improved V2 models.

For reference, the locations of the moorings and cross-sectional plots are shown in Figure 4.2.1 below of the V2 model domains.

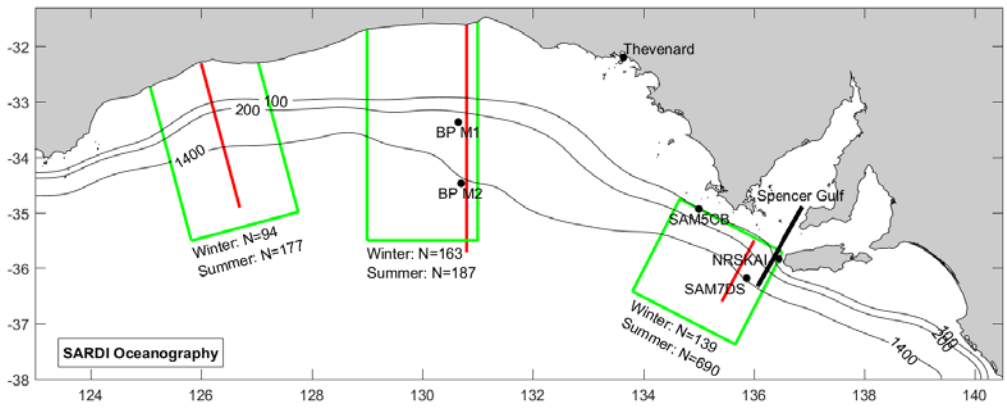

Figure 4.2.1 The ROMS model domain used in this study. The 100 m, 200 m and 1400 m isobaths are shown. The mooring locations of SAM5CB (Coffin Bay), NRSKAI (Kangaroo island), SAM7DS (deep 600 m mooring) and the BP moorings BPM1 (shelf edge) and BPM2 (shelf slope) are shown. The thick straight black line indicates the repeat SAIMOS CTD line. The red lines denote the location of cross-sectional (seasonal averaged) model results that are presented below. The green boxes denote the domains for which all available temperature data is obtained so as to compare with the (red line) cross section model results. The number N of temperature data casts for each green box is indicated for summer and winter.

4.2.1 Wintertime Summary:

Large scale current structures:

The ROMS and SHOC model circulation are generally similar to that expected (outlined above) and appears to be largely driven by i) winds, ii) the eastward LC, and iii) the 200 - 800 m deep upwelling in the west where the westward deep FC is thought to be strongest. In the east, an eastward SAC is found that is largest over the shelf break; the SAC acts as an extension of the LC.

The winter averaged results for circulation for each model are qualitatively in agreement. Both ROMS and SHOC show the penetration of a warm eastward LC in the west and as far as the Eyre Peninsula. The modelled LC is generally trapped near the shelf break with weaker currents in shore in the far west and central GAB. The (winter-average) LC speeds can be up to 20 cm/s at the surface and generally decrease with depth due to the thermal wind shear associated with the downwelling noted above. Evidence is also found (see below) for the existence of a westward FC at depths below 400 m.

Model/data comparison of winter mean currents:

A comparison of winter-time depth-averaged major (principal) axis current as inferred from mooring data and each model was also made. For the central GAB, (130.8 ^{o} E), the ROMS and SHOC model results were in good agreement with the BP mooring data from both the shelf (15 cm/s to the east) and deep mooring (1 cm/s to the west). The latter result, the deep westward currents found from ROMS at 126 ^{o} E, and the water mass analysis of Richardson (2015) all support the notion of a slow westward FC current near the 1000 m isobath and seaward. Such a current (2 cm/s) could transport matter 155 km to the west over a 3-month period. The much-faster (20 cm/s) LC could transport near surface water by 1550 km to the east over the same period.

A comparison of model results for depth-averaged currents was also made for 3 moorings from the Kangaroo Island and Eyre Peninsula region. Again the agreement of the models with data was good.

Downwelling:

The winter averaged temperature from both models and data exhibit downwelling to depths of 400 m or so across the GAB. Apart from the geostrophic balance of the LC, such downwelling is also expected to arise from both bottom boundary layer (BBL) transport of the LC, as well as the formation of dense (cold, salty) water in the shallow coastal regions of the GAB where evaporation exceeds precipitation all year round. Indeed, in qualitative agreement with observations the ROMS model results show the existence of relatively saline bottom water on the shelf and coastal regions of the eastern GAB and Spencer Gulf.

Deep thermohaline structure:

Below depths of 400 m, the modelled isotherms are generally flatter in agreement with the data. An exception here is in the far west (126 ^{o}E), where the ROMS and observed isotherms indicate upwelling that may be associated with the FC expected for the region.

Eddy Fields:

A second feature of both model results and data is the presence of both high and low pressure eddies in the deep ocean and near the shelf and slope. The modelled eddies can have diameters of 100-200 km or so with surface speeds of 20 cm/s and can strongly influence the deep shelf slope circulation. Altimeter derived maps of the surface eddy fields also indicate eddies to exist in the deep ocean but with smaller speeds of 5-10 cm/s. A detailed comparison of model results with altimeter data was made (Appendix 3) for summer and winter and the modelled eddies found to be too large as indicated and too intense in current speed. In addition, some of the model eddies also appear to be an artifice of the open boundary conditions adopted. Some improvements were found in the V2 model eddy field results (e.g., by using higher values of horizontal diffusion in SHOC), but in general, the model eddy fields and impacts may be unreliable.

4.2.2Winter Plan View Results:

Plots of ROMS and SHOC SST and depth averaged velocities, averaged over the 2011-2012 winters, are presented in Figure 4.2.2 and Figure 4.2.3. The curved velocity vectors are obtained as streamlines to enhance eddy-like features. Seasonal-averages of the SHOC layer-average velocities are available online, for example [near-surface speed, winter 2011].

Both the depth-average circulation and the SST are generally similar over the shelf despite the presence of the unrealistically large and intense offshore eddies. This gives confidence that the shelf results at least have hind-cast skill. This will be shown in a comparison with mean seasonal current meter mooring data made below.

In Figure 4.2.4 an equivalent average of the National Oceans and Atmospheric Administration (NOAA), Advanced Very High Resolution Radiometer (AVHRR) satellite temperature data is presented. Both models reproduce the expected eastward wind driven flow over the shelf as well as the westward

intrusion of relatively warm LC water along the shelf break and its extension as the SAC farther east. The LC water for both models is perhaps 0.5 ^{o}C too warm compared to the data.

Model results for mean winter bottom temperature and salinity were compared with that obtained from the CSIRO Atlas of Regional Seas (CARS; Ridgway et al., 2002) and available SARDI CTD, Argo and tagged sea lion (IMOS) data (Figure 4.2.5). For depths below 1500 m, the comparisons were restricted to results for that depth. The results for temperature (not shown), indicate that the models over-predict bottom temperature on the shelf by about 0.5 ^{o}C, and under-predict observed temperatures over the shelf slope. In the gulfs, little data were available and the ROMS model indicates warmer temperatures than those given by SHOC; the ROMS values are closer to those found in an extensive modelling/observational study made of Spencer Gulf (Middleton et al., 2013).

Model results for bottom salinity are not shown. The salinity data (Figure 4.2.5) was quality checked and the amount of reliable salinity data is much less than that for temperature due to bio-fouling and calibration issues. Regions with no data are white. The model bottom salinities are generally fresher than the data by 0.5 – 1 ppt. ROMS indicates higher salinities than SHOC in the gulfs and are in better agreement with other numerical and observational studies (e.g., Middleton et al., 2013; Lennon et al., 1987) and clearly show the expected winter outflow of dense salty bottom water from the eastern side of Spencer Gulf and to depths of 250 m or so (Godfrey et al.,1986).

A winter observational study (June 1994) of salinities in the GAB (Petrusevics et al., 2009) determined the vertical salinity difference (bottom minus surface), shown in Figure 4.2.6. These results indicate that a plume of fresh surface water (or salty bottom water) is found to extend from the head of the Bight to the Eyre Peninsula. The maximum anomaly is found near Thevenard with a magnitude of 0.4 ppt and is, as for Spencer Gulf, attributed to the net wintertime cooling and evaporation that is a feature of the region. Model results of the salinity anomalies for ROMS and SHOC are shown in Figure 4.2.7 and Figure 4.2.8. The ROMS results indicate the strongest anomalies are to be found within and adjacent to Spencer Gulf as expected from the above results. Within the GAB, the ROMS results show the largest salinity anomalies occur on the outer shelf and not near the coast as found by Petrusevics et al.,. (2009). The salinity anomalies for SHOC are small compared to those indicated by both Petrusevics et al., (2009) and ROMS.

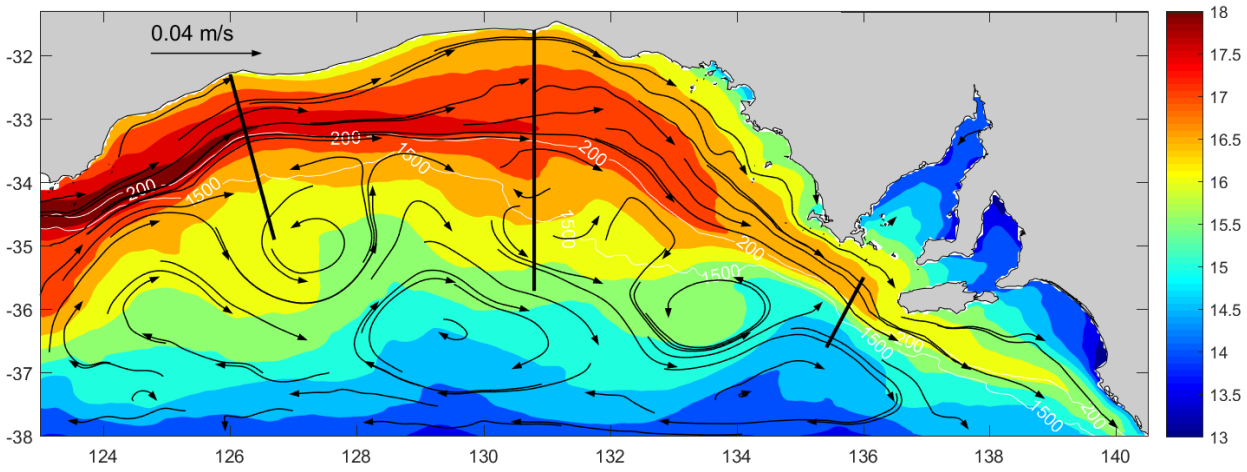

Figure 4.2.2 The ROMS 2011-2012 winter and depth-averaged currents. Units: m/s and a vector arrow of length 0.04 m/s is shown. In addition, the model SST winter averaged is presented with the colour bar in ^{o} C. The cross sections for analysis below are indicated by the thick black lines. The 200 and 1500 m isobaths are indicated by the white lines.

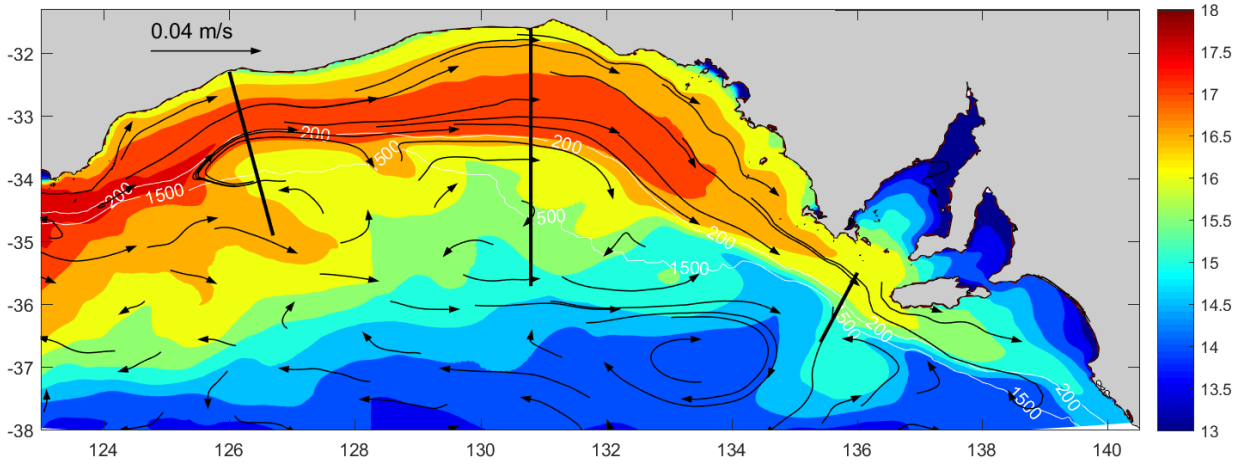

Figure 4.2.3 The SHOC 2011-2012 winter and depth-averaged currents. Units: m/s and a vector arrow of length 0.04 m/s is shown. In addition, the model SST winter averaged is presented with the colour bar in ^{o}C. The cross sections for analysis below are indicated by the thick black lines. The 200 and 1500 m isobaths are indicated by the white lines.

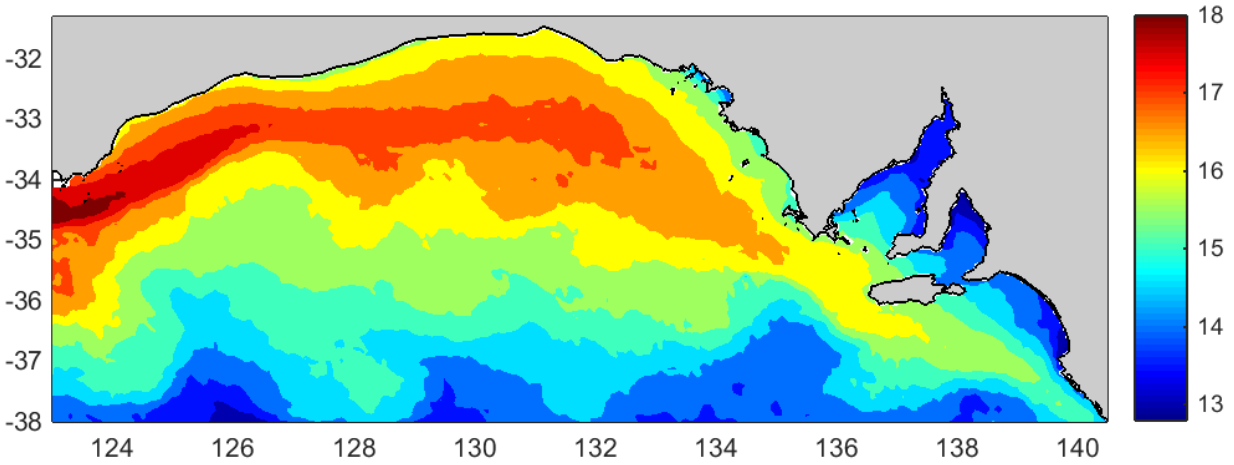

Figure 4.2.4 The observed SST 2011-2012 winter average using the NOAA AVHRR satellite data (same domain and colour bar as in Figure 4.2.2 and Figure 4.2.3)

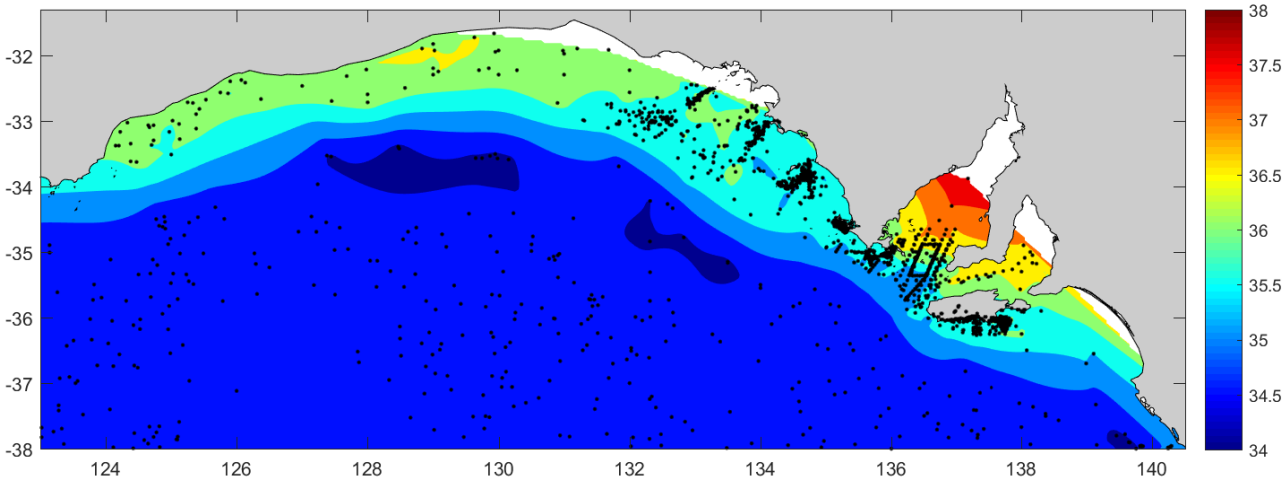

Figure 4.2.5 The observed winter salinity at either the bottom or 1500 m using all available CTD, sea lion, ARGO float data (black points).

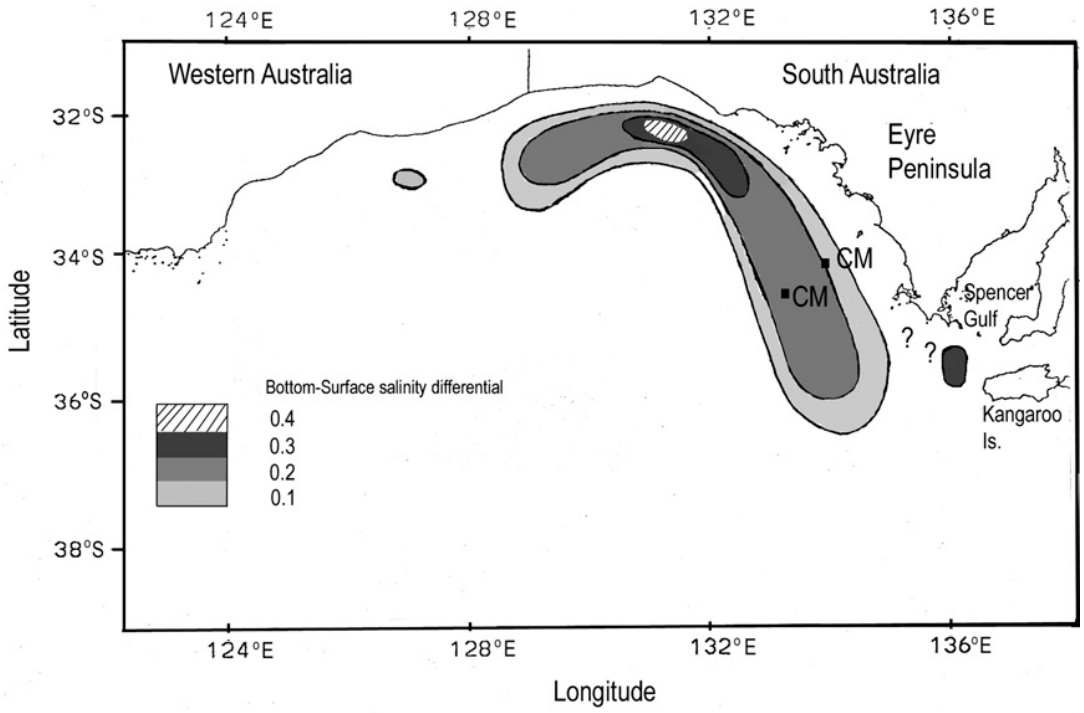

Figure 4.2.6 The observed bottom minus surface sea level anomaly for June 1994 as obtained by Petrusevics et al., (2009): units ppt

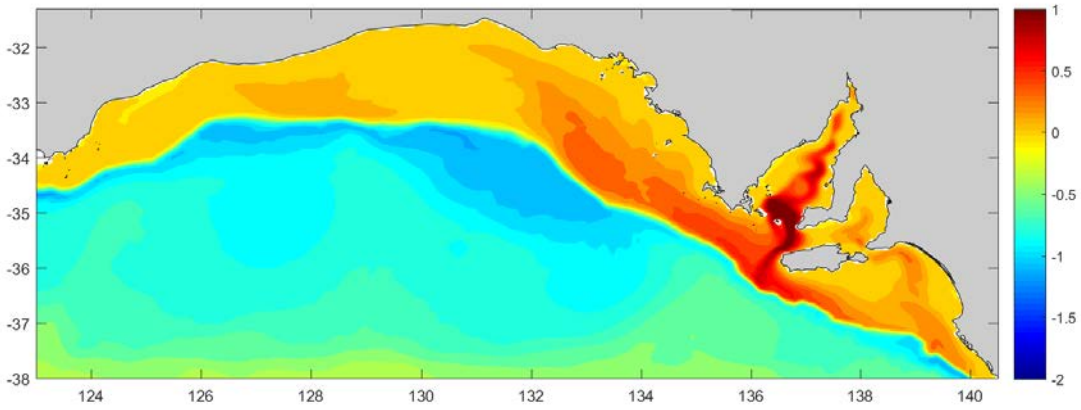

Figure 4.2.7 The ROMS 2011-2012 winter-average vertical salinity anomaly: bottom minus surface: units ppt.

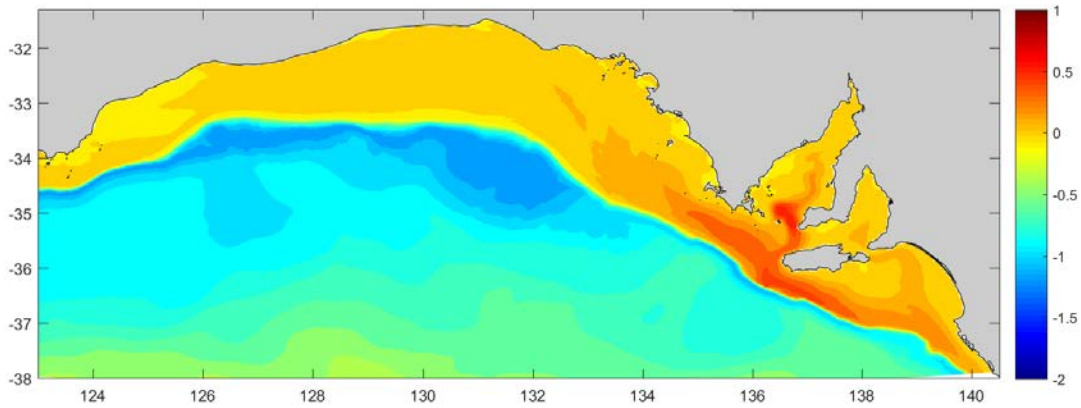

Figure 4.2.8 The SHOC 2011-2012 winter-average bottom salinity anomaly: bottom minus surface: units ppt.

4.2.3 Winter Cross-Sectional Results

The above comparisons are complemented by an examination of winter-average results at the three cross sections outlined in Figure 4.2.1. With the exception of the data from the 4 moorings in the GAB and off Kangaroo Island, we have only temperature CTD cast data for comparison; reliable salinity data being too sparse for meaningful section comparisons. The cross-sections of temperature data were determined using cast data from each of the boxes shown in Figure 4.2.1.

It should also be noted that for each cross-section, the shelf/slope topographies contoured in grey (e.g., Figure 4.2.10 to Figure 4.2.13) are those used by the respective model (sigma or z coordinates). For the plots of observed temperature, the topography is from the Geosciences Australia topographic data set. Since each differs so do the pictured shelf/slope regions. Results are presented both for depths of 0 to 400 m and 400 to 1500 m include the regions of proposed petroleum exploration. For both, the offshore

limits are as shown in Figure 4.2.1. Note that due to the unrealistic eddies, model results are only presented for the shelf cross-sections from the coast to the 400 m isobaths. Comment on deep water results will be made where data exists.

Section 126 ^{o}E: far western GAB

Model results (not shown) for winter averaged velocity show a LC largest at the shelf edge (20 cm/s) and a weaker eastward flow (5 cm/s) near the coast: the latter likely wind driven. Data for temperature are limited but presented in Figure 4.2.9. For the shelf section (0 to 400 m), an offshore eddy structure exists but may be unrealistic due to the paucity of data. Notably, for depths 400 -1500 m, the data in Figure 4.2.9 (and the ROMS model) show deep upwelling. Such deep upwelling and associated deep slope-trapped westward currents are signatures of the FC (Middleton and Bye 2007).

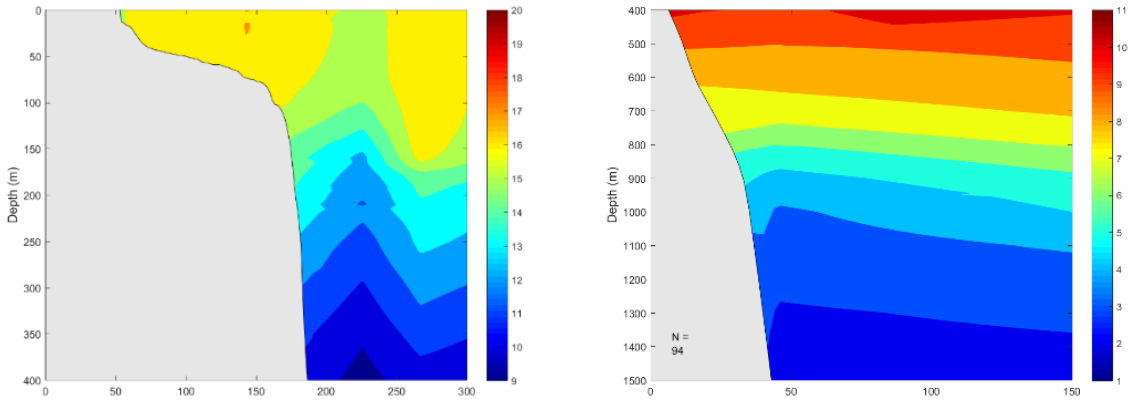

Figure 4.2.9 126 ^{o} E shelf cross-section: Left Panel coast to 400 m; Right Panel 400 to 1500 m. Contour plot of observed winter average temperature. Colour bar indicated.

Section 130.8 ^{o}E: central GAB

The ROMS alongshore velocities to depths of 400 m are contoured in Figure 4.2.10 and show the LC to be trapped to the shelf break/slope as found at the 126 ^{o} E section and with a comparable magnitude (< 10 -20 cm/s). Eastward currents are weaker (~ 3 - 5 cm/s) inshore and over the 80 -100 m isobaths. The onshore wind driven Ekman transport presumably raises coastal sea level and, through geostrophy, leads to the 5 – 10 cm/s eastward coastal currents (CC) that are larger than those at mid-shelf.

Offshore of the LC, a very weak westward current is found at depths below 300 m (Figure 4.2.10). The intensification of this westward current with depth and reduction in amplitude of the eastward LC with depth are both qualitatively consistent with the thermal wind shear that results from the downwelling of model (and observed) isotherms in the top 400 m (Figure 4.2.12 and Figure 4.2.13). The downwelling is consistent with that expected for the eastward wind field and associated Ekman transport and BBL transport of the LC.

Table 4.2.1 The mean of major axis depth-average velocities for the models and data (m/s) for winter 2011/2012 average. For the BP moorings, eastward and northward current components (u/v) are presented. –see Appendix 1 and Figure 4.2.1

Source	NRSKAI	SAM5CB	SAM7DS	BPM1 shelf edge	BPM2 shelf slope
Mean Observed	0.20	0.18	0.10	0.15/-0.01	-0.01/-0.01
Mean ROMS	0.34	0.22	0.16	0.10/-0.01	-0.02/-0.07
Mean SHOC	0.29	0.16	0.04	0.15/-0.02	-0.01/0.00

The location of the BP moorings is also indicated by the black dots in Figure 4.2.10. A description of the mooring details is given in Appendix 1 and locations in Figure 4.2.1. Depth-averaged eastward currents (winter means) are presented in Table 4.2.1. For the BPM1 (shelf) mooring (water depth 200 m), the ROMS and SHOC eastward averages are close to that found from the mooring data (10 - 15 cm/s). Both mooring and ROMS also indicate mean southward flows of about 1 cm/s. For the BPM2 site (water depth 1400 m), both the ROMS and mooring data indicate a weak westward averaged flow of 1 cm/s or so.

The SHOC results for the alongshore currents in the top 400 m, (Figure 4.2.11) show a LC over the shelf break (depths 100 - 200 m) (Figure 4.2.10) that is similar to that from ROMS. The SHOC alongshore currents over the shelf show a weaker flow mid-shelf and westward flow near the coast.

In agreement with the ROMS output and data, the temperature structure of SHOC (Figure 4.2.12) also indicates downwelling to depths of 400 m and with a flatter thermal structure at depths of 400 - 800 m (not shown). Over the shelf, both data and model indicate well mixed water with temperatures of 16 – 17 ^{o} C.

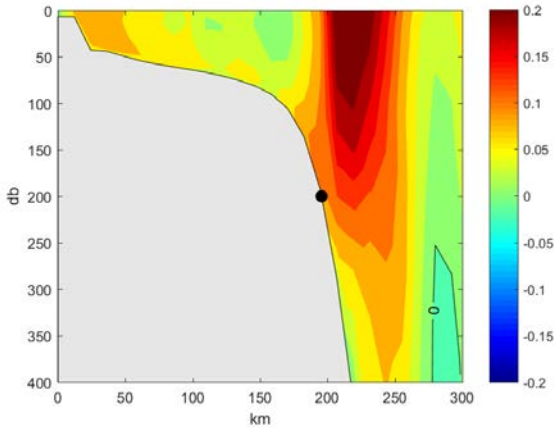

Figure 4.2.10 130.8 º E shelf cross-section- coast to 400 m, with contour plot of the ROMS 2011-2012 winter average along-isobath velocity. Contour level 0.02 m/s. Positive values are to the east. Right panel: The black dot indicates the site of the BPM1 mooring.

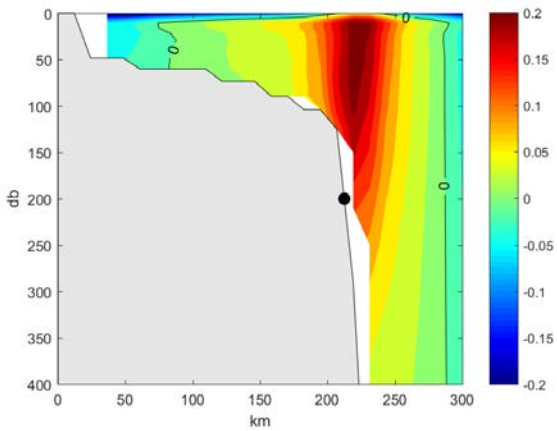

Figure 4.2.11 130.8 º E shelf cross-section- coast to 400 m, with contour plot of the SHOC 2011-2012 winter average along-isobath velocity. Contour level 0.02 m/s. Positive values are to the east. The black dot indicates the site of the BPM1 mooring.

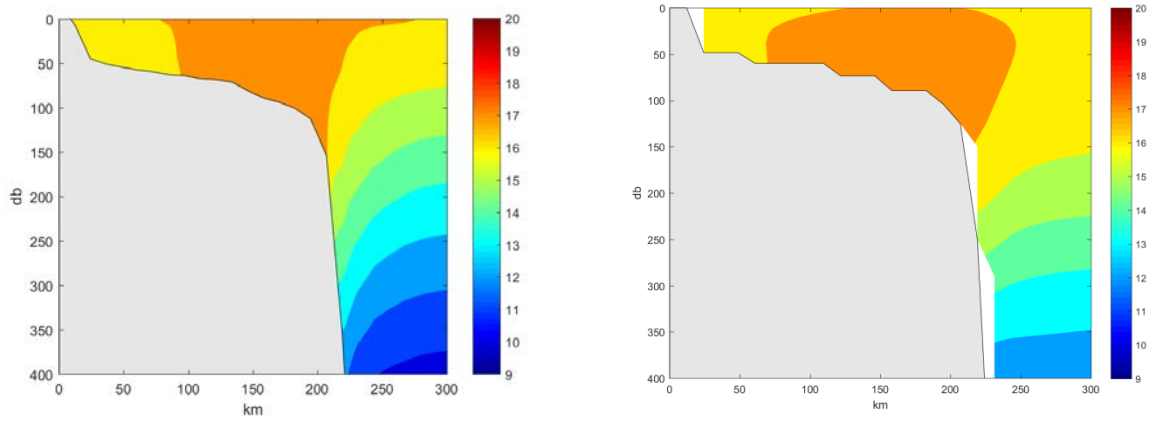

Figure 4.2.12 130.8 º E shelf cross-section – coast to 400 m. Contour plot of the ROMS (left) and SHOC (right) 2011-2012 winter average temperature. Colour bar indicated.

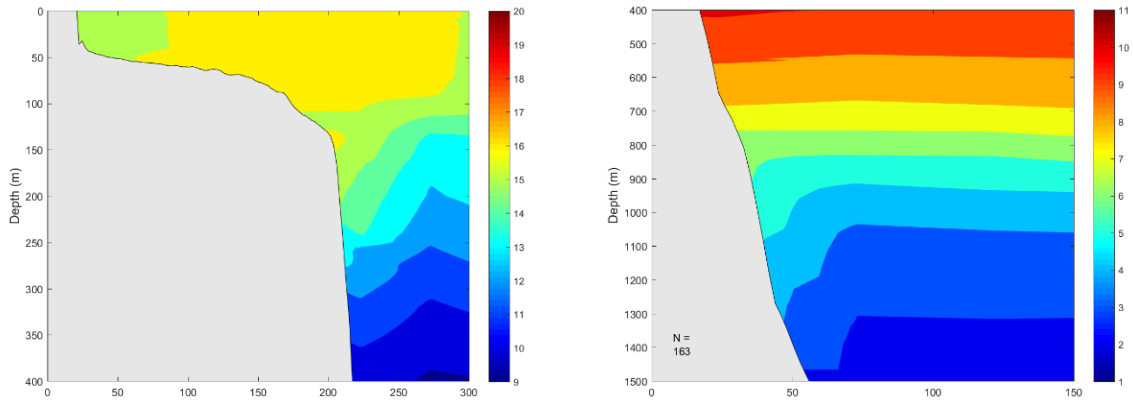

Figure 4.2.13 130.8 º E shelf cross-section. Left Panel: coast to 400 m. Contour plot of observed winter average temperature. Right Panel: 400 to 1500 m. Contour plot of observed winter average temperature. Colour bar indicated.

Section 136 ºE: far eastern GAB

The cross-section here begins at the 100 m isobath to focus on the shelf and slope rather than Spencer Gulf. The model results for winter averaged velocity are presented in Figure 4.2.14 and the winter averaged alongshore currents for both models exhibit a strong 20 cm/s along-isobath flow to the south-east over the shelf and shelf slope; the currents for ROMS are notably stronger than for SHOC. As noted, the current here is best called the South Australian Current (SAC) as the effects of the LC are thought to be small in the far eastern GAB (Cirano and Middleton, 2004).

Farther offshore, a weaker 5-10 cm/s north westward flow is found in SHOC and associated with a low pressure/sea level eddy (Figure 4.2.3): it therefore may be spurious.

The deep mooring SAM7DS was deployed at a depth of 516 m (see Figure 4.2.1) and the winter mean depth-averaged current was to the south-east at around 10 cm/s (Table 4.2.1). The approximate location of the mooring is indicated by the black dot in Figure 4.2.14. The ROMS model has a depth averaged velocity of 16 cm/s to the south-east and about twice that of the 10 cm/s found from the mooring. The SHOC model indicates a smaller depth-average velocity of 4 cm/s which is closer to the observations and consistent with the more extensive south-westward (SAC) indicated in Figure 4.2.14.

Two other moorings were deployed in the region (Figure 4.2.1). The NRSKAI mooring was deployed offshore of Kangaroo Island at a depth of 110 m. The mean along-isobath flow for the winter data was 20 cm/s and smaller than that from both models (~ 30 cm/s) – see (Table 4.2.1). The second mooring SAM5CB, was deployed off the Eyre Peninsula on the 100 m isobath. The observed winter mean flow to the south-east was 18 cm/s and similar to that predicted by ROMS (22 cm/s) and SHOC (16 cm/s).

In the top 100 m, and near the coast, both models and data indicate water to be generally well mixed with a temperature of about 16 ºC (Figure 4.2.15). On the slope and to depths of 300 m, both models exhibit strong downwelling which is only weakly evident in the data and at depths of 150 m. In fact the observations (Figure 4.2.16) indicate an offshore eddy-like structure but which may be related to insufficient data.

For depths greater than 400 m, the observations and models indicate either weak downwelling or upwelling (Figure 4.2.17 and Figure 4.2.18) and a flatter structure at greater depths.

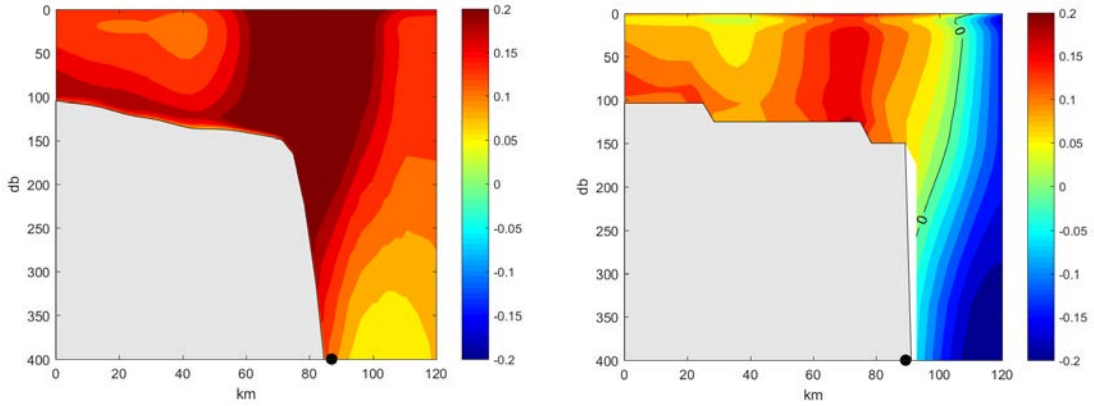

Figure 4.2.14 136 º E shelf cross-section- coast to 400 m. Contour plot of the ROMS (left) and SHOC (right) 2011-2012 winter average along-isobath velocity. Contour level 0.02 m/s. Positive values are to the east. The black dot indicates the approximate site of the SAM7DS mooring.

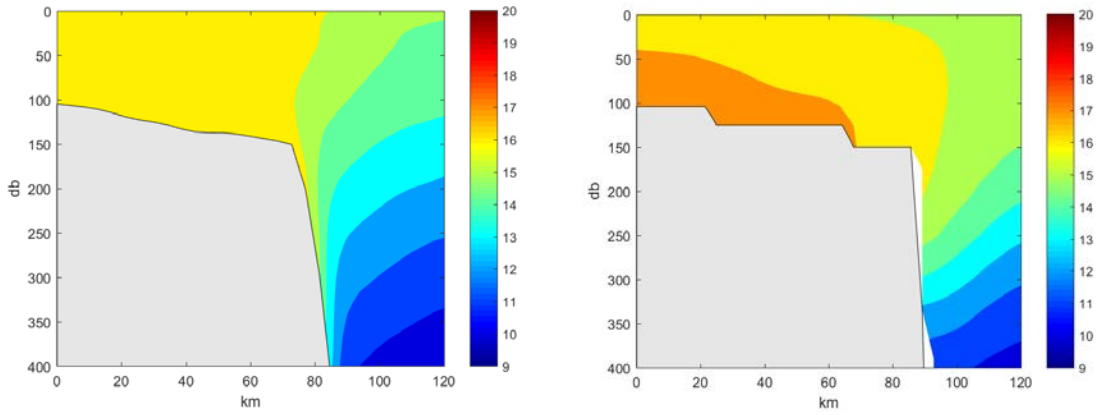

Figure 4.2.15 136 º E shelf cross-section – coast to 400 m. Contour plot of the ROMS (left) and SHOC (right) 2011-2012 winter average temperature. Colour bar indicated.

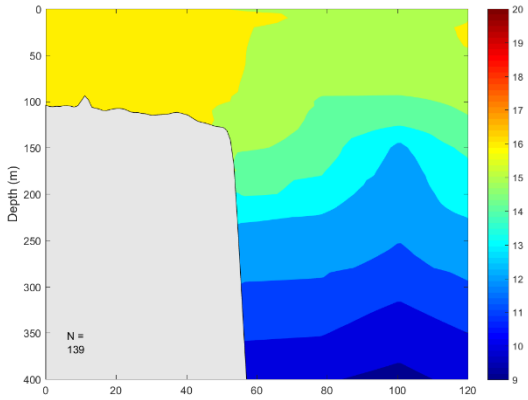

Figure 4.2.16 136 º E shelf cross-section – coast to 400 m. Contour plot of observed winter average temperature. Colour bar indicated.

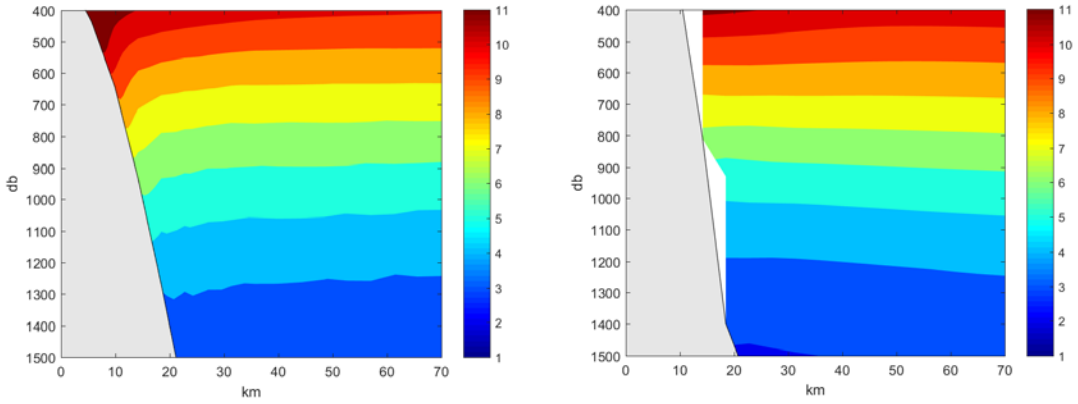

Figure 4.2.17 136 º E shelf cross-section – 400 to 1500 m. Contour plot of the ROMS (left) and SHOC (right) 2011-2012 winter average temperature. Colour bar indicated.

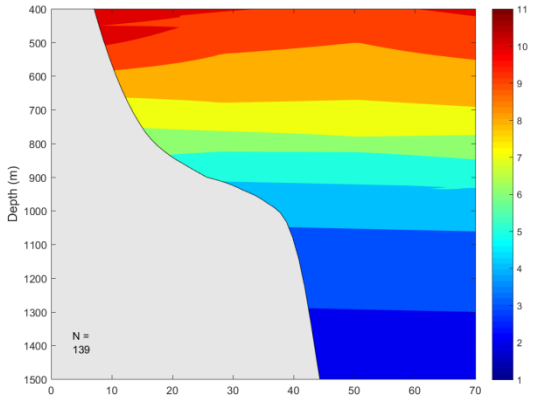

Figure 4.2.18 136 º E shelf cross-section – 400 to 1500 m. Contour plot of observed winter average temperature. Colour bar indicated.

4.3 Summer model/data comparison

4.3.1 Summertime Summary

Large scale current structures:

In summary, the ROMS and SHOC model circulation are similar to that expected (outlined above) and consists of several current features that influence and are influenced by the thermohaline fields and downwelling. In particular, the ROMS and SHOC results indicate the expected anti-cyclonic circulation in the central GAB, with a westward upwelling favourable CC and southward (topographic Sverdrup) transport over the shelf and eastward SAC. Middleton and Platov (2003) show that the Sverdrup transport can be reduced (or reversed) if water over the shelf of the western GAB is much lighter (warmer) compared to that in the east - the Joint Effect of Baroclinicity and Topographic Relief.

For both models, the SAC was also found in the eastern GAB. Inshore of the SAC (and over the shelf), both models and data exhibit weak westward and eastward flows that are respectively consistent with an upwelling and downwelling favourable circulation. This is due to the fact that neither (weak) flow dominates near the coast during summer since upwelling in the eastern GAB occurs as several events during summer. Farther to the west and in the central GAB, a westward coastal flow associated with upwelling is found in ROMS and SHOC.

Model/data comparison of summer mean currents:

ROMS indicates the amplitude of the SAC to be about 10 cm/s in the west and central GAB. The ROMS depth average speed over the 200 m isobath and central GAB is 10 cm/s to the east and in good agreement with mooring data (6 cm/s). SHOC generally indicates a much stronger SAC (> 20 cm/s) and the depth average is 15 cm/s and about twice that of the data. Both ROMS and SHOC indicate the depth averaged flow over the 1400 m isobath (central GAB) to be to the west (2 - 4 cm/s) and in good

agreement with the data (1 cm/s) and suggests the presence of a westward FC. In the eastern GAB the mooring and model mean velocities can be to the west (Coffin Bay) or south (off Kangaroo Island) and a consistent upwelling or downwelling flow field is not found as noted above.

Downwelling:

Both models and data indicate downwelling has occurred in the top 400 m. Such downwelling in the east is likely a residual from the previous winter. However, in the west to central GAB, the downwelling is also likely driven by the convergence of Sverdrup transports as described above and by Middleton and Platov (2003). These authors also outline how this convergence can act to enhance the strength of the SAC. These results and those for winter, strongly suggest that downwelling is found all year round in the western to central GAB as also indicated by an analysis of neritic carbonate benthic sediments (Middleton et al., 2014). Active summertime shelf edge downwelling was also found in idealised numerical experiments assuming an (initially flat) distribution of nitrates (see Section 8.2.2).

Coastal Upwelling:

Surface upwelling is not found in the far western GAB even though the mean summer winds are approximately directed in the alongshore direction: this is consistent with the analysis of Middleton and de' Oliveira (2017). Upwelling is indicated by the SST data along the Bonney Coast (BC) and off the Eyre Peninsula, but less so in the models. The lack of consistency may be due to the relatively weak upwelling currents for the eastern GAB. Both ROMS and to a larger extent SHOC exhibit SST patterns that are consistent with the data and with upwelling between the BC and the Eyre Peninsula.

Deep thermohaline structure:

The data and ROMS (but not SHOC) also indicate the existence of deep upwelled water (depths 500 - 1000 m) over the slope of the western to central GAB. This dense water sits lower in the water column, should lower sea level and through geostrophy, is expected to enhance the eastward SAC (Middleton and Platov, 2003). As noted, the SHOC model does not exhibit deep upwelled water, (reasons unknown), but does indicate a stronger and more extensive SAC to that given by ROMS or Middleton and Platov, 2003).

Eddy Fields:

Both models indicate low pressure/sea level eddy formation with scales of 100 - 200 km radii, although as found for winter, some modelled eddies are unrealistically large and intense, particularly in the case of ROMS.

4.3.2 Summer Plan View Results

During summer, and on the West Australian coast, the eastward LC is reduced in magnitude due to opposing winds and has a much smaller impact on the circulation in the GAB as is evident by the weaker inflow in the far west of the model domains (Figure 4.3.1 and Figure 4.3.2). The analysis by Akhir (2009) suggests that there is a weak upwelling favourable "Cresswell" Current along the nearshore region of the far western GAB that turns north along past Cape Leeuwin to combine with the Capes Current (Gersbach et al., 1999). On the other hand the analyses of SST data and dynamics made by Middleton and de Oliveira (2017) suggest that upwelling should be small in the far western GAB. This important result is supported by the analysis and SST data (Figure 4.3.1 to Figure 4.3.3) and indicates nutrients in the central GAB cannot come from the west.

The ROMS and SHOC model mean summer and depth averaged shelf circulation is shown in Figure 4.3.1 and Figure 4.3.2. As found for winter the shelf edge flow is predominantly directed to the east and along the shelf edge where it forms the year-round SAC. The SAC can extend as far as Kangaroo Island. Near the coast, and in both models (notably SHOC), westward-directed alongshore currents (associated with upwelling) are found to extend from the Bonney Coast to the western GAB. In the central GAB, the currents exhibit a southward turning towards the shelf edge (Figure 4.3.1).

The likely dynamical cause of these features was outlined above and in the modelling studies by Herzfeld and Tomczak (1999) and Middleton and Platov (2003). In summary, the ROMS and SHOC model results are consistent with these dynamics are:

- Near the coast and between the Bonney Coast and central GAB, the coastal currents are directed to the west and lead to upwelling. Coastal upwelling is weak in the western GAB.
- Within the wide central GAB, an anticyclonic (anticlockwise) gyre is found where the seaward arm of this gyre is associated with the shelf edge SAC within the GAB and a southward transport over the wide central GAB.
- Downwelling in the central GAB is found to depths of 300 m and deep upwelling in the far west. These will be illustrated by the cross-sectional plots below.

The deep water eddy field found for both ROMS and to a lesser extent SHOC (Figure 4.3.1 and Figure 4.3.2), are again unrealistically too intense (see Appendix 3).

Farther off the shelf, ROMS shows very strong westward flow near 38 °S. This appears to be a model artefact, and suggests that the boundary conditions are not letting the SAC to exit the model domain towards the south-east.

The ROMS SST results (Figure 4.3.1) are in reasonable agreement with the data as a consequence of driving the model towards the observations as the model steps forward. Notably, the SHOC SST results mimic the observations and the expected cool water upwelling from the BC to the western Eyre Peninsula (without using those SST estimates to influence the model).

Bottom temperatures (sea floor depths 0 to 1500 m) are presented in Figure 4.3.5: for clarity and for water depths greater than 1500 m, results are presented for the 1500 m depth only. Results (not shown) for both ROMS and to a lesser extent SHOC exhibit bottom temperatures that are too warm by a degree or more over the shelf and slope.

Observational results for the summer averaged bottom salinity are shown in Figure 4.3.6. The ROMS results (not shown) are in reasonable agreement with the data and reproduce the slightly more saline water found in the eastern GAB, as well as the very salty water found in the gulfs. Unlike winter, and as expected (Middleton and Bye 2007; Middleton et al., 2013), the exchange between the gulfs and shelf is absent during summer. The SHOC results (not shown) do not reproduce the differences in salinity across the GAB and water inside the mouth of the gulfs is too fresh by about 0.5 ppt.

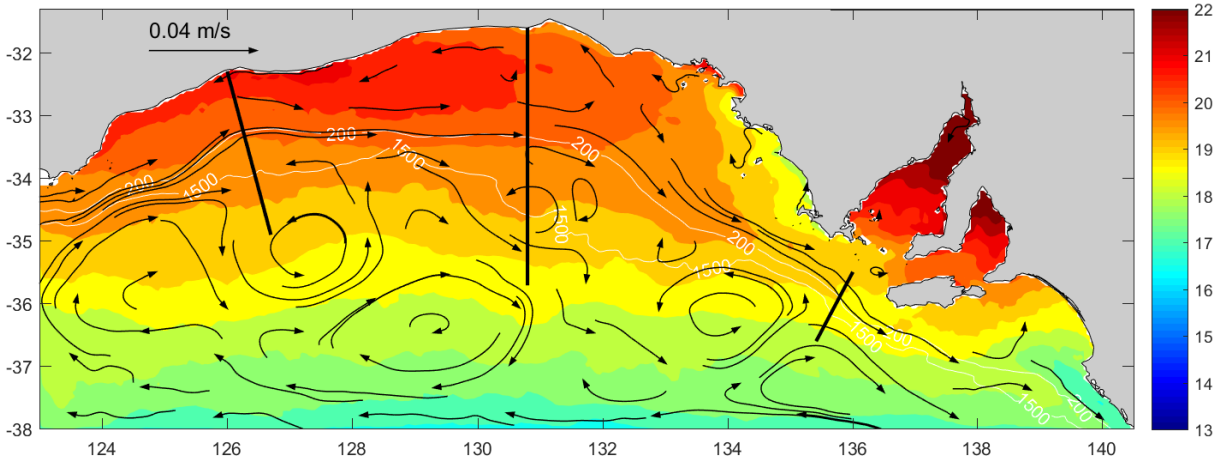

Figure 4.3.1 The ROMS 2011-2012 summer and depth-averaged currents. Units: m/s and a vector arrow of length 0.04 m/s is shown. In addition, the model SST summer averaged is presented with the colour bar in ° C. The cross sections for analysis below are indicated by the thick black lines. The 200 and 1500 m isobaths are indicated by the white lines.

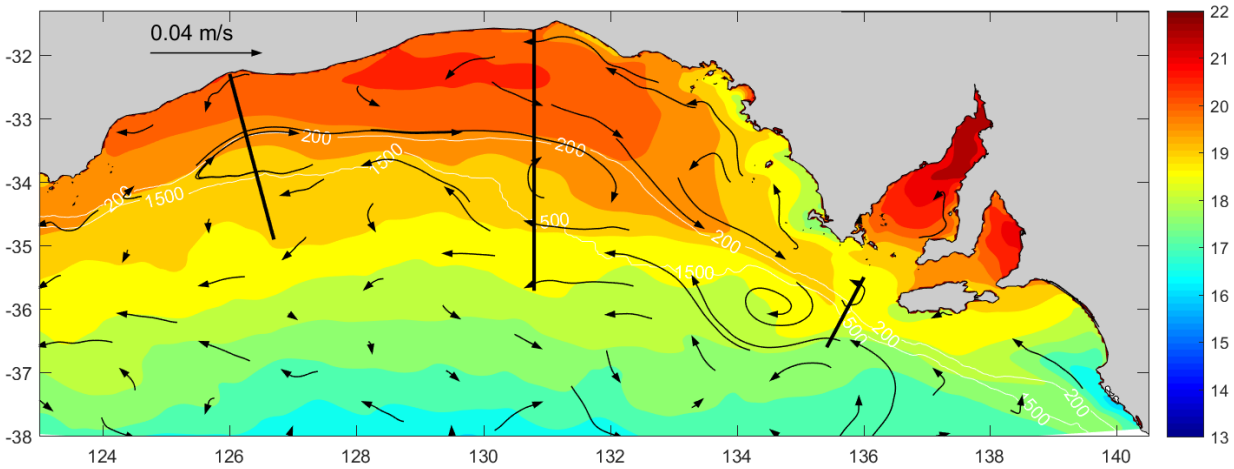

Figure 4.3.2 The SHOC 2011-2012 summer and depth-averaged currents. Units: m/s and a vector arrow of length 0.04 m/s is shown. In addition, the model SST summer averaged is presented with the colour bar in ° C. The cross sections for analysis below are indicated by the thick black lines. The 200 and 1500 m isobaths are indicated by the white lines.

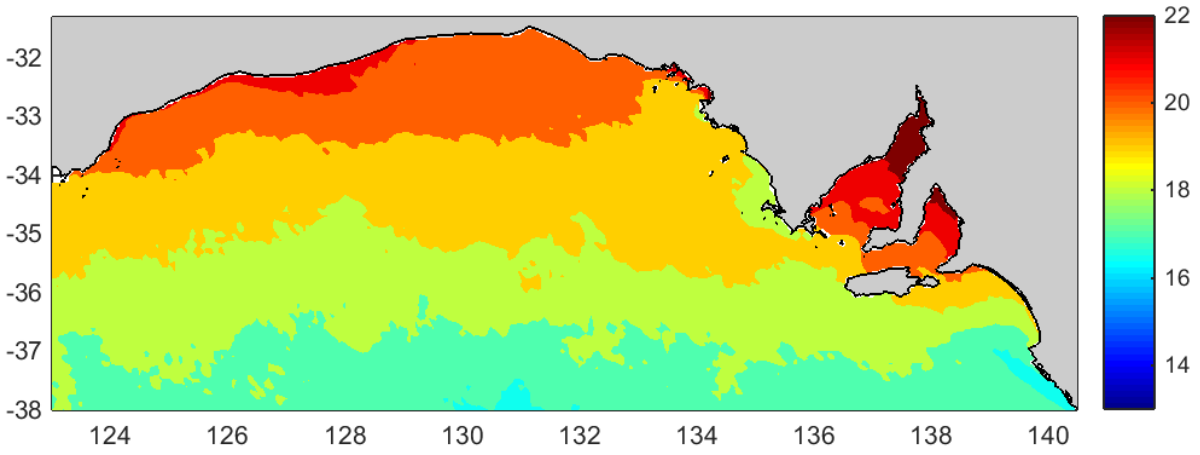

Figure 4.3.3 The observed SST 2011-2012 summer average using the NOAA AVHRR satellite data (same domain and colour bar as in Figure 4.3.1)

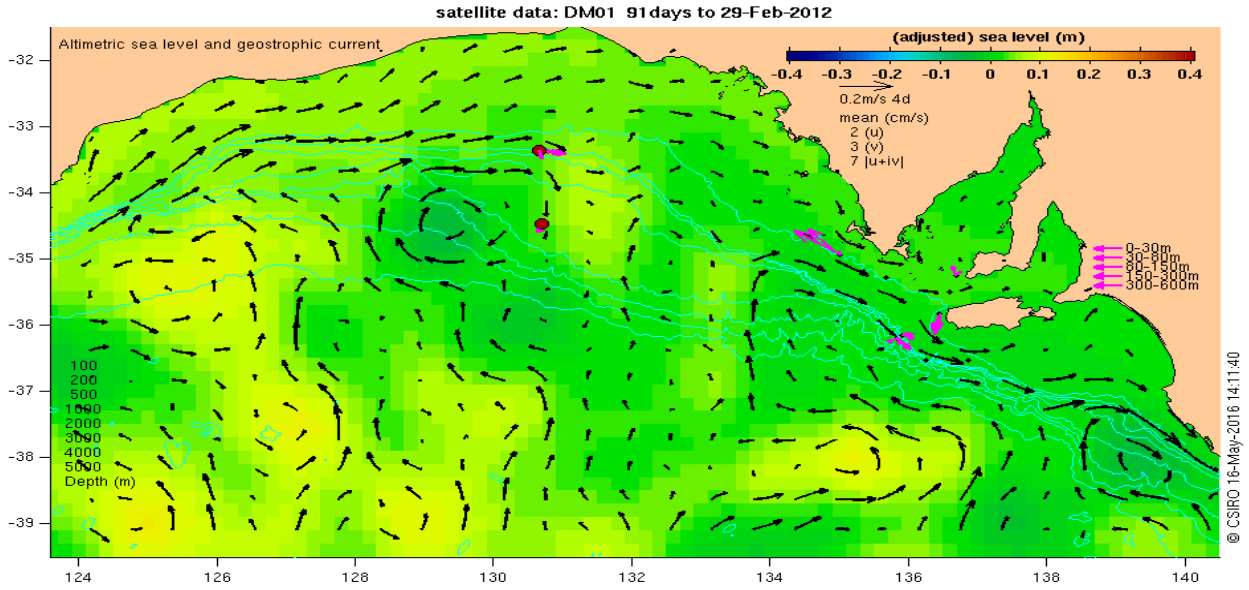

Figure 4.3.4 Observed (by satellite altimeter and tide-gauges) sea level, geostrophic surface velocity and ADCP currents (in magenta) for summer 2011-12. http://www.marine.csiro.au/~griffin/BPGAB/DM01/eta_season05_layer0.html

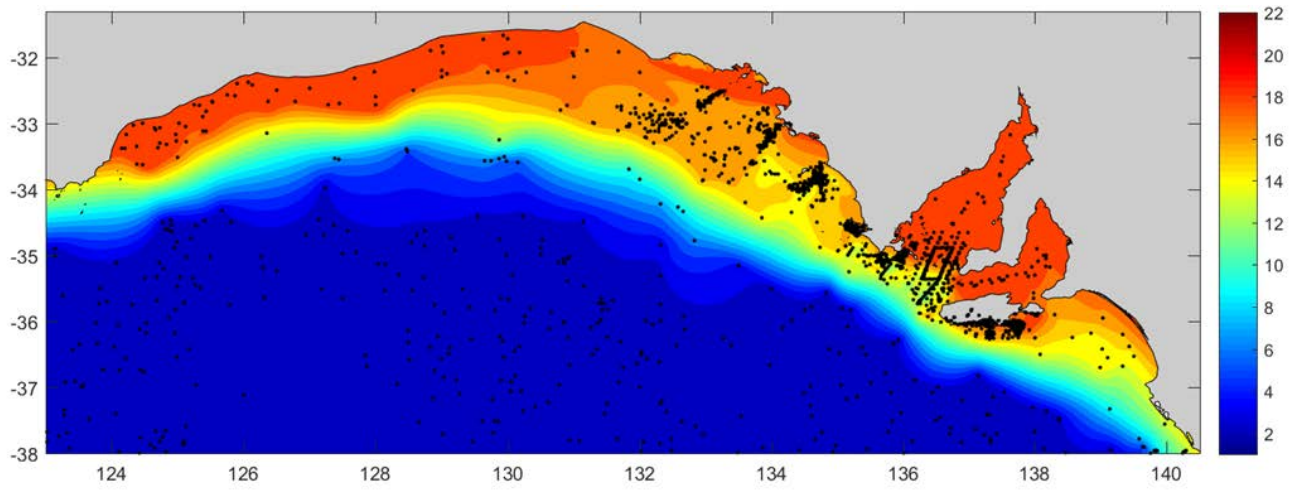

Figure 4.3.5 The observed summer temperature at the sea floor or 1500 m using all available CTD, sea lion, ARGO float data (black points).

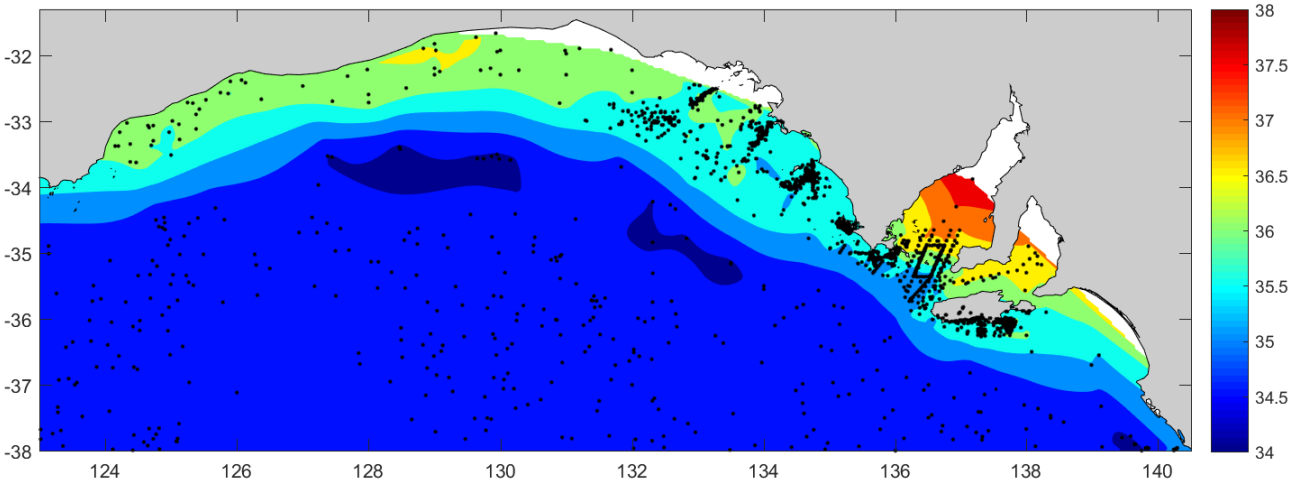

Figure 4.3.6 The observed summer salinity at the sea floor or 1500 m using all available CTD, seal, ARGO float data (black points)

4.3.3 Summer Cross-Sectional Results

The above comparisons are complemented by an examination of summer average results at the three cross sections outlined in Figure 4.2.1. Again, with the exception of the data from the 4 moorings in the GAB and off Kangaroo Island, (Figure 4.2.1), we have only temperature cast data for comparison. (The amount of salinity data is too limited for reliable cross-sections). Thus, only observed temperature results are presented along with some comments on the model results.

Section 126 ^{o}E: far western GAB

The plan-view ROMS model results for currents for this cross-section (Figure 4.3.1) suggest the alongshore velocities are generally weak (5 cm/s or less) and to the west with the exception of an eastward shelf break trapped current (SAC) with speeds of up to about 10 cm/s. The inshore westward current is likely wind driven.

The plan-view SHOC alongshore velocity field (Figure 4.3.2) indicates an eastward flow over the shelf edge that is much weaker than that from ROMS. Seasonal maps of SHOC velocity show that a cyclonic eddy happened to be at the location of the cross section in [2011] but in [2012] there was an anticyclone.

Both the SHOC and ROMS temperature fields (not shown) indicate that water has been downwelled to depths of 400 m although the observations indicate the downwelling to be weaker (Figure 4.3.7).

At depths greater than 400 m, the ROMS model and data indicates deep upwelled water while SHOC indicates downwelling near the slope; the former result is consistent with the upwelling shown in the observations (Figure 4.3.7) and existence of a FC in the far west of the GAB.

Further evidence for this deep upwelling comes from the hydrographic section made by Schodlok and Tomczak (1997a) during November 1995 and 120 ^{o}E and shown in Figure 4.3.8. In the top 500 m (upper panel; Figure 4.3.8), strong downwelling is found while at greater depths between 500 and 1000 m strong upwelling is found. These authors (Schodlok and Tomczak 1997b), also estimated a net transport to the west of 35 Sv between the coast and 39 ^{o}S. This deep westward transport was identified as a "northern" boundary current (the FC) as found in the model of Middleton and Bye (2003) and from wintertime data by Cresswell and Peterson (1993).

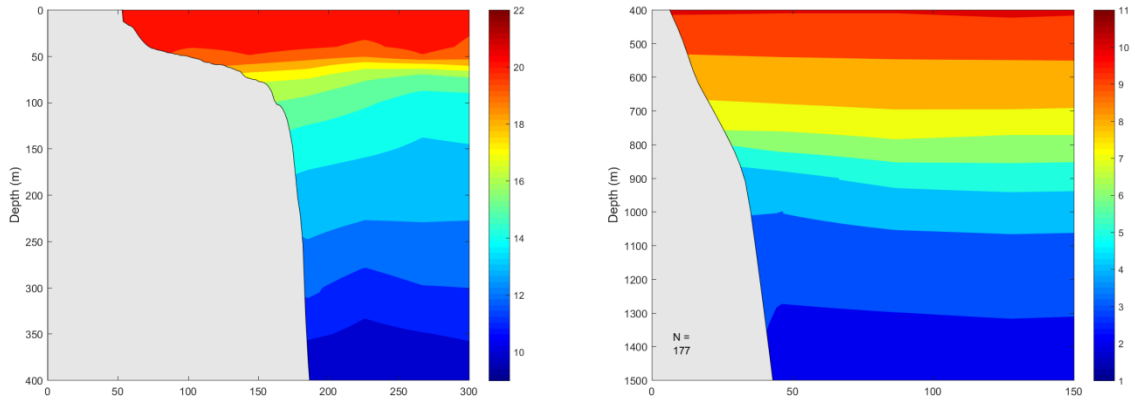

Figure 4.3.7 126 ^{o} E shelf cross-section. Left Panel:coast to 400 m. Right Panel: 400 to 1500 m. Contour plot of observed summer average temperature. Colour bar indicated.

Section 130.8 ^{o}E: central GAB

The alongshore ROMS velocity field (Figure 4.3.9) exhibit an eastward SAC trapped over the shelf break and of order 10 cm/s. The ROMS depth and summer averaged current are to the east and from Table 4.3.1 equal to 10 cm/s and similar to that of the shelf mooring BPM1 (6 cm/s). Either side of the SAC (i.e.

both north and south) the flow is to the west. The inshore depth-averaged westward flow might be driven by the upwelling favourable winds, although there are no in situ observations to confirm this for 2011 and 2012. Offshore, the westward flow in ROMS is consistent with that obtained by the simpler modelling study of Middleton and Platov (2003) and consistent with a FC at depth.

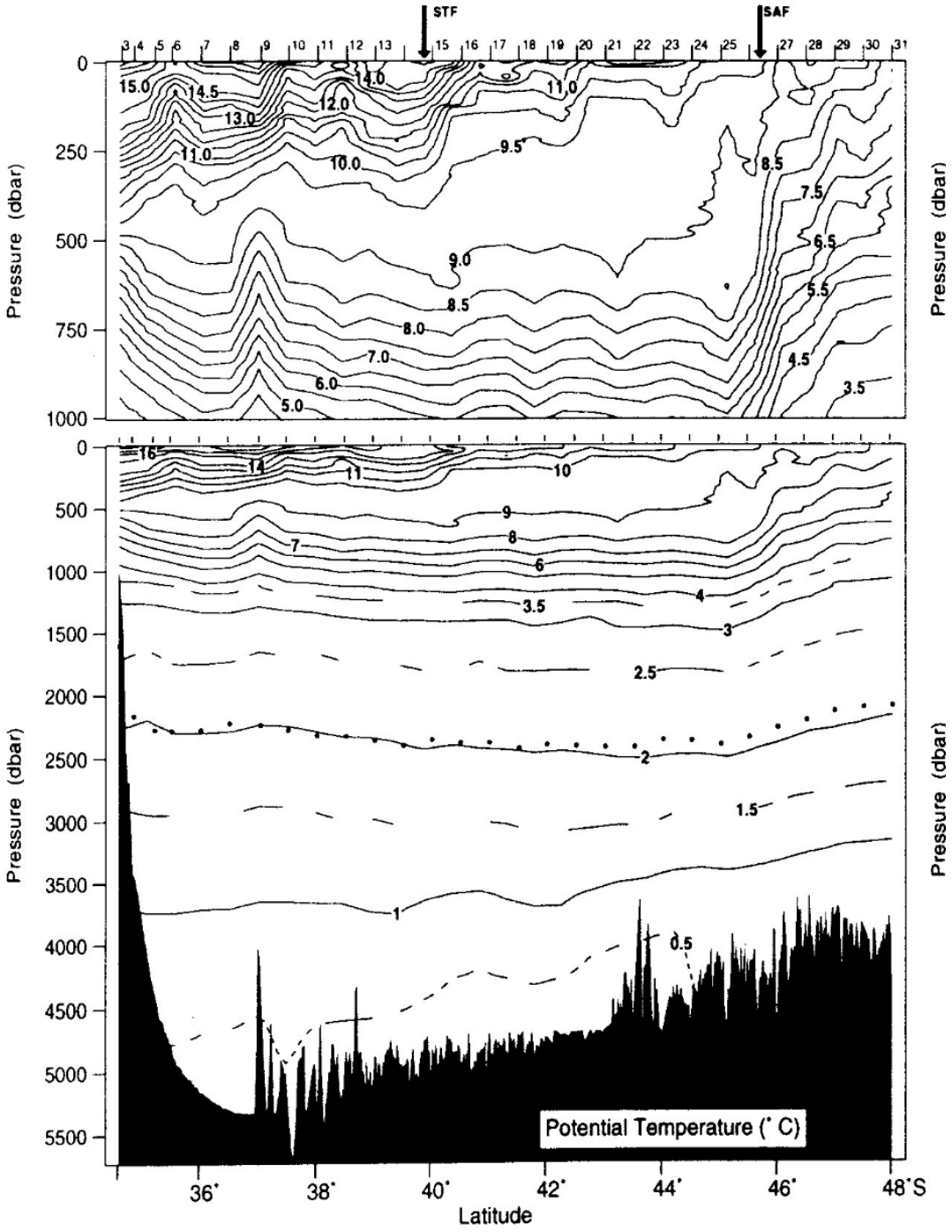

Figure 4.3.8 A hydrographic section of potential temperature taken at 120 ° E in November 1994 by Schodlok and Tomczak (1997a). The plot illustrates the existence of dowelled water in the top 500 m and upwelled water at depths of 500 – 1000 m.

The central GAB temperature transect for both ROMS and the data (Figure 4.3.11 and Figure 4.3.12) indicate downwelling along the shelf break and at depths between 100 and 250 m. Such a result is expected from a summertime convergence of Sverdrup transports. At depths below 400 m, both the ROMS and data generally indicate deep upwelled water and from the discussion above, is again a likely contributor of the summer SAC:;the upwelled dense water sits "lower" in the water column and the resultant trough in sea level that drives the SAC through geostrophic balance. Results for the ROMs depth-averaged velocity at the deep BPM2 slope mooring site (Table 4.3.1) are also in very good agreement with the mooring data with a very small westward time and depth-average velocity of 1- 2 cm/s. Inshore of the SAC, the ROMS currents (Figure 4.3.9) are to the west and consistent with a local upwelling favourable current.

Table 4.3.1 The mean of major axis velocities for the models and data (m/s) for summer 2011/2012 averages. For the BP moorings, eastward and northward current components (u/v) are presented. The mooring locations are presented in Figure 4.2.1 and Appendix 1.

Source	**NRSKAI**	**SAM5CB**	**SAM7DS**	**BPM1 shelf edge**	**BPM2 shelf slope**
Mean Observed	0.06	-0.16	0.03	0.06/-0.01	-0.01/-0.02
Mean ROMS	0.05	-0.02	0.01	0.10/-0.01	-0.02/-0.03
Mean SHOC	0.04	-0.03	0.00	0.15/-0.02	-0.04/0.02

The cross-shelf results from SHOC present a similar SAC circulation to ROMS but is stronger and up to 20 cm/s (Figure 4.3.10) and everywhere to the east. At the BPM1 shelf edge mooring, the depth averaged ROMS and SHOC currents are also stronger and 10 -15 cm/s, - larger than that of the data (6 cm/s; Table 4.3.1). In agreement with the data and ROMS, downwelling over the shelf break and slope is also found (Figure 4.3.12; left panel).

Both the ROMS, SHOC and observations for temperature indicate upwelled isotherms near the coast (Figure 4.3.11 and Figure 4.3.12). The observed temperature field (Figure 4.3.12) is also upwelled between depths of 500 - 800 m and consistent with that expected for the FC.

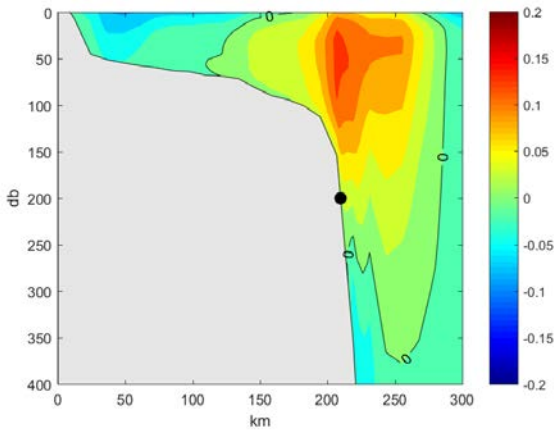

Figure 4.3.9 130.8 º E shelf cross-section- coast to 400 m with contour plots of the ROMS 2011-2012 summer average along-isobath velocity. Contour level 0.02 m/s. Positive values are to the east.

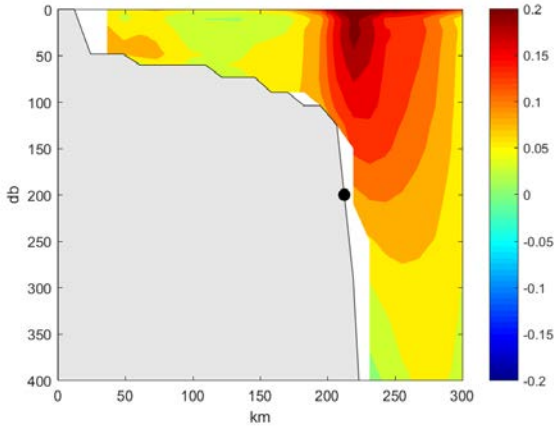

Figure 4.3.10 130.8º E shelf cross-section- coast to 400 m with contour plots of the SHOC 2011-2012 summer average along-isobath velocity. Contour level 0.02 m/s. Positive values are to the east.

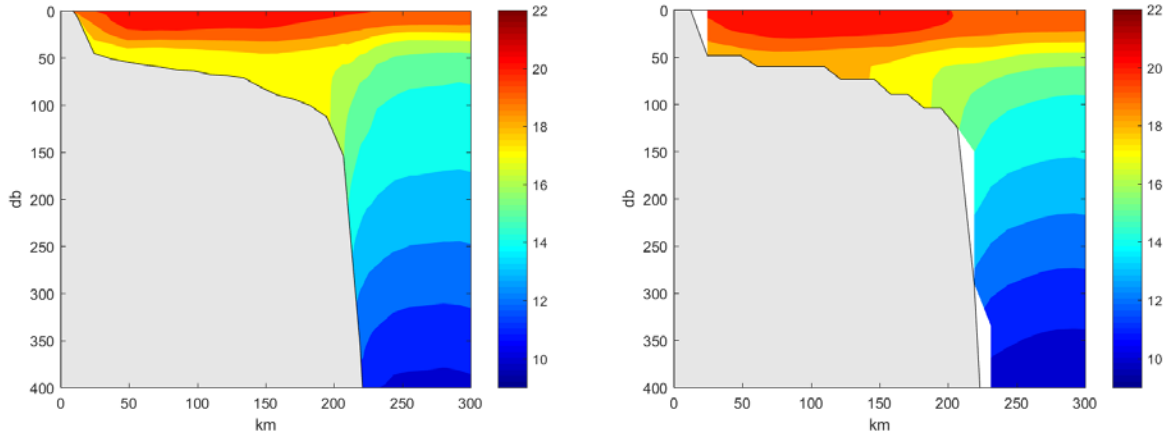

Figure 4.3.11 130.8º E shelf cross-section – coast to 400 m. Contour plot of the ROMS (Left) and SHOC (Right) 2011-2012 summer average temperature. Colour bar indicated.

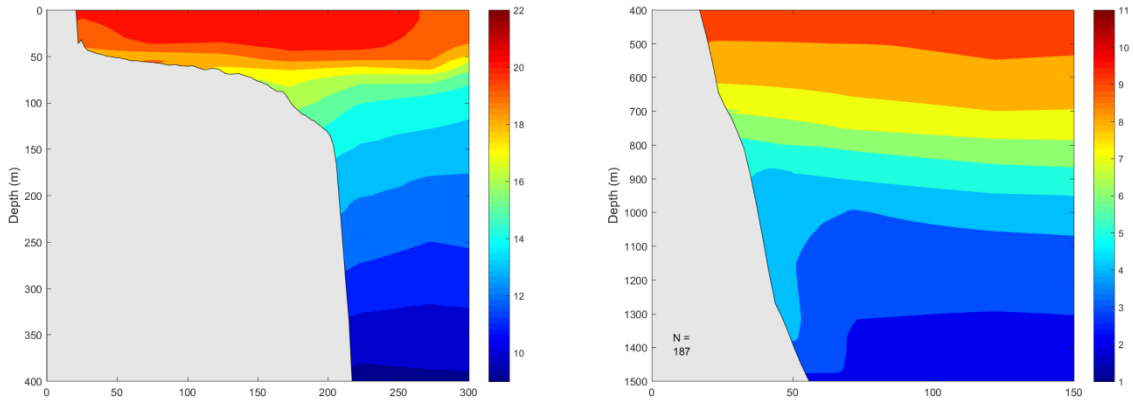

Figure 4.3.12 130.8 º E shelf cross-section. Left Panel: coast to 400 m. Contour plot of observed summer average temperature. Colour bar indicated. Right Panel 400 m to 1500 m.

Section 136 ^{o}E: far eastern GAB

The cross-section here begins at the 100 m isobath and is aligned in the north-east, south-west direction to focus on the shelf and slope circulation. In addition, the mean flow in the coastal regions (depths less than 100 m) should tend to follow isobaths and, if upwelling favourable, be directed to the north-west, south of Kangaroo Island, then to the north to the immediate west of Kangaroo Island and then to the west north-west at the mouth of Spencer Gulf and south of the Eyre Peninsula.

Results for this section are presented in Figure 4.3.13 to Figure 4.3.17. For ROMS, (Figure 4.3.13; left panel), a strong and extensive SAC to the SE is found over the shelf break and slope. The maximum amplitude is about 20 cm/s while the depth averaged value of 9 cm/s is larger (Table 4.3.1) than that of 3 cm/s derived from the 516 m depth SAM7DS ADCP mooring. Inshore of the shelf edge, and in contrast to SHOC (Figure 4.3.13; right panel) the mean flow is to the SE and not consistent with upwelling favourable currents. As noted above, and shown below, events of upwelling do occur but the weak mean currents can be downwelling favourable.

Downwelled isotherms at depths of 150 - 300 m are found in the ROMS and SHOC results and in crude agreement with the data (Figure 4.3.15). The origin of this downwelling is unknown but may result from the previous winter.

Comparisons of the ROMS depth and summer averaged currents were also made with the SAM5CB and NRSKAI moorings (Table 4.3.1). For the former off the Eyre Peninsula, the data and models indicate a flow of 16 cm/s and 2 - 3 cm/s respectively and to the NW expected for upwelling. For NRSKAI, both the data and the models indicate a 4 -6 cm/s flow to the SSE (expected for downwelling).

The SHOC model indicates a strong SAC (20 cm/s) but also a weak upwelling CC over the shelf.

The observations and models (Figure 4.3.15 and Figure 4.3.16) indicate neither strong upwelling nor downwelling.

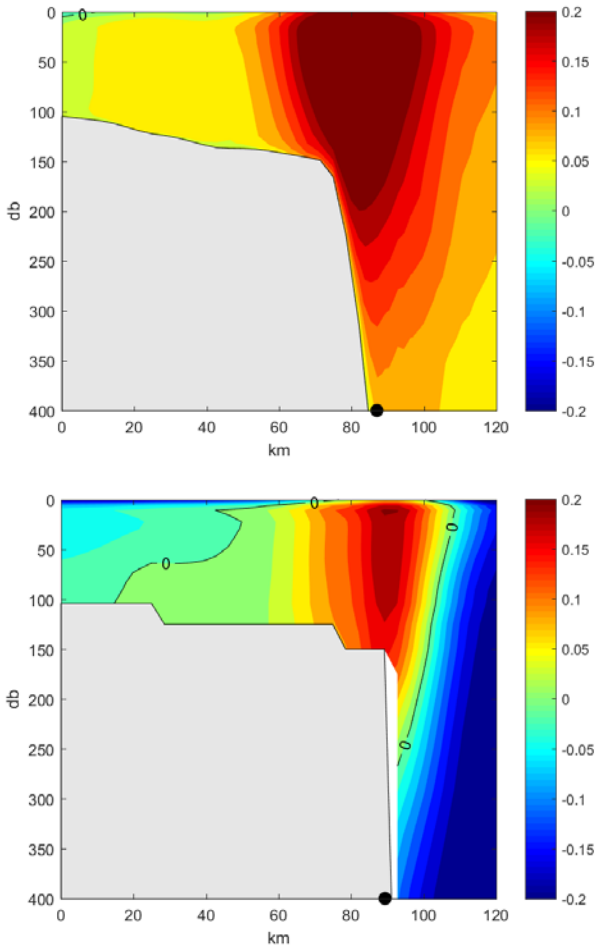

Figure 4.3.13 136 º E shelf cross-section- coast to 400 m, with contour plot of the ROMS (left) and SHOC (right) 2011-2012 summer average along-isobath velocity. Contour level 0.02 m/s. Positive values are to the east. The black dots indicates the approximate site of the SAM7DS mooring.

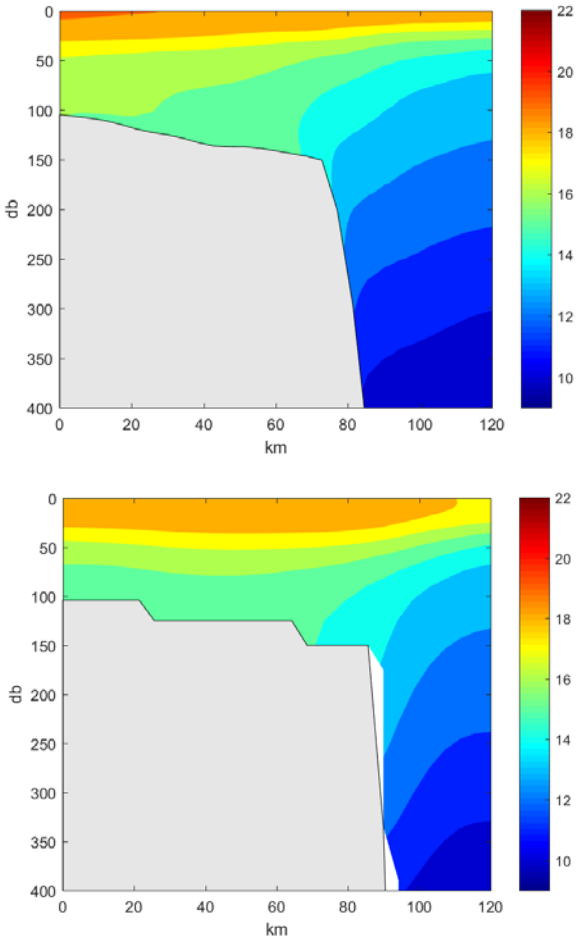

Figure 4.3.14 136° E shelf cross-section – coast to 400 m. Contour plot of the ROMS (Left) and SHOC (Right) 2011-2012 summer average temperature. Colour bar indicated.

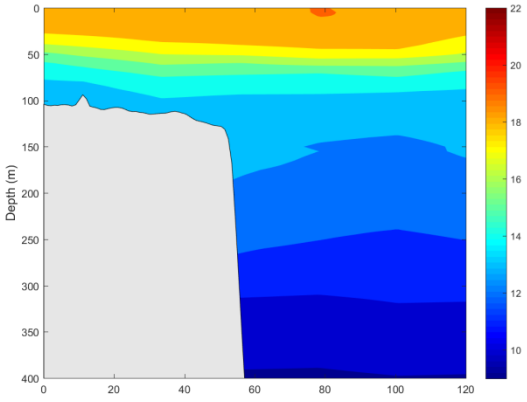

Figure 4.3.15 136° E shelf cross-section – coast to 400 m. Contour plot of observed summer average temperature. Colour bar indicated.

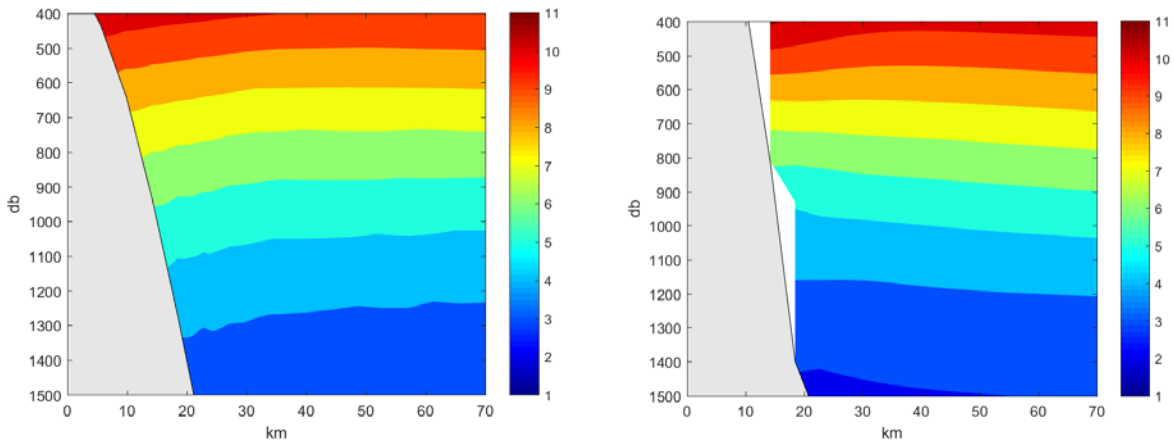

Figure 4.3.16 136 º E shelf cross-section – 400 to 1500 m. Contour plot of the ROMS (Left) and SHOC (Right) 2011-2012 summer average temperature. Colour bar indicated.

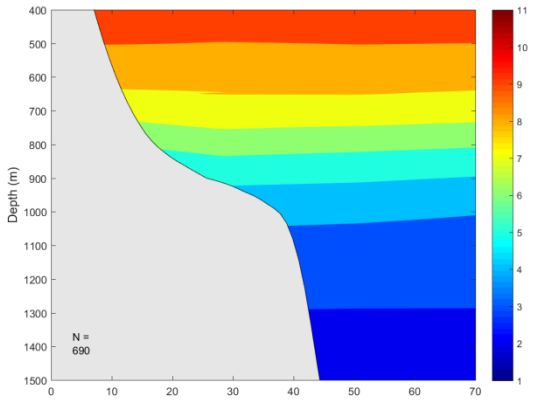

Figure 4.3.17 136 º E shelf cross-section – 400 to 1500 m. Contour plot of observed summer average temperature. Colour bar indicated.

5. THE REGIONAL SCALE: HYDRODYNAMIC MODELLING AND OBSERVATIONS

5.1 Summary

Comparisons are made between model and observed times series of velocity, temperature and salinity at five moorings and two other sites within the GAB shown in Figure 5.1.1. Mooring details are outlined in Appendix 1. Comparisons are made below in several spectral bands beginning with the "tidal" band (0-36 hour periods), the "weather band" (3– 30 day periods) and then the "seasonal" band (30 day averages). In addition, comparisons are made with the Southern Australian Integrated Marine Observing System (SAIMOS) CTD repeat line data that extends from the mouth of Spencer Gulf to the shelf edge (Figure 5.1.1). Comparisons are made for the two year period, 2011-2012, during which two moorings were operative in the vicinity of the BP leases (Nov 2011 to Dec 2012).

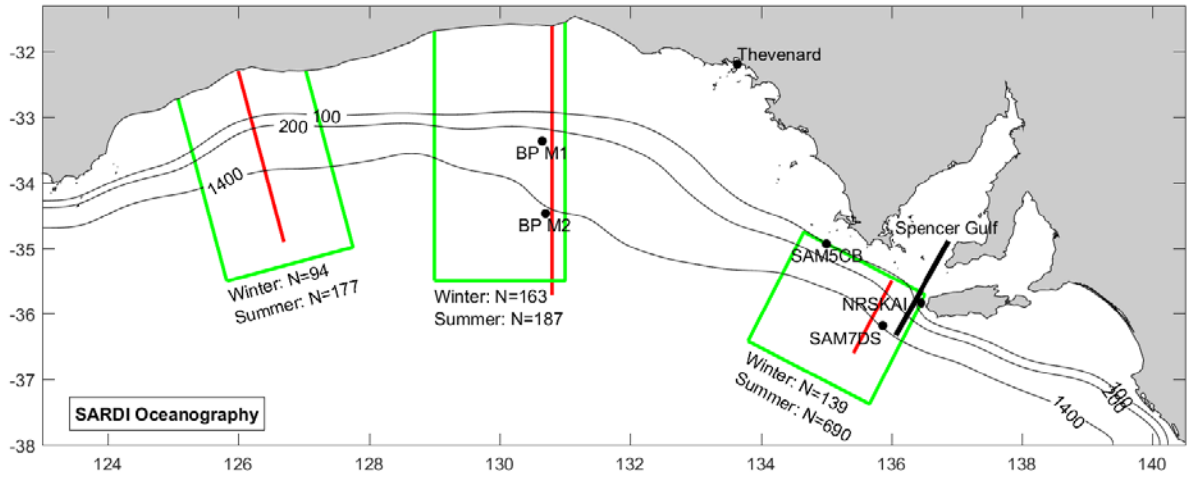

Figure 5.1.1 The ROMS model domain used in this study. The 100 m, 200 m and 1400 m isobaths are shown. The mooring locations of SAM5CB (Coffin Bay), NRSKAI (Kangaroo island), SAM7DS (deep 600 m mooring) and the BP moorings BPM1 (shelf edge) and BPM2 (shelf slope) are shown. The thick straight black line indicates the repeat SAIMOS CTD line. The red lines denote the location of cross-sectional (seasonal averaged) model results that are presented below. The green boxes denote the domains for which all available temperature data is obtained for comparison with the (red line) cross section model results. The number N of temperature data casts for each green box is indicated for summer and winter.

Ocean Currents and Sea Level:

For the three tidal, weather and monthly bands, the observed currents from the shelf moorings were typically in the range 10 - 20 cm/s but up to 50 cm/s notably for the weather band and during wintertime storms. For the offshore moorings (depths greater than 200 m), the depth-averaged currents in these bands were typically 10 cm/s or less.

Both models were better able to hind-cast observations of currents on the shelf (NRSKAI, SAM5CB) and notably in the weather-band and seasonal band (monthly averages). Here the squared correlation r^2

between the model and observations were typically between 0.6 and 0.9. Note, the squared correlation is a measure of the variance that is explained by the models, but with an arbitrary scale factor. In the tidal band SHOC was able to better reproduce tidal band currents ($r^2 > 0.5$) than ROMS. The influence of large amplitude internal tides and/or near-inertial baroclinic waves is clear at BP [M1] and [M2], where the tidal-band velocity is sometimes in antiphase at various depths.

For the tidal and weather bands of the shelf slope moorings, much less hind-cast skill was generally obtained ($r^2 \sim 0.3$) although ROMS and SHOC were able to reproduce some aspects of the winter and time averaged currents. The lesser skill in deeper water is well-known to result from the chaotic dynamics associated with baroclinic instability, and thermohaline circulation which is dependent on the temporally integrated effects of advection and diffusion of temperature and salinity. Deep water eddies are much less predictable than the quasi-linear dynamics associated with shelf currents driven by wind forcing.

Model output was also obtained at a head of the GAB site to examine the possibility of resonance due to inertial waves forced by the daily (24 hr) sea breeze which can be up to 10 m/s and shown to be important off Perth (Mihanovic et al., 2016). In a preliminary spectral analysis, only SHOC exhibited significant energy at the inertial period of 22 hrs and further investigation is needed. An examination of other model output did not reveal any special or unusual flow features for the region although further work remains to be done.

Model results for sea level (not shown) also compared very well with data from the Thevenard coastal tide gauge in both the tidal and weather bands.

Temperature and salinity:

Both SHOC and ROMS were able to reproduce monthly averaged SST quite well although in the case of ROMS, this was forced through strong nudging to the SST data.

Strong tidal band variations in the observations of temperature (and salinity) were also found at both the deep water shelf and slope BP moorings at depths of 100 – 200 m or so. These were not well reproduced by the models and again, likely for the reason noted above.

Finally, model temperature and salinity results for the cross-shelf SAIMOS survey transect were also compared with data for an April and February period of 2012. The model results replicate the observed upwelling in a qualitative manner. For the April transect, the ROMS results indicate the expected discharge (Middleton et al., 2013) of salty water from Spencer Gulf.

5.2 Summary tables of statistics for depth-averaged current variability

The BP moorings consisted of single-level current meters, that is, “point” data at discrete depths in the water column. For these moorings, the depth averages were found by weighting each instrument in proportion to its “layer thickness” – the depth interval with upper and lower surfaces defined by the halfway point between the current meter and the instruments above and below it. The currents above and below the top and bottom instruments respectively were excluded from the average.

The SAIMOS ADCP (Acoustic Doppler Current Profiler) moorings obtained profiles at evenly spaced intervals. The average is the simple arithmetic average over all bins in the profiles. The bin thicknesses at NRSKAI and SAM5CB were 4 m, whereas the bin thickness at SAM7DS was 6 m. More details are available in Appendix 1.

Here the statistics of variability in the depth-averaged currents over the two-year simulations are compared. Three frequency bands were chosen:

1. High frequency (periods one hour to 36 hours) or “tidal band”
2. Mid frequency (periods three days to thirty days) or “weather band”
3. Monthly averages or “seasonal band”

The methods for filtering to create the three bands are described in the relevant sections below.

The high-frequency band is dominated by tides and inertial oscillations; the low-frequency band is dominated by wind-forced coastal trapped waves and local weather events, and the monthly averages are dominated by the seasonal effects.

The major or principal axis of variation was determined from the covariance of the u (east-west) and v (north-south) variability (Table 5.2.1). Positive (negative) angles are taken in the counter-clockwise (clockwise) direction rotated from east. For example, for the high frequency tidal band at the NRSKAI, the ROMS angle for the major axis direction is – 68 degrees and approximately to the SSE. Currents are defined to be positive in this SSE direction and negative to the NNW.

*Table 5.2.1 Major axis rotation angles computed for the 2011/2012 period, for the high- and mid- frequency bands (the monthly means are formed from the mid-frequencies so have the same rotation). *Variability at SAM7DS does not show a strong preferred direction.*

Source & filtering	Mooring NRSKAI	Mooring SAM5CB	Mooring SAM7DS*	Mooring BPM1 (shelf)	Mooring BPM2 (slope)
High frequency Observed	-73	-68	-72	82	60
High frequency ROMS	-68	-86	-4.5	78	67
High frequency SHOC	-70	-80	-2.6	75	57
Mid frequency Observed	-77	-44	-46	-1.3	-50
Mid frequency ROMS	-80	-35	-47	0.24	-46
Mid frequency SHOC	-77	-33	-47	-10.0	-40

In Table 5.2.2, the squared correlation (r^2) between the model and data depth-averaged major axis velocities and for each frequency band based on all available data for each instrument during 2011/2012. As noted, the correlations are highest for the weather-band and monthly averages of the shelf data and smallest for the deep moorings.

Table 5.2.2 The squared correlation (r^2) between the model major axis velocities and mooring data based on all available data for 2011/2012.

Source & filtering	NRSKAI	SAM5CB	SAM7DS	BPM1 shelf edge	BPM2 shelf slope
High frequency ROMS/Observed	0.20	0.55	0.01	0.38	0.32
High frequency SHOC/Observed	0.27	0.54	0.02	0.35	0.31
Mid frequency ROMS/Observed	0.63	0.76	0.03	0.14	0.00
Mid frequency SHOC/Observed	0.73	0.86	0.04	0.14	0.01
Monthly mean ROMS/Observed	0.90	0.88	0.03	0.18	0.09
Monthly mean SHOC/Observed	0.83	0.88	0.00	0.01	0.01

For completeness, Table 5.2.3 provides the mean and standard deviation for all available major axis current data in 2011/2012 and each instrument and frequency band. As noted above, for the three bands, the observed currents from the shelf moorings were typically in the range 10 -20 cm/s but up to 50 cm/s, notably for the weather band and during wintertime storms. For the offshore moorings (> 200 m depths), the depth-averaged in these bands currents were typically 10 cm/s or less.

Mean statistics and plots for eastward and northward, rather than major axis, are given in the case of the BP shelf slope data due to uncertainty in determining a reliable major axis.

The winter and summer averaged major axis velocities for model and data (m/s) are presented in Table 4.2.1 and Table 4.3.1.

Table 5.2.3 The mean (upper number in cell) and standard deviation (lower number) for model and data major axis velocities at each mooring site based on all available information for 2011/2012: units m/s.

Source & filtering	NRSKAI	SAM5CB	SAM7DS	BPM1 shelf edge	BPM2 shelf slope
High frequency	-0.13	-0.02	0.01	0.01	-0.02
Observed	0.07	0.03	0.04	0.04	0.01
High frequency	-0.19	-0.05	0.02	0.02	-0.03
ROMS	0.04	0.03	0.05	0.05	0.01

Source & filtering	NRSKAI	SAM5CB	SAM7DS	BPM1 shelf edge	BPM2 shelf slope
High frequency	-0.14	-0.02	0.02	0.02	-0.01
SHOC	0.05	0.02	0.03	0.03	0.01
Mid frequency	0.00	0.00	0.00	0.00	0.00
Observed	0.10	0.16	0.07	0.07	0.03
Mid frequency	0.00	0.00	0.00	0.00	0.00
ROMS	0.12	0.13	0.05	0.05	0.05
Mid frequency	0.00	0.00	0.00	0.00	0.00
SHOC	0.14	0.12	0.04	0.05	0.02
Monthly mean	0.13	0.06	0.13	0.13	0.02
Observed	0.06	0.12	0.05	0.05	0.05
Monthly mean	0.19	0.12	0.11	0.11	0.03
ROMS	0.13	0.10	0.06	0.06	0.07
Monthly mean	0.15	0.06	0.15	0.15	0.03
SHOC	0.11	0.10	0.08	0.08	0.04

5.3 High-frequency (tidal band) currents

"High frequency" time series were formed by high-pass filtering using a Butterworth filter with cutoff period of 36 hours.

For the tidal band, plots of the depth-averaged major axis currents are presented in Figure 5.3.1 for a typical two-week period in April. At the Kangaroo Island mooring ("NRSKAI") the tidal amplitudes are typically 2 cm/s and larger than those at the Coffin Bay mooring (SAM5CB) where amplitudes are about 5 cm/s, and larger again than at the deep SAM7DS mooring.

Visually, both the ROMS and SHOC models reproduce the observations at NRSKAI reasonably well, both in amplitude and the phase of the fluctuations. The squared correlations for the high-passed data is small and around 0.20. The models have even better skill reproducing the high-frequency variation at SAM5CB where r^2 is above 0.63. At the deep water mooring SAM7DS, the models do not reproduce the high-frequency tidal variability well.

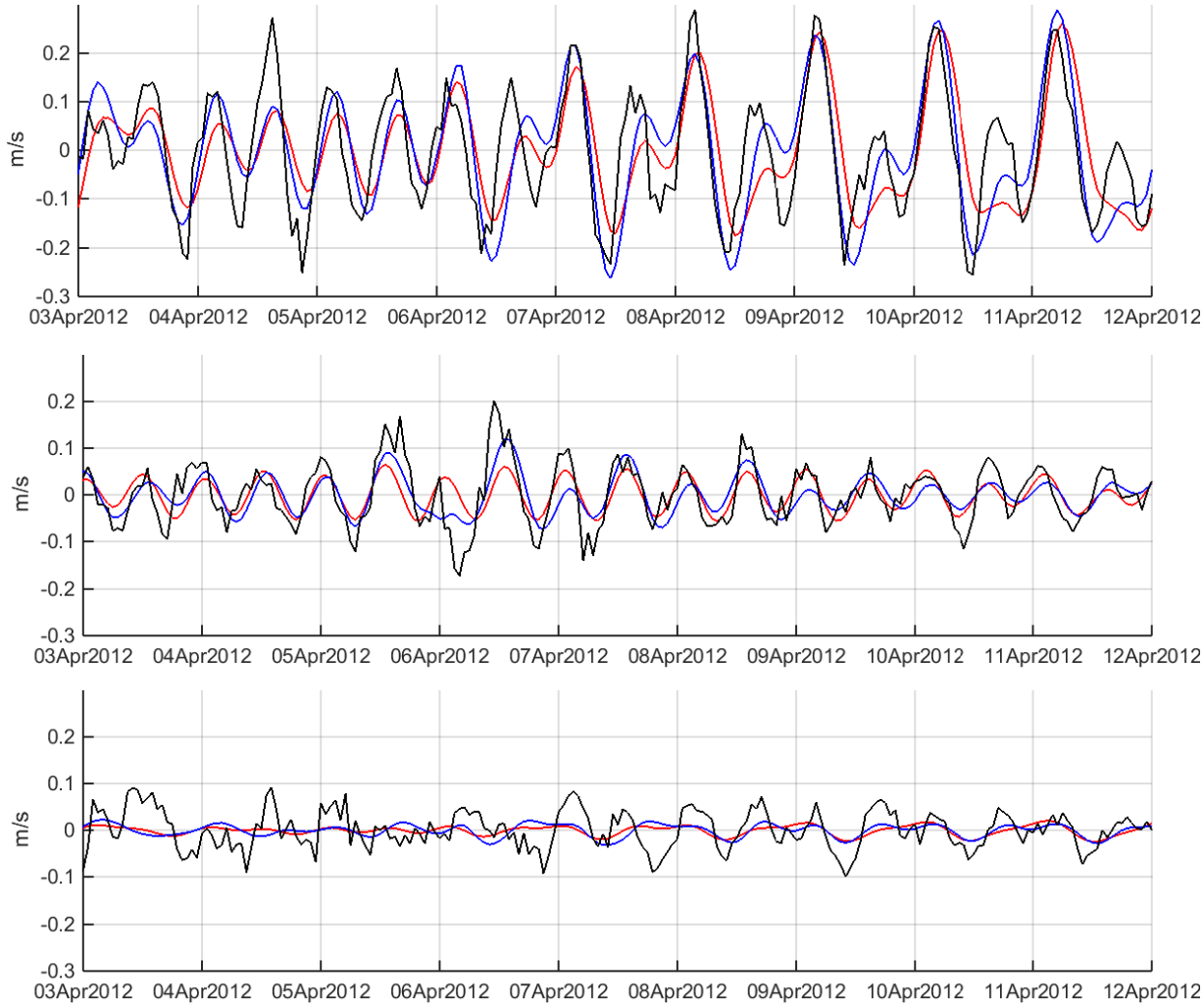

Figure 5.3.1 Vertically-averaged major axis tidal band velocities at SAIMOS moorings NRSKAI (upper), SAM5CB (middle), and SAM7DS (lower). A typical single fortnightly period is shown. Black: observations, red: ROMS, blue: SHOC.

Comparisons were made for tidal band depth-mean velocity between the models and the deep BP moorings (Figure 5.3.2). Results for the east-west direction are shown (east is positive). Currents at the shallower shelf mooring are typically 7 cm/s in amplitude while those in the much deeper slope mooring (depths to 1400 m) are much smaller (1-2 cm/s). The SHOC model reproduces the tidal variability better than ROMS.

Surprisingly, for BPM2, the values for r^2 seem small (~0.3) where from Figure 5.3.2, the 9 day snapshots suggest the two models to reproduce the observations extremely well. However, the 9 day time-series snapshots shown in the figures may not reflect the goodness of fit for the bulk of the data since all available BPM2 data (one year) are used to compute the correlations.

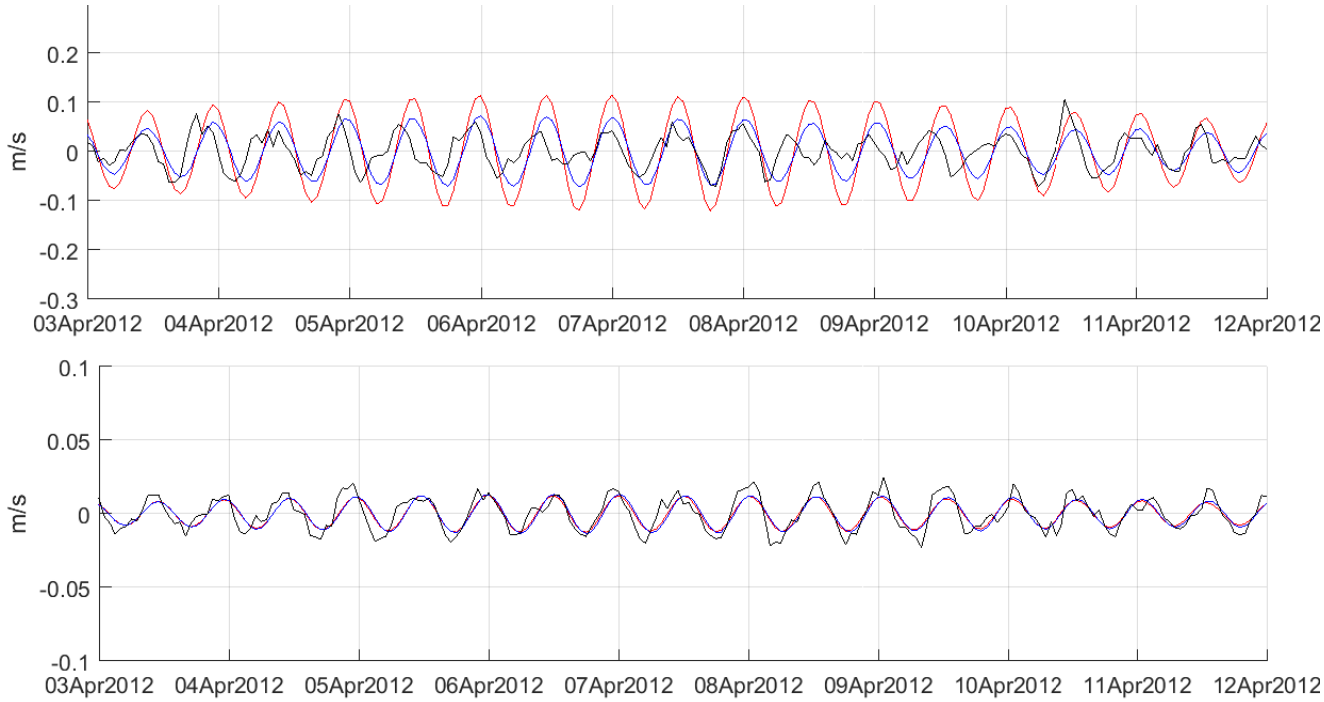

Figure 5.3.2 Vertically-averaged east-west tidal band velocities at BP shelf mooring (upper) and BP slope mooring (lower). Note change of scale. The vertical averages were taken between the depths of the top and bottom current meters. A typical single fortnightly period is shown. Black: observations, red: ROMS, blue: SHOC

5.4 Mid-frequency (weather band) currents

"Mid-frequency" (weather band) currents were formed by bin-averaging the time series data at a 3 day period. This approach was adopted in order to reduce gaps due to patchy current meter data.

For the weather band variability the principal axis angles of rotation are given in Table 5.2.1. Because of the way the major axes are defined, positive values at SAM5CB corresponds to flow to the east whereas positive flow at NRSKAI indicates flow to the south, south-east. For example on the 15th June the flow is to the east at SAM5CB, and to the south at NRSKAI (Figure 5.4.1 and Figure 5.4.2), expected for a continuous ribbon of along-isobath downwelling coastal flow. The weather band flow is directed predominantly along isobaths, as expected for flow with periods greater than 3 days or so.

Overall, the squared correlations for both models accounts for much of the weather-band variability: at the Coffin Bay site, more than 76% of the variance (or variability) of the observed currents is explained by the models. At site SAM7DS, there is little correlation between the model and observed currents (not shown): wind driven effects do not dominate here.

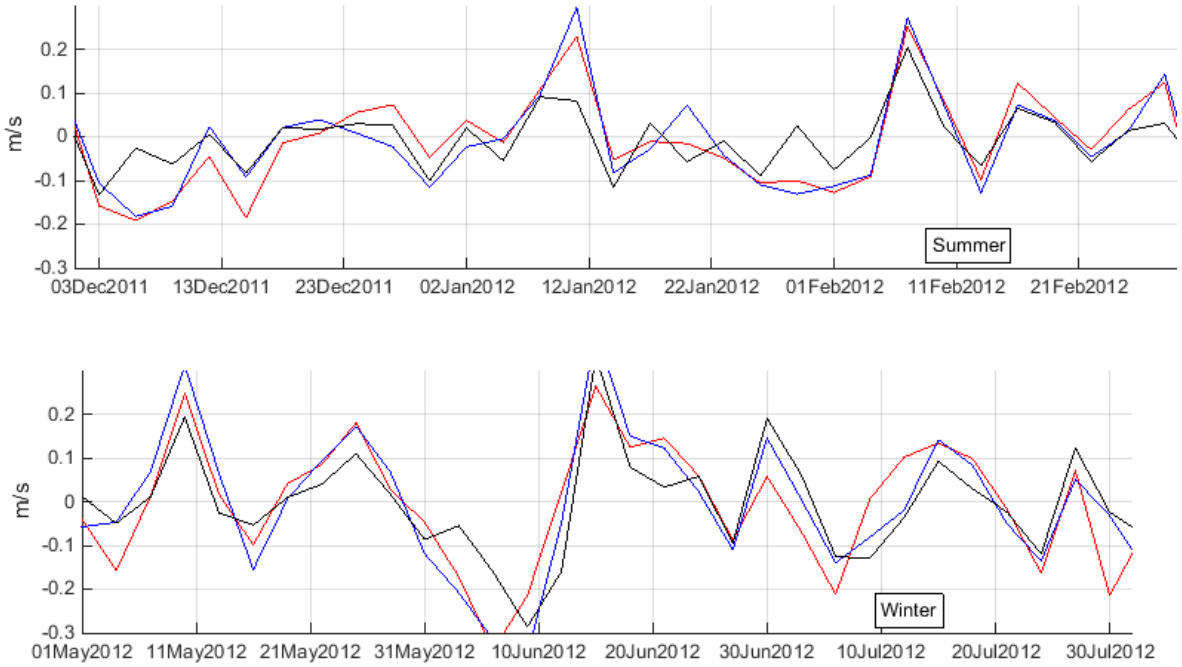

Figure 5.4.1 Weather band, vertically-averaged, major-axis velocity at NRSKAI summer (upper), and winter (lower) moorings during 2011/2012. Vertical averages were taken between the depths of the top and bottom ADCP bins. The duration of the model run is shown. Black: observations, red: ROMS, blue: SHOC.

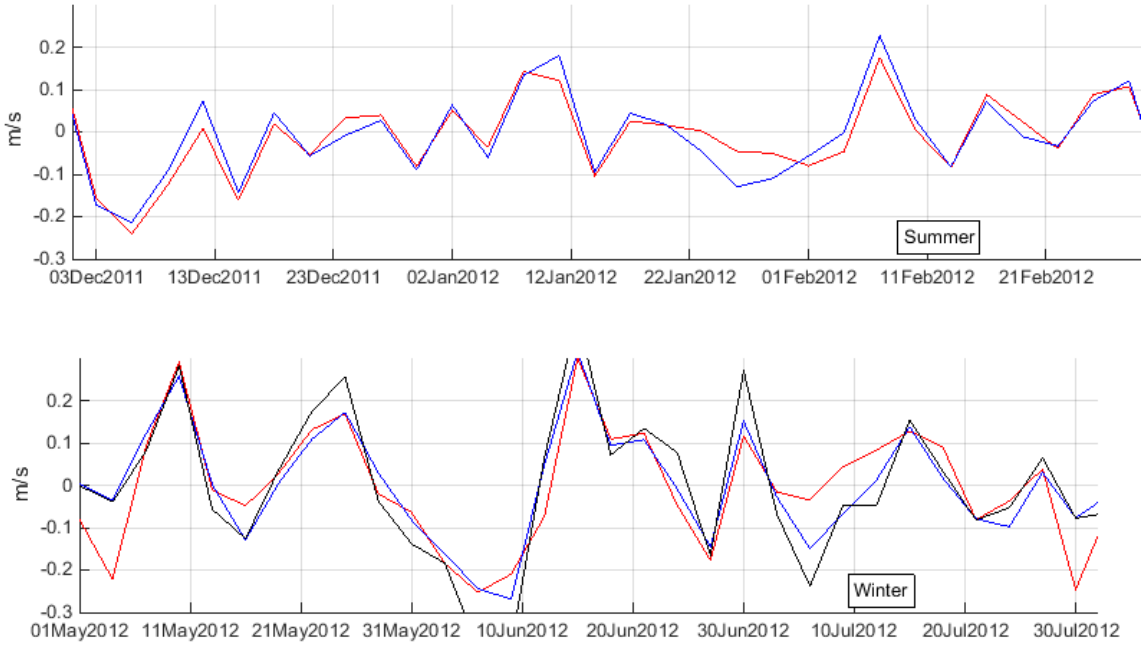

Figure 5.4.2 Weather band, vertically-averaged, major-axis velocity at SAM5CB summer (upper), and winter (lower) moorings during 2011/2012. Vertical averages were taken between the depths of the top and bottom ADCP bins. The duration of the model run is shown. Black: observations, red: ROMS, blue: SHOC.

The meteorology associated with two wind driven events is shown in Figure 5.4.3 and Figure 5.4.4 which show the mean sea level (atmospheric) pressure (MSLP) on the 10th and 15th of June 2011.

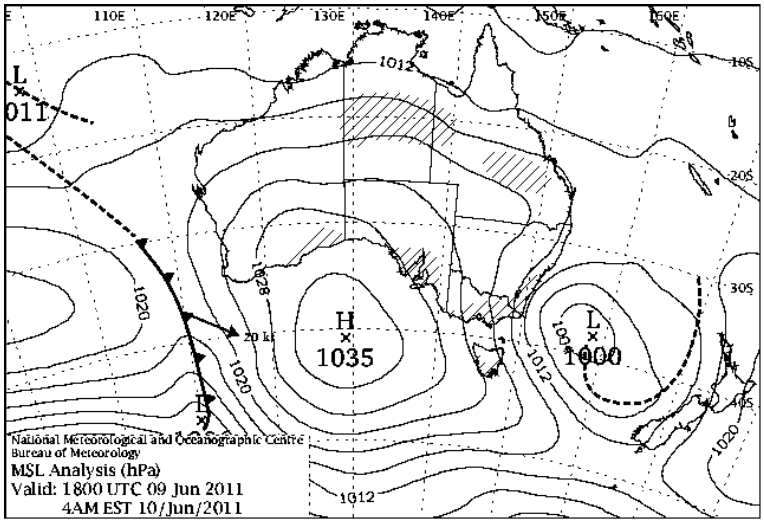

Figure 5.4.3 The mean sea level atmospheric pressure (MSLP) on the 10th June 2011. Units hector-pascals.

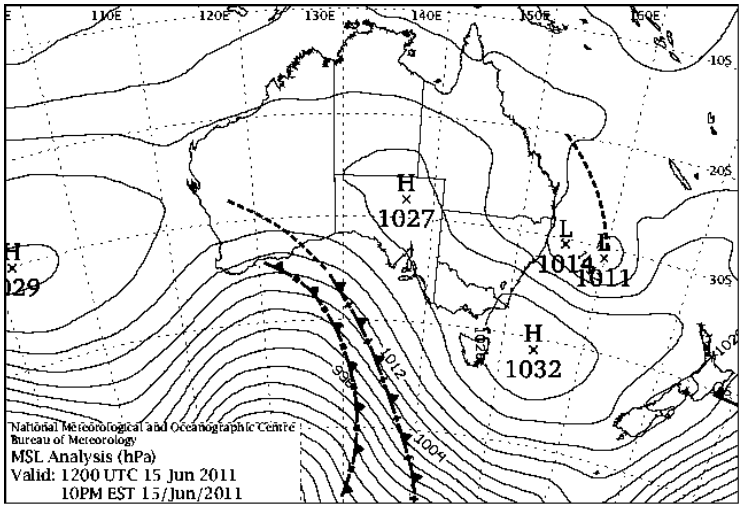

Figure 5.4.4 The mean sea level atmospheric pressure (MSLP) on the 15th June 2011. Units hecto-pascals.

The meteorology associated with two strong wind-driven events is shown in Figure 5.4.3 and Figure 5.4.4. For the 10th June, the high pressure system drives flow to the west (north) at the Coffin Bay (Kangaroo Island) mooring sites as shown in Figure 5.4.1 and Figure 5.4.2. For the 15th of June, the high

pressure system is replaced by an advancing front (Figure 5.4.4) and the winds are to the south-east. These winds drive currents to the east (south) at the Coffin Bay (Kangaroo Island) mooring sites as shown in Figure 5.4.2 and Figure 5.4.1. That is, in the direction of the principal axes chosen and positive for eastward (southward) currents at the Coffin Bay (kangaroo Island) mooring sites.

Moreover, the MSLP plots illustrate the type of variability found in the wind forcing during winter (and summer) where the region is characterised by eastward propagating high and low pressure systems and fronts.

For the BPM1 and BPM2 mooring data in the central GAB the weather-band variability is smaller than that described above for the shelf with currents of order 10 cm/s or less. The models provide a poor hind-cast of this deep water data and graphical results are not presented.

5.5 Monthly-average variability

Monthly averaged currents were created by bin-averaging over 30-days.

The SAIMOS site (NRSKAI and SAM5CB) results are shown in Figure 5.5.1. Both sites show the model and data indicate a strengthening of the eastward currents during winter (June-August) with amplitudes of up to 20 cm/s or so. The squared correlations for both models are very high (r^2 ~ 0.9).

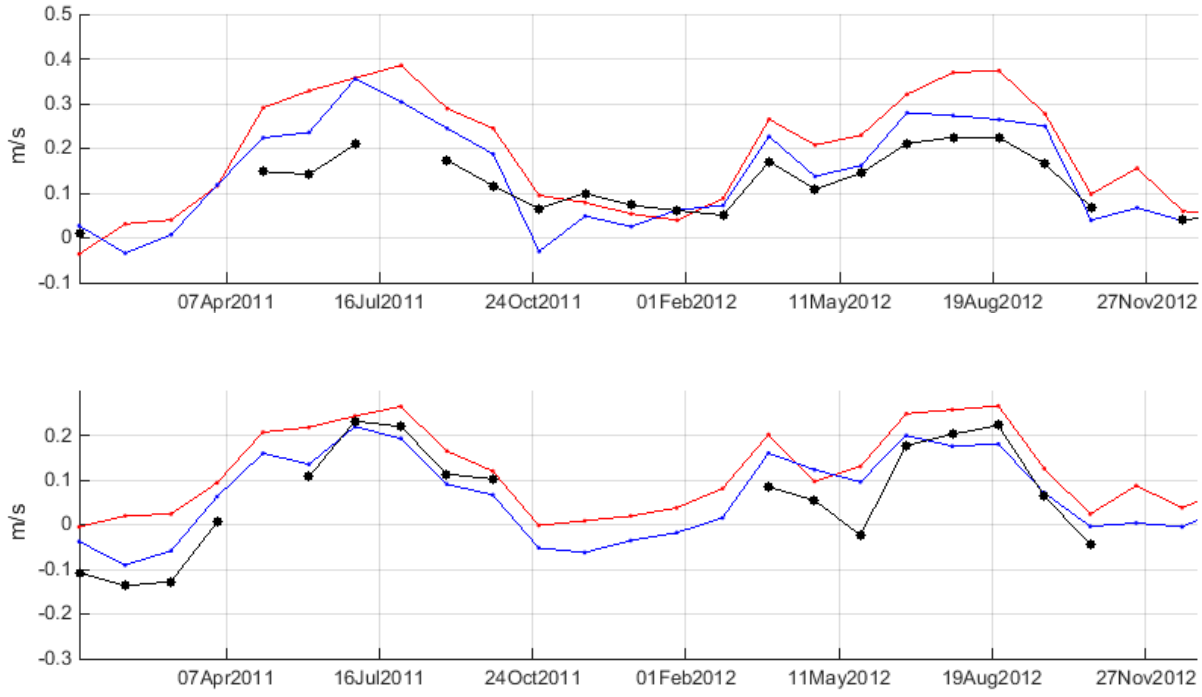

Figure 5.5.1 Monthly-averaged, depth-integrated, major axis currents at NRSKAI (upper) and SAM5CB (lower) moorings. The principal axis directions are given in Table 5.2.1. Vertical averages were taken between the depths of the top and bottom ADCP bins. Black: observations, red: ROMS, blue: SHOC.

At the BP mooring sites the 30 day running averages of currents are very similar to the results obtained using a weather band filter and the current variability is not well hind-cast by the models. Graphical results are therefore not presented.

5.6 Vertical shear

Table 5.6.1 Depths of layers for vertical shear estimates.

	NRSKAI Depth (m) below surface	SAM5CB Depth below surface
Top	10-30	10-22
Middle	40-75	38-74
Bottom	90-105	82-86
Total Depth	110	96

The data at NRSKAI and SAM5CB were divided into three layers: top, middle and bottom (Figure 5.6.1). The layer depths were chosen on the basis of each of the three data sources (ADCP current meter, and two models) each having values at the respective levels. The choices were also limited by the ADCP having no data above 10 m below the surface, or below 6 m above the bottom. The time series of major axis currents for the NRSKAI mooring and for the two-year duration of the model runs are plotted in Figure 5.6.1 and Figure 5.6.2. Results for Coffin Bay are very similar and not presented.

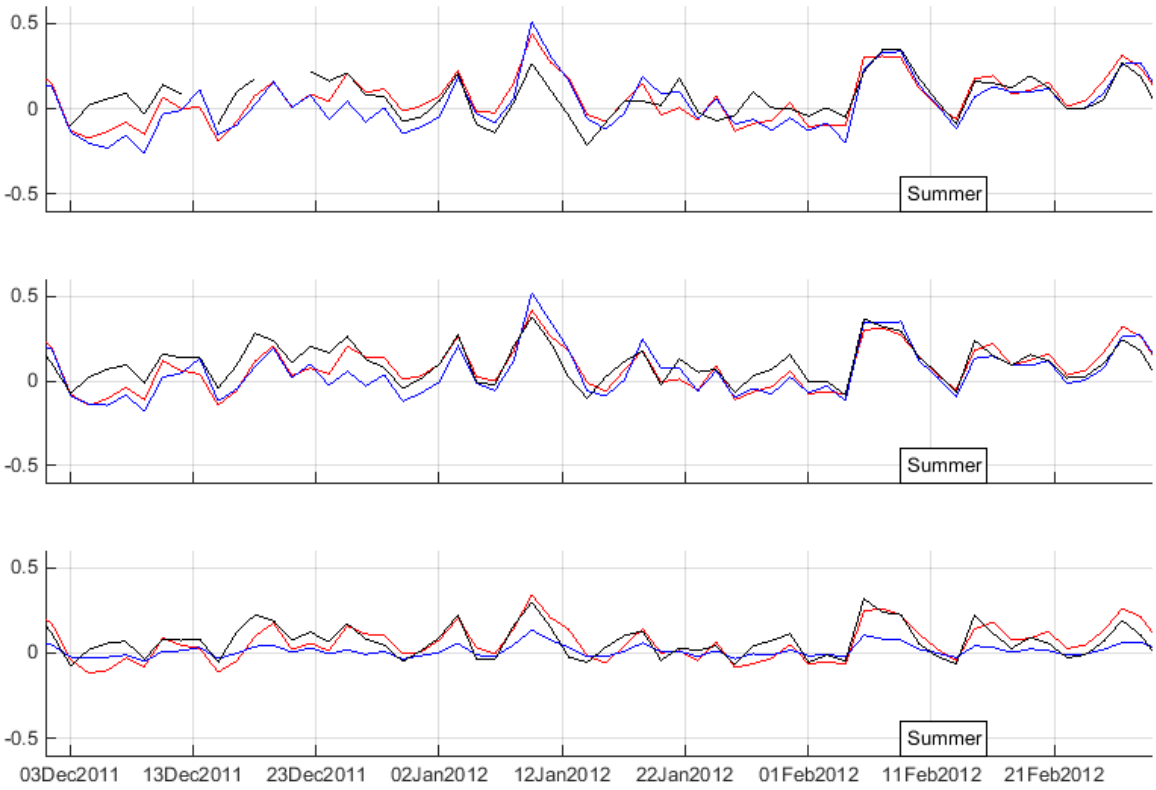

Figure 5.6.1 Major axis currents at three different levels at NRSKAI mooring (water depth 110 metres) during summer 2011/2012. Units m/s). Currents were low-pass filtered to remove tides, then a vertical average was taken over each of the three levels. Upper panel: top level. Middle panel: middle level. Lower panel: bottom currents. Black: observations, red: ROMS, blue: SHOC. Positive values imply velocities are directed poleward: to the south-south-east.

Visually, at both sites, the horizontal velocities of each of the three layers are similar, indicating that the shear due to density gradients or boundary layer effects are not strong: note that the surface and bottom Ekman layers are missed due to the restrictions in near surface and bottom data.

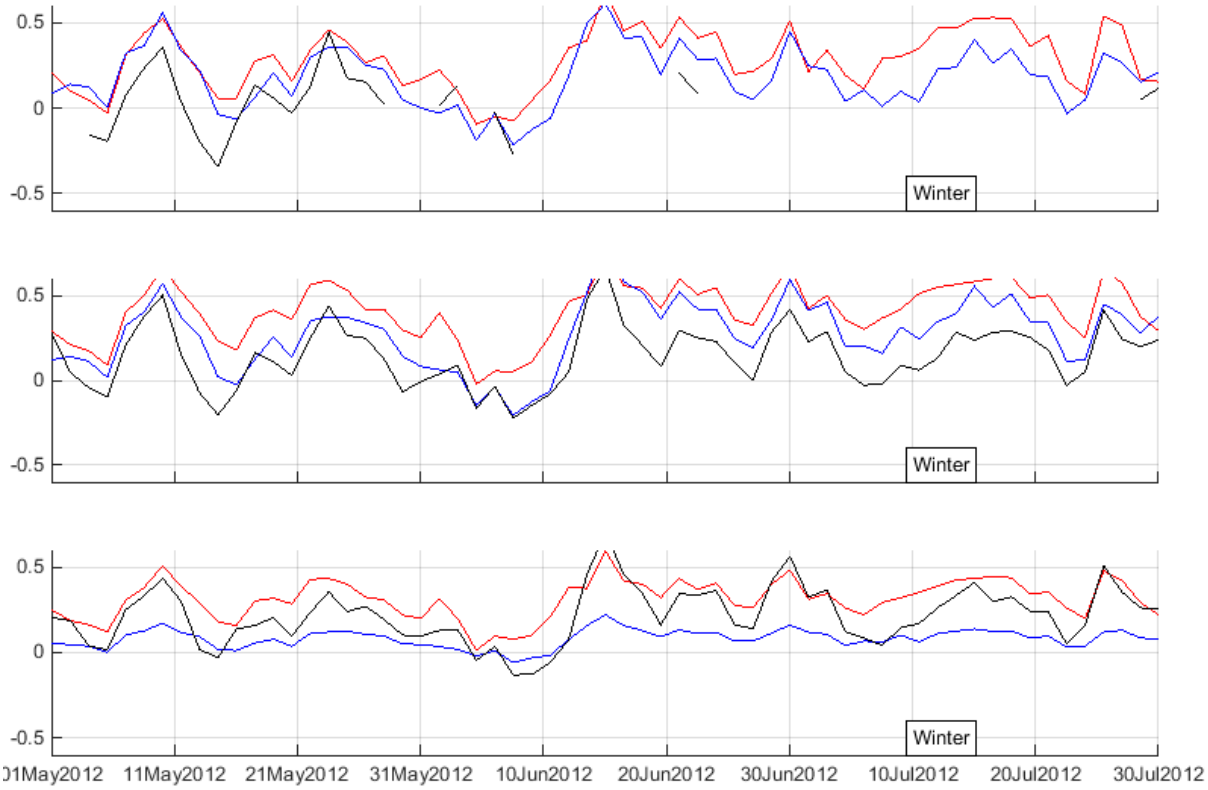

Figure 5.6.2 Major axis currents at three different levels at NRSKAI mooring (water depth 96 m) during winter 2012. Units m/s). Currents were low-pass filtered to remove tides, then a vertical average was taken within each of the three levels. Upper panel: top level (10-22 metres below surface). Middle panel: middle level (38 to 74 metres below surface). Lower panel: bottom currents (82 to 86 metres below surface). Black: observations, red: ROMS, blue: SHOC. Positive values imply velocities are directed poleward: to the south-south-east.

Both models replicate the observations reasonably well and notably during the summer period. Similar results were found for Coffin Bay and are not shown.

5.7 Temperature and salinity

An initial comparison is made below between time series of observed temperature and salinity data and model output. On the shelf and in coastal regions, both quantities are affected by atmospheric forcing as well as oceanic currents and diffusion and therefore the skill in model hind-casts is expected, and found, to be lower than that for shelf currents. On the deep shelf slope, hind-cast skill is also likely degraded by the presence of unresolved or poorly represented eddies, inertial waves and internal tides.

Results for the shelf:

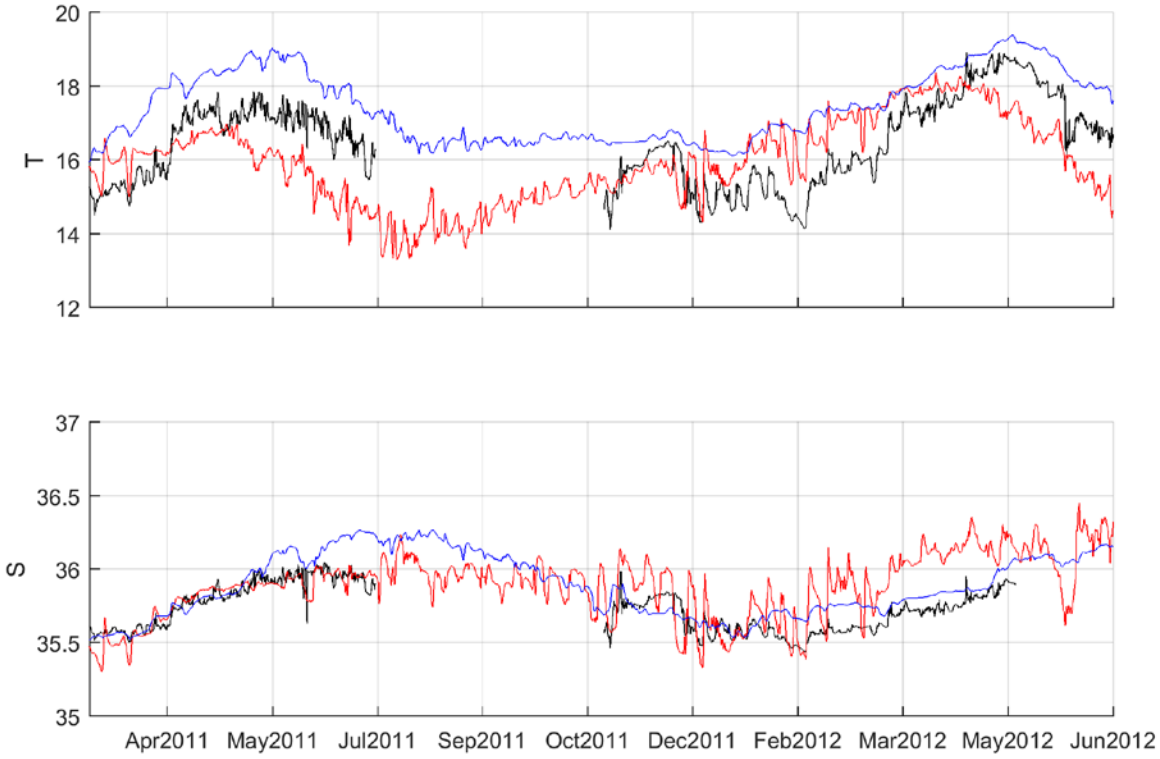

Figure 5.7.1 Bottom temperature (upper) and salinity (lower) at SAIMOS mooring SAM5CB. Black: observations, red: ROMS, blue: SHOC. Temperature at 95 db (95 m below surface). A data gap exists for the period July-October 2011 and the June 2012 salinities are unreliable, and have been omitted. Units are ^{o} C for temperature T and ppt for salinity S.

The results in Figure 5.7.1 show more than a year of hourly near bottom temperature (T) and salinity (S) observations and model output at the Coffin Bay mooring site and at a depth of 95 m or approximately 10 m from the sea floor.

Both models capture the seasonal cycles evident in the data. For temperature, SHOC is about 2 ^{o}C too warm. ROMS does slightly better but suggests a stronger tidal and/or weather band variability that is not found in the data or SHOC. For salinity, both models reproduce some segments of the observations.

In summary model errors of up to 2 ^{o}C and 0.25 ppt are found for temperature and salinity.

Results for the shelf edge and slope: Temperature is illustrated below for depths of 14 m and 197 m (shelf edge Mooring BPM1) and at depths of 120 m and 1420 m (shelf slope mooring BPM2).

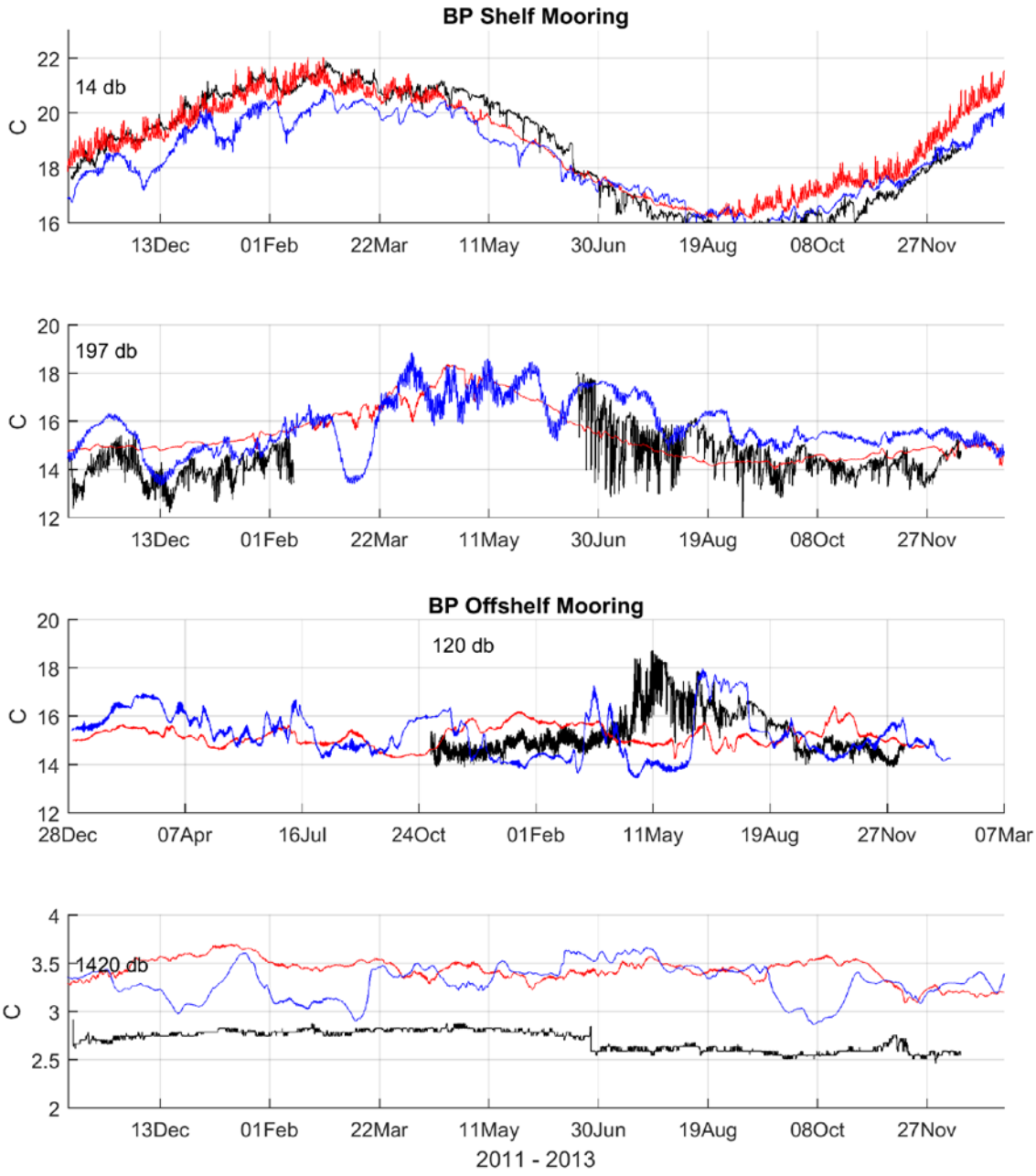

Figure 5.7.2 Unfiltered temperature at the top and bottom instruments at the BP moorings. Black: observations, red: ROMS, blue: SHOC. Note 1 db = 1 m in depth. Units are ° C for temperature T.

For the near surface (upper panel), the seasonal signal is again resolved by the models but differences with the data are again up to 2 °C as found above. For the deepest (1420 m) mooring the bottom panel

in Figure 5.7.2 shows no seasonal cycle at all, almost no variability and a temperature close to 2.5 ^{o}C. The lack of variability is generally modelled by ROMS. Both models are generally too warm by about 0.5 to 1.0 ^{o}C.

Of most interest in Figure 5.7.2 are the temperature observations at depths of 197 m (shelf mooring; 2nd panel) and 120 m (off-shelf mooring; 3rd panel). The data at these sites indicates strong variations in the tidal band of about 2 ^{o}C that are only partly reproduced by the models.

As an initial investigation of this variability, auto spectra of the observations were determined based on the standard two-sided Welch discrete Fourier transform which uses 50% overlapping segments and windowing to reduce the variance of the frequency estimates. A single-sided spectrum is created by using only positive frequencies, with amplitudes doubled. The width of and variance of the lowest frequency bin is then halved. A check is performed by summing the estimates, which must equal the time domain variance. (This also enables comparison between different methods that enforce the same condition). The estimates are divided by frequency to form the final "power spectrum".

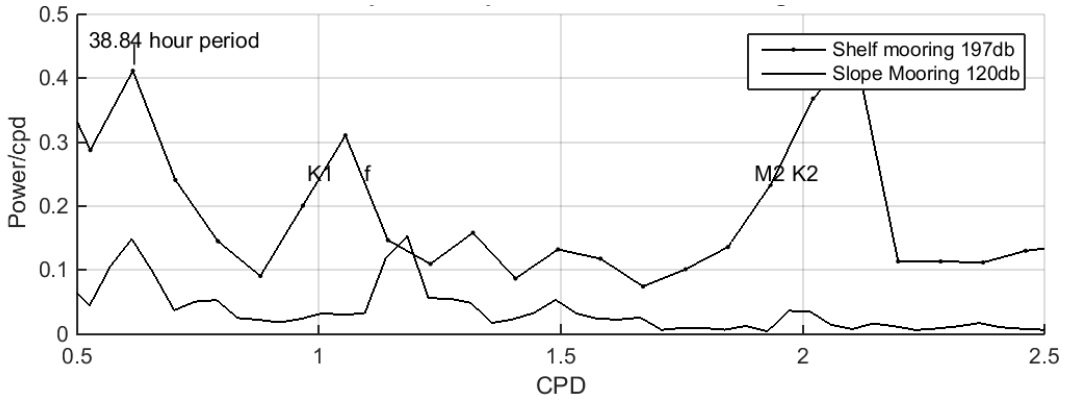

Figure 5.7.3 Power spectrum of temperature at two BP Current Meters (CMs) located at depths of 197 m and 120 m. The period of observations used is the period of high variability in the 197 m depth data in Figure 5.7.2. The frequencies of the semi-diurnal tides (~ 12hr period) M2 and K2 are indicated along with the diurnal daily tide K1 and inertial frequency f. Vertical units (^{o}T)^{2}/CPD). Horizontal units Cycles per day (CPD).

For the 197 m depth mooring data, the spectra were calculated using 48 days of data starting June 20th 2012; a period of maximum variability. For the 120 m depth mooring data, the spectra were calculated using 48 days of data starting 23rd April 2012.

The spectrum in Figure 5.7.3 suggests that the variability at each site occurs at different frequencies (and mechanisms). For the 197 m depth shelf mooring (BPM1; upper curve) temperature variability appears to be mostly associated with both the diurnal and semi-diurnal tides. For the 120 m depth outer slope mooring BPM2, the tidal variations in temperature appear to be more associated with inertial waves. Further investigation is warranted as the role of internal tides on the shelf slope circulation of the GAB is completely unknown but may be important to mixing on the shelf slope.

Results for sea surface temperature (SST)

A comparison of over one year of model output is presented in Figure 5.7.4 with (satellite) SST as observed at the BP mooring sites (upper two panels) and at the Coffin Bay mooring (bottom panel) . Note that each of the time series differ in that the satellite data are obtained as monthly averages, SHOC and ROMS as 20 minute and 10 day snapshots. For ROMS, the strong nudging of SST to the data was adopted and the agreement with the data is within 0.25 °C.

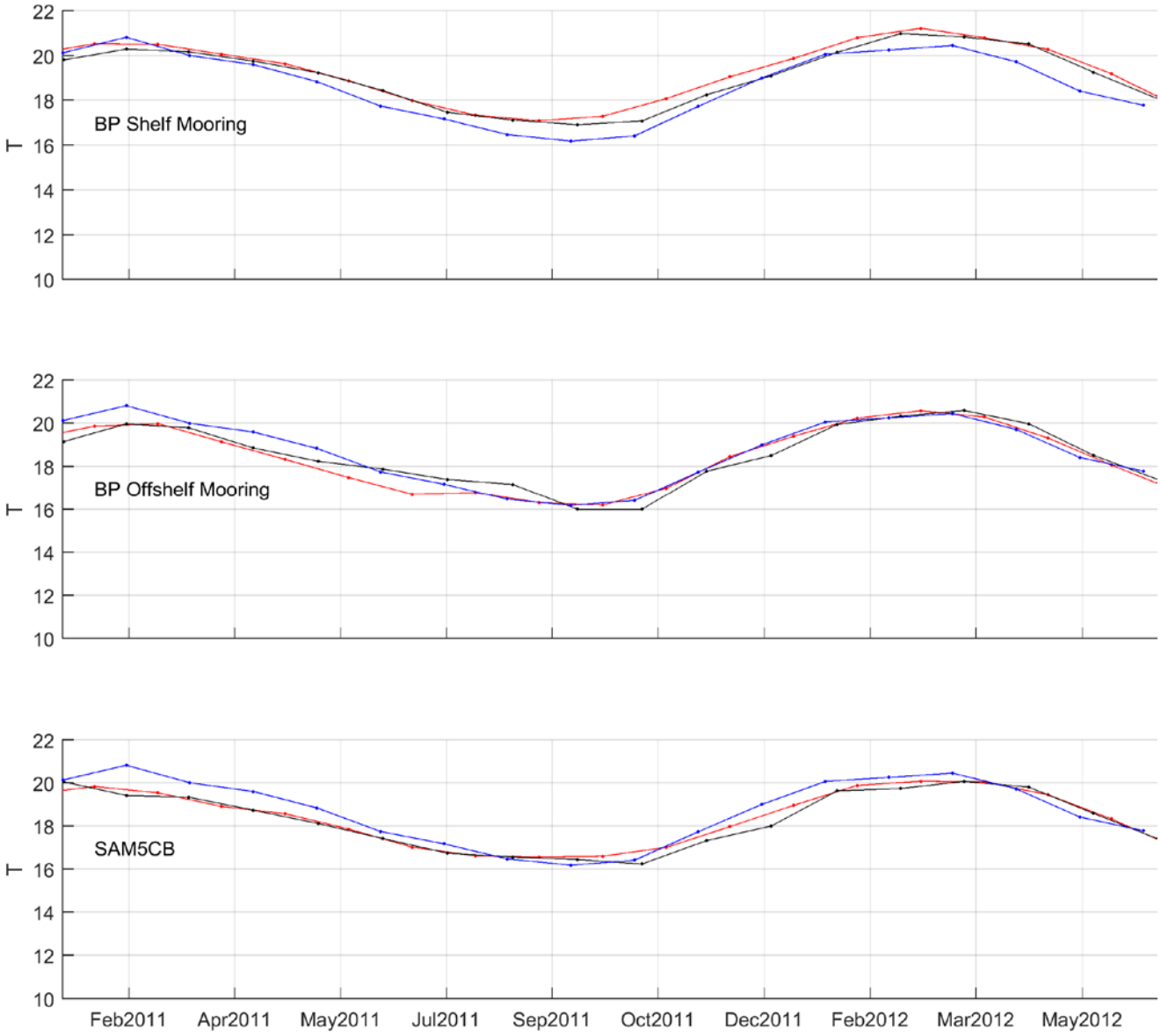

Figure 5.7.4 ROMS, SHOC and monthly mean NOAA AVHRR observed SST. Black: observations, red: ROMS, blue: SHOC.

Results for the Spencer Gulf CTD transect

A key feature of the physics of Spencer Gulf is the dense salty discharge out of Spencer Gulf that occurs in autumn and winter. A second feature of the region is the upwelling that occurs during summer in response to events of seasonal south-easterly airflow. The ability to simulate these features is used as a test of the models.

Winter gulf discharge: Cross sectional data illustrating this were not available for the model period of simulation. However, the discharge is illustrated in the plan-view model results Figure 4.2.7 and Figure 4.2.8 as well as in other studies (Middleton and Bye 2007; Middleton et al., 2013). For ROMS a cross-sectional illustration of the warm, salty outflow is shown in Figure 5.7.5.

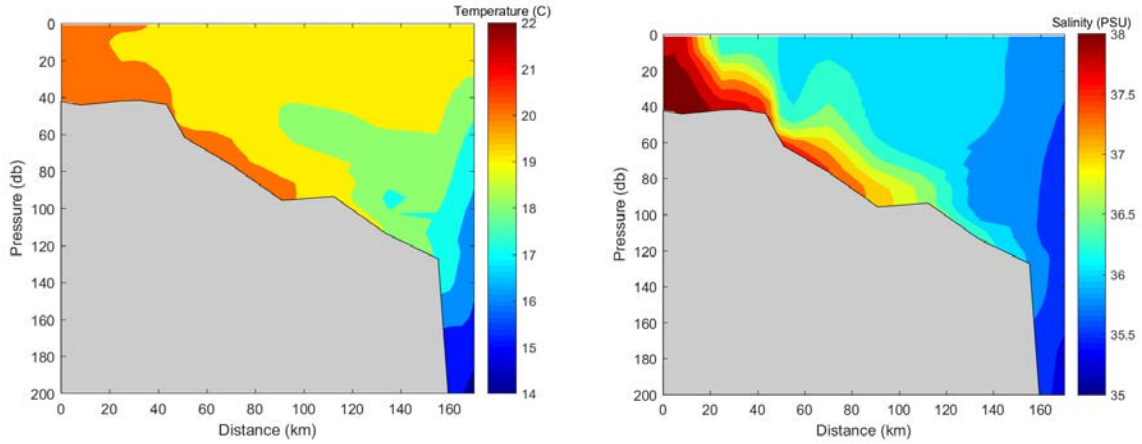

Figure 5.7.5 ROMS (T/S) transect on the 19th April 2012. Left panel temperature (° C); Right panel salinity (psu or ppt).

Summer upwelling: A set of temperature and salinity cross-sections for SAIMOS observations, ROMS, and SHOC are shown in Figure 5.7.6 to Figure 5.7.8, respectively. These transects are for 19th February 2012 (summer), when we expect dense (fresh, cold) water to have been upwelled to the mouth of Spencer Gulf. The SAIMOS transect shows a well-mixed surface layer to depths of 40-50 m. Spencer Gulf mouth water has temperatures of 21 °C and salinities of 36.35 ppt while off Kangaroo Island the surface to bottom water temperature ranges from 18 °C (surface) to 14 °C at depth, with cold (14 °C) and fresh (35.5 ppt) water at depths of 200 m.

The ROMS results are qualitatively similar to the observations with fresh (36 ppt) cold (16-17 °C) water upwelled to the gulf mouth. The summer SHOC results also exhibit upwelling, although somewhat weaker than that produced by ROMS.

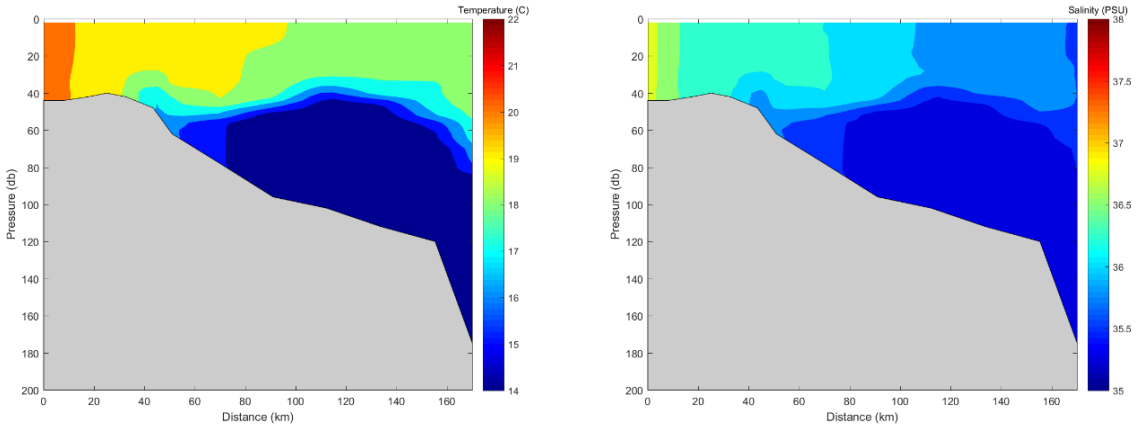

Figure 5.7.6 SAIMOS (CTD) transect on the 19th February 2012. Left panel temperature (° C); Right panel salinity (psu or ppt).

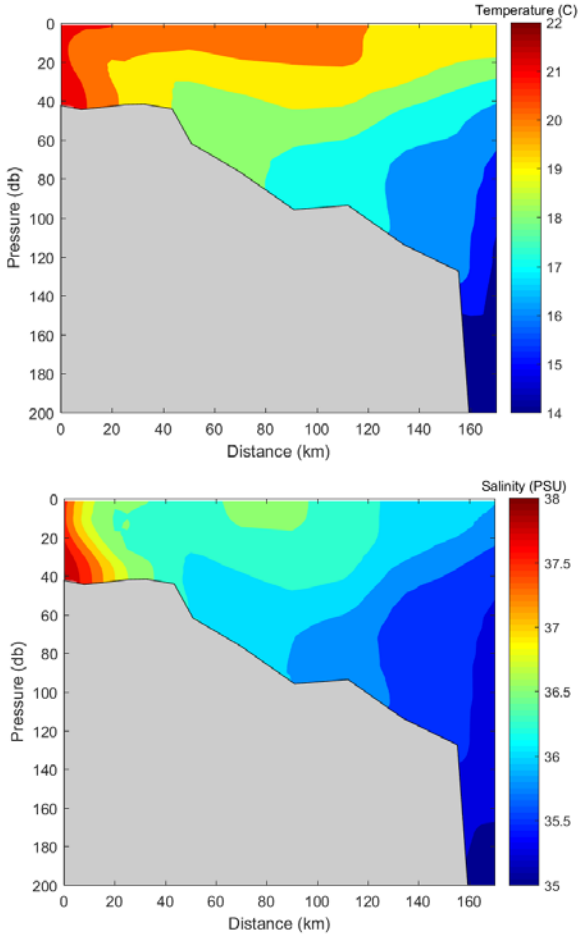

Figure 5.7.7 ROMS (T, S) section on the 19th February 2012. Left panel temperature (° C); Right panel salinity (psu or ppt).

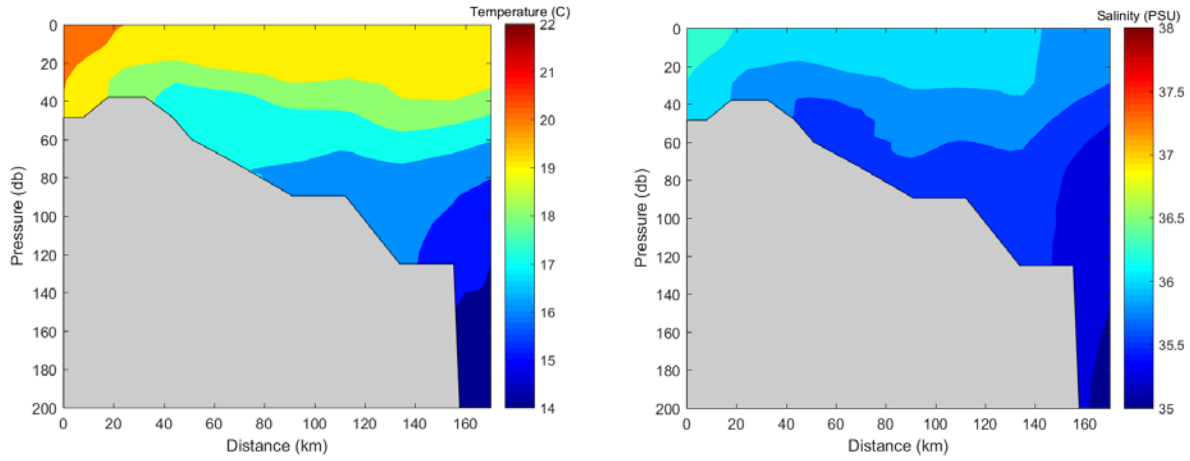

Figure 5.7.8 SHOC (T, S) section on the 19th February 2012. Left panel temperature (° C); Right panel salinity (psu or ppt).

5.8 Glider Analysis

Three seaglider missions have been completed by the IMOS Glider facility under contract to the GABRP. These are the only seaglider missions ever to have visited the central GAB. Seagliders are designed for deep-sea missions (off the continental shelf) so all deployments and retrievals were conducted near the 200 m isobath out from Port Lincoln. The goal of each mission was to get to 130.7 °E and back, sampling across the continental slope as many times as battery longevity allowed. Three missions were conducted rather than just the two planned because the first had to be curtailed mid-mission because of a severe battery problem.

The first mission (Sept- Oct 2014, 26 days, 495 km) only got as far west as 131.7 °E before a battery problem occurred, obliging the operators to turn off all sensors and return east. So only a few short transects (Figure 5.8.1) were completed. The two salient features of the observations were 1) depressed shallow isotherms near the 200 m isobath (compared to offshore) associated with the LC, 2) anomalously warm (compared to CARS 2009, which is based on limited data) surface mixed layer, and 3) raised deep isotherms farther offshore.

Gliders can only follow their planned track if the ambient flow speed is less than the glider's glide speed through the water, which is about 0.25 m/s. The glider encountered NNE flow of this magnitude on 8 October, while trying to proceed WSW. Little headway could be made so the glider's heading was altered to NW. We cannot, therefore, say if the deep uplift of the isotherms observed at the turning point (-2 °C anomaly at 700 m, as shown in Figure 5.8.1) represents the extreme of the feature. This anomaly is probably best described as a transient cyclonic eddy because of 1) its high amplitude and 2) the clockwise veering of the flow as the glider proceeded NW, but it could also be described as evidence of the FC, if we consider that to comprise a sequence of cyclonic eddies.

The second mission (April-May 2015, 51 days, 1420 km) also observed deep cold anomalies (-2 °C anomaly at 700 m, see Figure 5.8.2) but on this occasion they were mostly along the 130.7 °E transect across the Ceduna Plateau. The surface mixed layer was thinner than the climatological average, but not

colder. The shallow depressed isotherms associated with the SAC were observed on all four visits to the upper slope, especially the eastern three.

The third mission (March-May 2016, 75 days, 2639 km, Figure 5.8.3) encountered weak, generally westward flow from the launch point to the start of the 130.7 °E transect. A small but notable feature sampled on this leg was a 400 m-thick lens of anomalously warm (+1° C) and salty (+0.1 psu) water sampled on 18 March. The diameter of this anticyclonic feature was about 50 km at which point the tangential velocity was about 10 cm/s. Fluorescence was very high in the center of this eddy, but only at the base of the mixed-layer, explaining why there is no anomaly visible in MODIS imagery of chl-*a* for 16 March (the best available image).

Westward flow was seen on much of the next leg (northward along 130.7 °E), but not during the subsequent SE-ward leg when the flow changed from eastward to strongly west south-west ward midway along that leg. Satellite imagery (Figure 5.8.4) shows that that transition occurred just before a southward meander of the LC was encountered. Satellite altimetry places the centre of a large but weak cyclonic eddy between these two glider legs, explaining the general sense of the observed flow. The glider observations on the 12th April, (Figure 5.8.3) show that the interior of the eddy featured a point where the deep isotherms were raised, but shallower isotherms were depressed (see the -1.5 ° C,-0.2 psu) anomalies at 500 m-800 m, but +1.5 °C+0.2 psu anomalies for 500 m-300 m). The warm, salty waters of the LC were not encountered at depth (~100 m) at the subsequent visit to the shelf break on 20th April, consistent perhaps with upstream diversion of the LC offshore.

It is worth noting that strong coastal upwelling was occurring (Figure 5.8.4) when this third glider mission commenced. Imagery shows the upwelling had ceased by the end of the mission, after a period of strong westerly winds and eastward flow over the shelf. LC waters were encountered at depth during the last two shelf break visits on 28 April and 7 May, consistent with acceleration of that flow.

In summary, the glider missions have provided three detailed ‘snapshots’ that reveal the richness of the subsurface variability in the central GAB. More missions are needed before any general statements can be made of the deep hydrography of the GAB but it is clear; the GAB is not a region of particularly highly energetic mesoscale variability but is, as we had anticipated, a region of relatively slow, but nonetheless complex flows. Our observations are consistent with our existing understanding of the FC and the variability of the LC, while also highlighting that even the weak eddies of the GAB are strong enough to mask the presence of the FC.

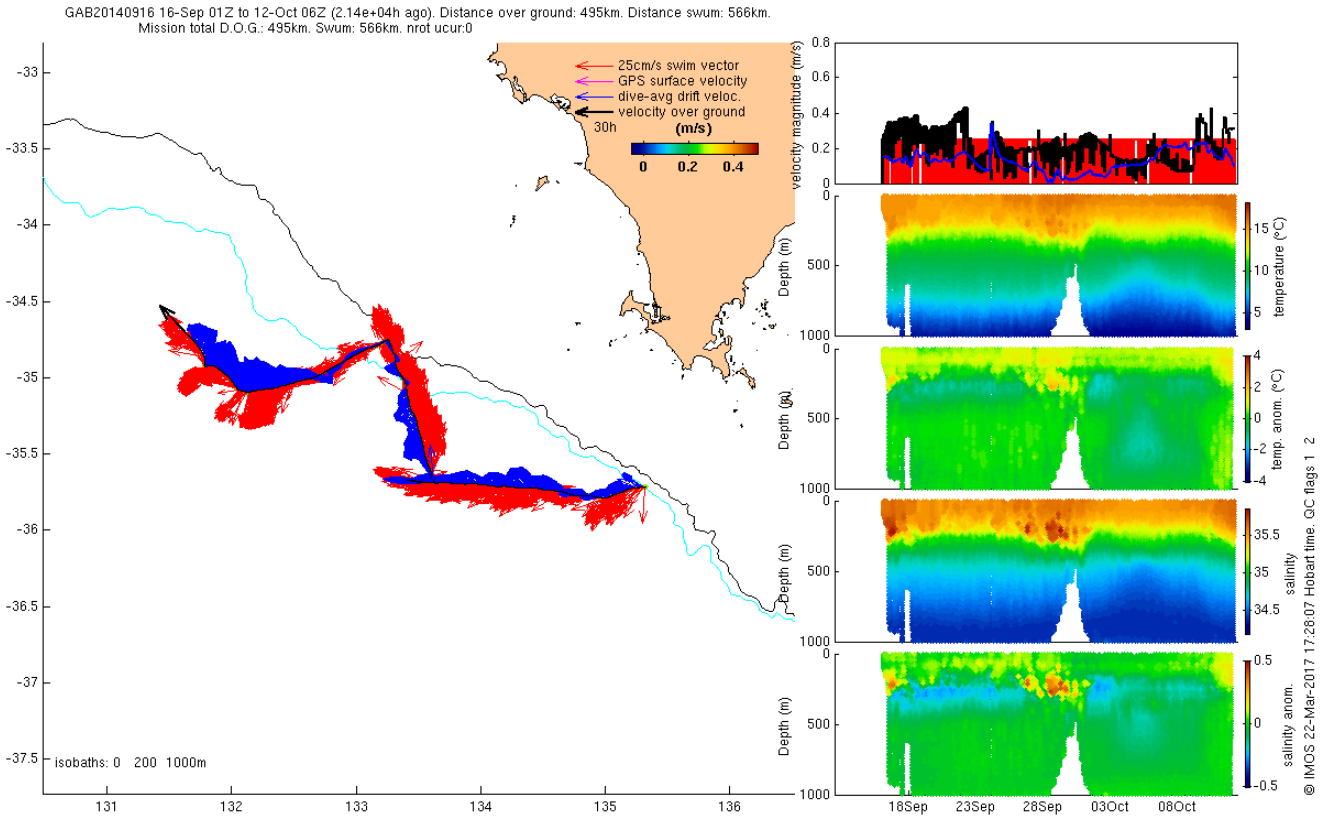

Figure 5.8.1 The first seaglider mission to the GAB. Summary of the track (left) and sensor data (right). The anomaly panels show the difference of the observations from the CARS2009 estimate for the exact day-of-year, place and depth.

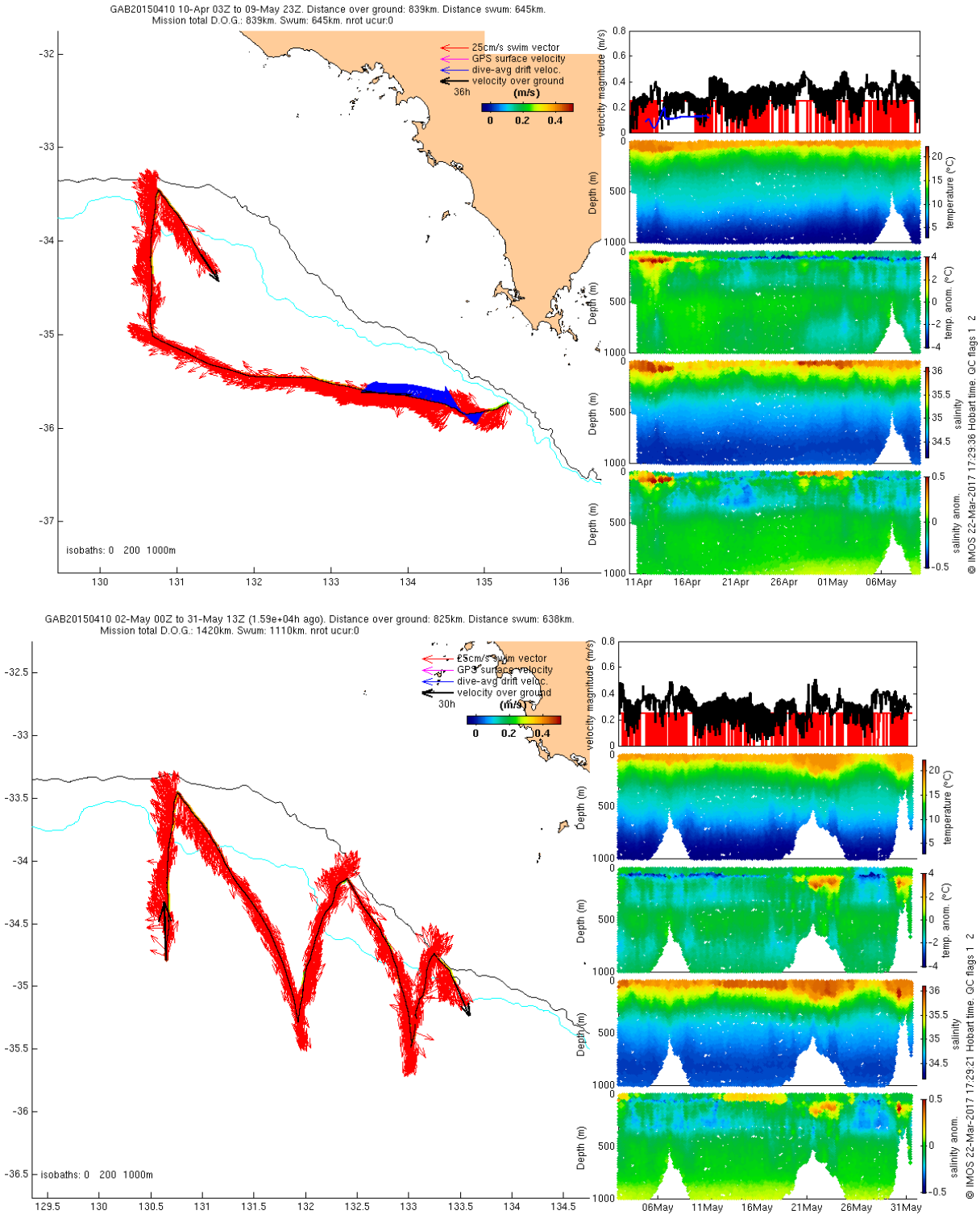

Figure 5.8.2 The second seaglider mission to the GAB. Summary of the track (left) and sensor data (right). The upper panels show the first 30 days, the lower panels show the last 30 days.

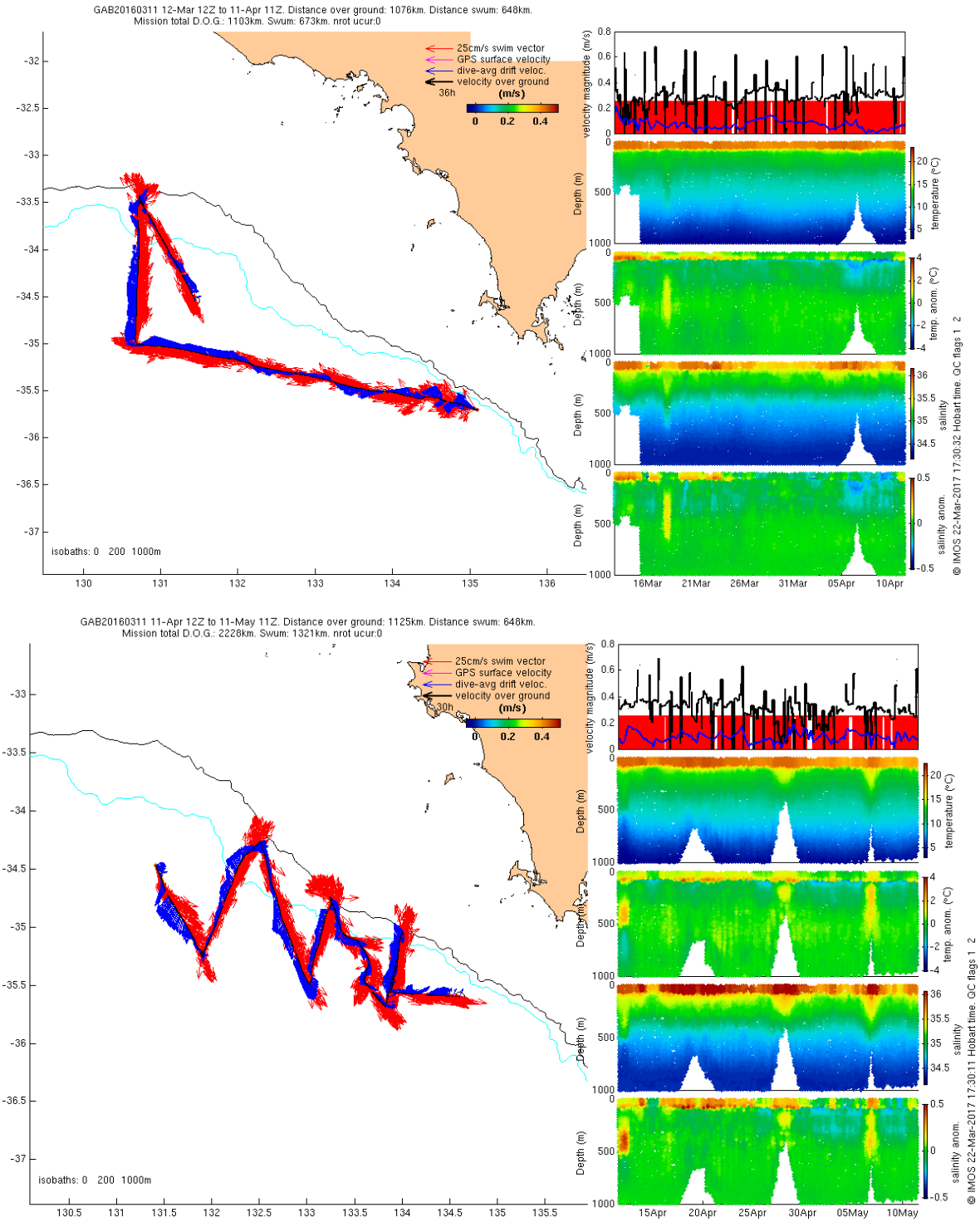

Figure 5.8.3 The third (final) seaglider mission to the GAB. Summary of the track (left) and sensor data (right). The upper panels show the first 30 days, the lower panels show the last 30 days.

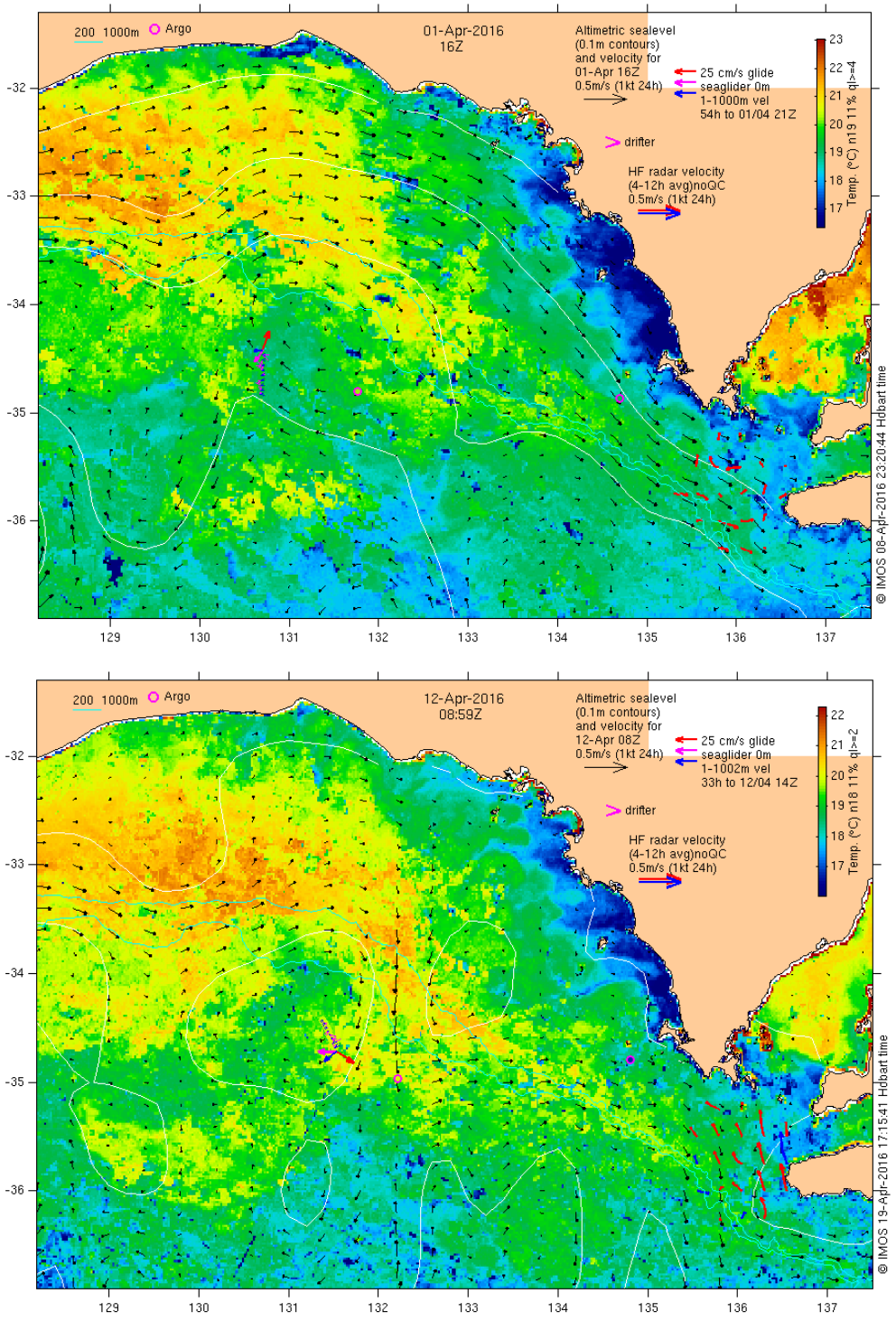

Figure 5.8.4 Satellite imagery of surface temperature and altimetric current velocity for when the glider was going northward up the 130.7°E leg (upper) and SE-ward down the next leg (lower).

6. PARTICLE TRACKING STUDIES

6.1 Summary

Particle movement over the shelf (depths < 200 m), is largely determined by the expected circulation features that include the eastward LC and SAC and surface Ekman transports driven directly by the winds.

During winter, these currents can move surface particles across the GAB and towards the coast and ultimately as far as the Bonney Coast (BC). At mid-to bottom depths offshore transport due to downwelling moves particles to the shelf edge where they are entrained into the eastward LC and SAC. Shelf particles can be entrained into Spencer Gulf by the expected two way exchange that arises due to wintertime flushing.

During summer, particles originally near the coast and GAB move little compared to winter, with longer residence times at the head of the GAB. The expected westward wind driven coastal flow is found in the GAB and off Kangaroo Island. Downwelling is found in the central GAB. Again, the SAC flow on the shelf edge is strongly directed to the east.

As noted, the model eddies are unrealistic in strength. However, the results show that shelf edge waters at depths of 100 m or more can be entrained into these eddies and deeper water. The opposite does not seem to occur in the GAB presumably since the shelf-edge downwelling found all year round “insulates” shelf waters from those at great depths. At the surface, and during winter, positively buoyant material (such as oil) from the deep ocean can reach the surface and be driven onshore by the surface Ekman transport. These simulations do not include the additional shoreward velocity experienced by buoyant material due to Stokes Drift.

Other tracking studies completed for other themes are summarised below in Section 6 under “service to other themes”.

6.2 ROMS Methodology - forward tracking in time

Patches of four particles in each of four adjacent model cells were used and the locations of all stored every 24 hours along with depths. In summary:

i. Particles will be deployed at each of the cross sections noted above and at 4 sites (patches) and 3 depths. The patch sites will be above the 50 m, 100 m, 200 m and 1400 m isobaths. The 3 initial particle depths will be the surface, bottom and mid-depth.
ii. Each patch will have 4 particles and be seeded at three 10 day intervals and all tracked for 70 days following release.
iii. For summer, the three dates of deployment (seeding) at every site (or patch) and depth noted above are 2, 12 and 22 January for each of the 4 years (2011, 2012, 2013, 2014). The particles are all tracked for 70 days following seeding (release).
iv. For winter, the three dates of deployment (seeding) at every site (or patch) and depth noted above are 2, 12 and 22 July for each of the 4 years (2011, 2012, 2013, 2014). The particles are all

tracked for 70 days following seeding (release) and so effectively cover a summer and winter season.

Due to space limitations, only results for 2013 are presented but these typify results for other years.

6.3 Results

The winter results for 2013 are presented in Figure 6.3.1 to Figure 6.3.3 where each plot respectively corresponds to the trajectories for the three cross shelf sections of particle release sites at 126.5 ^{o}E, 130.5 ^{o}E and 136 ^{o}E. Particle release sites (and trajectories) at the surface are shown in each of the upper panels and for water depths (wd) of 50 m (red), 100 m (purple), 200 m (green) and 1400 m (blue). The final particle locations after 70 days are indicated by the filled colour circles.

The middle panel plots correspond release sites and trajectories to mid water depths and again over the 50 m (red), 100 m (purple), 200 m (green) and the 1400 m isobaths (blue).

The bottom panel of each plot contains results for particle release sites and trajectories at the sea floor.

Note, all particles are neutrally buoyant and move with the horizontal and vertical velocities and sub-grid scale diffusion and generally do not remain at their initial depths. We consider first the winter results (Figure 6.3.1 to Figure 6.3.3) and then summer results (Figure 6.3.4 to Figure 6.3.6).

As noted above and in Appendix 3, while the shelf circulation is generally well modelled, the model deep water eddy fields are generally unrealistically strong so that the particle tracking results for depths greater than 200 m are at best only qualitative. Therefore, results for particles (blue) deployed at water depths of 1400 m will not be discussed. Graphical results are included as they at least give a qualitative guide of eddy impacts.

6.3.1 Winter Results

Figure 6.3.1 to Figure 6.3.3 each contain results for one of the three transects. For each transect, the top panel (surface particles) show the surface flow in water depths (wd) of 50 and 100 m (red and purple particles) to move to the east and towards the coast: both results consistent with that expected from the surface northward Ekman transport and eastward LC and SAC. Farther offshore in a wd of 200 m, the surface and mid-depth green particles (top and middle panels) display a similar eastward flow but generally more directed along-isobaths as expected for the LC. In general, the flow between the coast and 200 m isobaths moves from the far west and ultimately to the Bonney Coast.

There is evidence of downwelling and offshore sub-surface flow expected for the GAB in general. For all three transects, some mid-depth particles deployed at water depths less than 100 m (red and purple) migrate and are entrained into the deeper waters of the shelf edge LC and SAC –see Figure 6.3.1 to Figure 6.3.3; middle panels). For the far east transect at 136 ^{o} E, (Figure 6.3.3) red 50 m wd particles were deployed at the SW corner of Spencer Gulf. Some are later found in Spencer Gulf and some out on the shelf slope and in deeper waters. Those purple particles deployed on the shelf at wd's of 100 m, are subsequently found to move to wd's of 200 m or more (see Figure 6.3.3; mid and bottom panels): this movement results from the constriction in along-shelf flow off the Eyre Peninsula.

Implications for Nutrient Supplies to the central GAB. The above also shows that paths to the central GAB/shelf edge are from west to east so that nutrients needed to enrich the central GAB/shelf edge during winter would need to arise from either i) the far western GAB and/or ii) be supplied by the downwelled movement of coastal detritus where nutrients are stored in sediments.

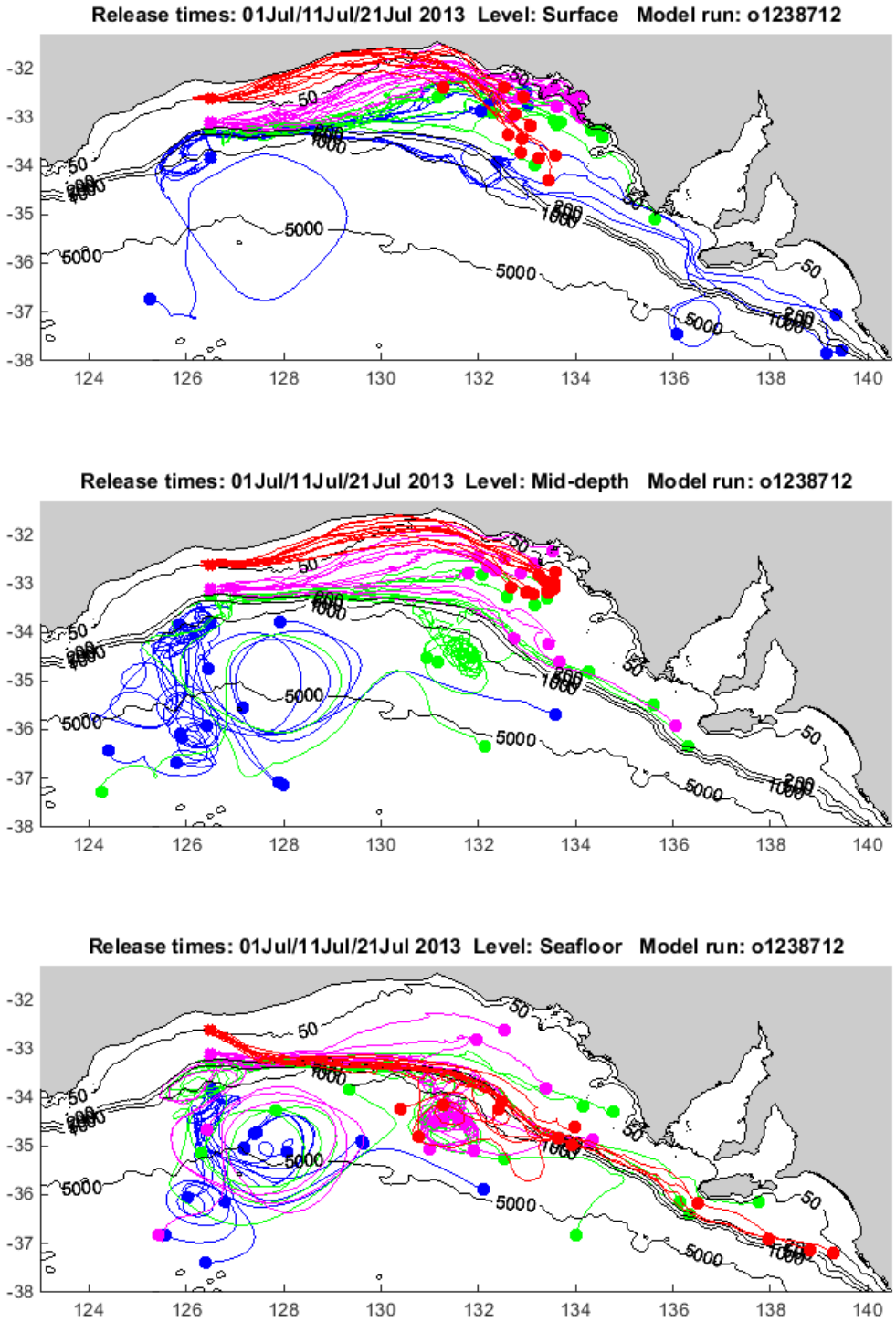

Figure 6.3.1 Plan view of float tracks for floats released at four sites along the western transect at 126.5 °E, at the surface (top panel), mid-depth (middle panel), and bottom (bottom panel), during winter 2013. The 4 sites are over the 50 m isobath in red, 100 m isobath in purple, 200 m isobath in green and 1400 m isobath in blue. Filled circles represent positions 70 days after release.

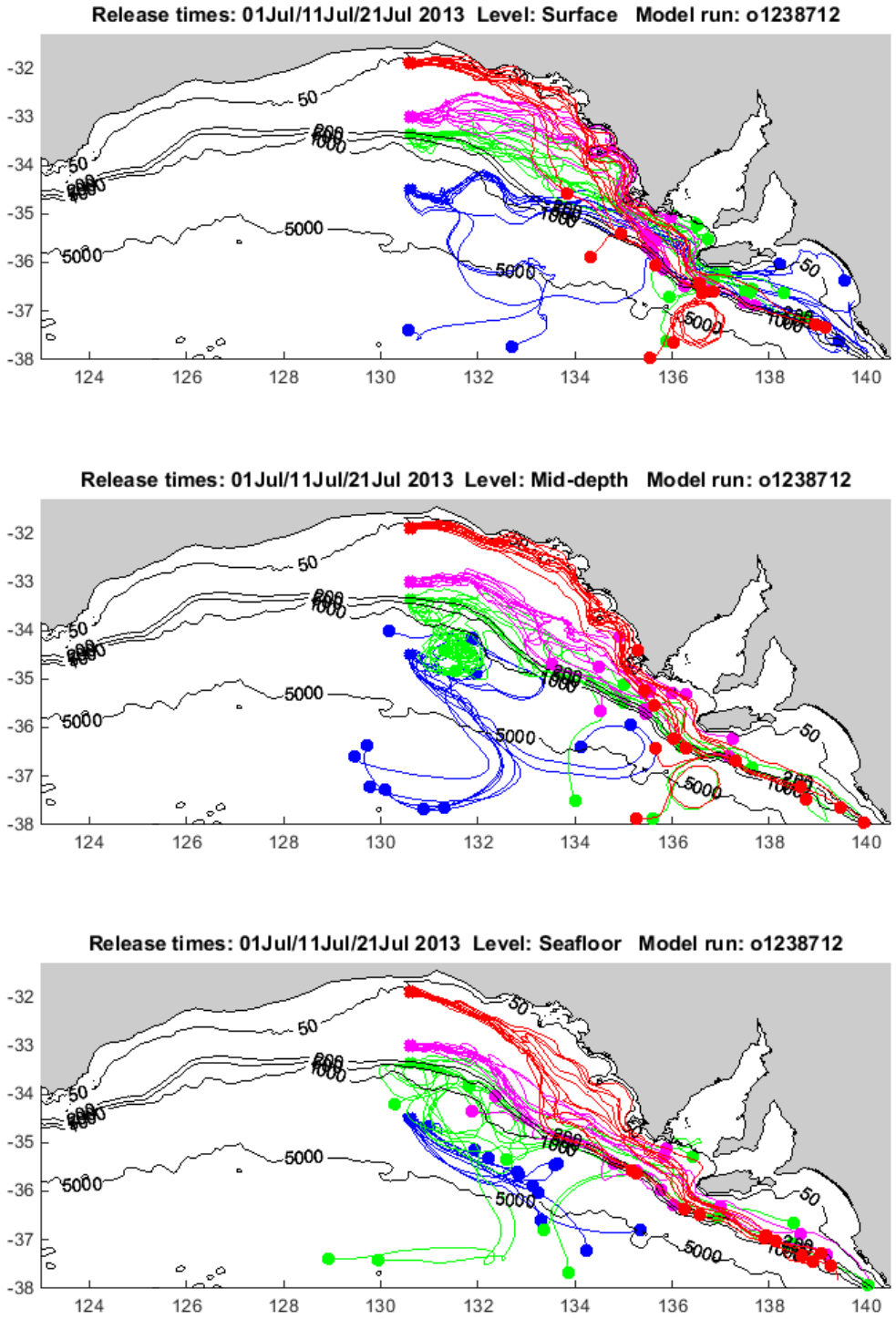

Figure 6.3.2 Plan view of float tracks for floats released at four sites along the central GAB transect at 130.5 °E, at the surface (top panel), mid-depth (middle panel), and bottom (bottom panel), during winter 2013. The 4 sites are over the 50 m isobath in red, 100 m isobath in purple, 200 m isobath in green and 1400 m isobath in blue. Filled circles represent positions 70 days after release.

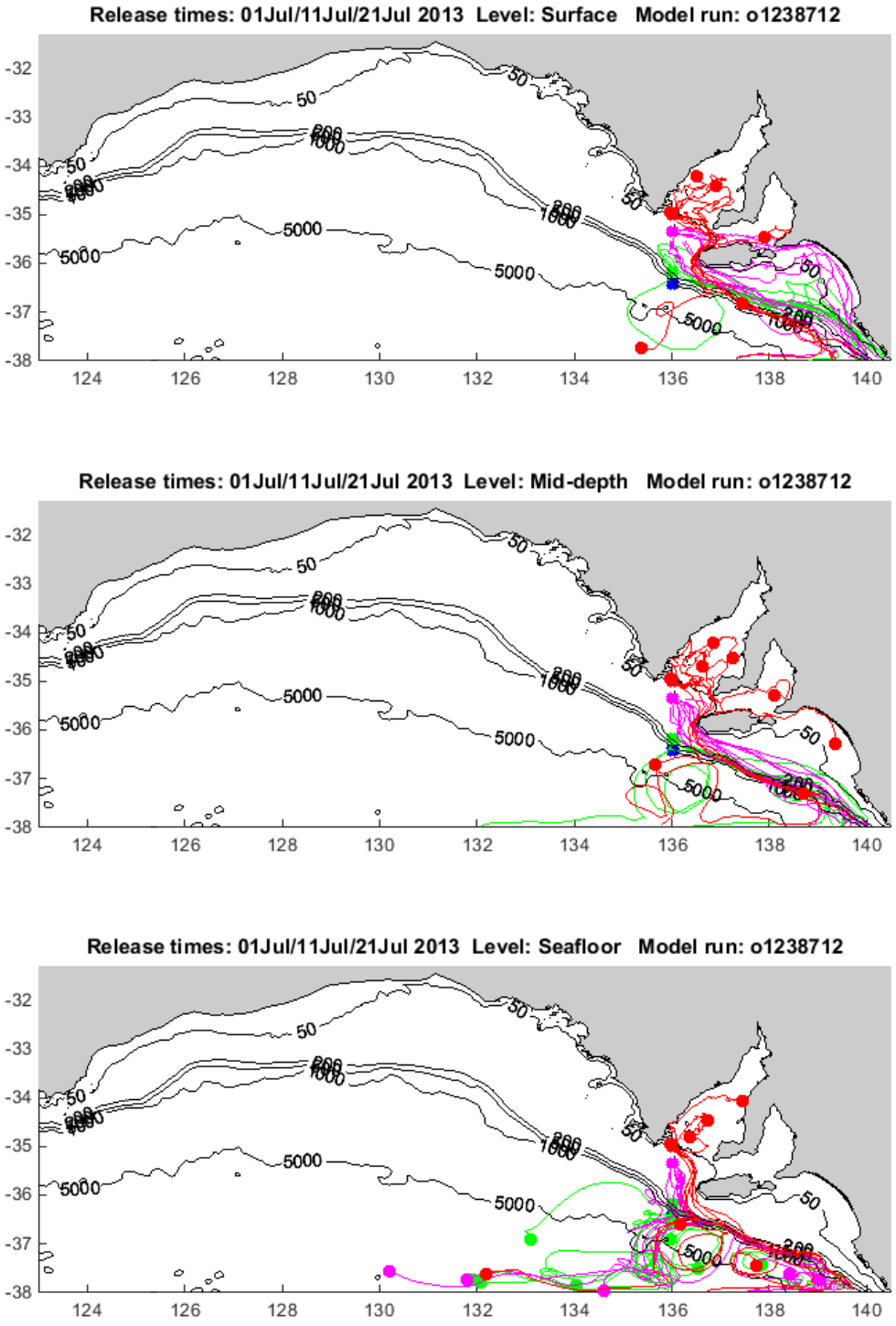

Figure 6.3.3 Plan view of float tracks for floats released at four sites along the western transect at 136 °E, at the surface (top panel), mid-depth (middle panel), and bottom (bottom panel), during winter 2013. The 4 sites are over the 50 m isobath in red, 100 m isobath in purple, 200 m isobath in green and 1400 m isobath in blue. Filled circles represent positions 70 days after release.

6.3.2 Summer Results

Figure 6.3.4 to Figure 6.3.6 contain the results for the three summer 2013 transects with notations as outlined above for winter. For all three transects, particles deployed at the surface in general exhibit an offshore flow consistent with the offshore surface Ekman transport.

For the 126.5 ^{o}E transect, the surface and mid-depth shelf and shelf break flow (red, purple and green move little compared with that during winter (Figure 6.3.4). A chaotic spread of particles is found farther east and may be the result of time-varying east and west-ward winds due to the passage of cold fronts and high pressure systems. In the case of the initial mid-depth flow at 100 m (green) there is a strong drift to the east following the SAC (Figure 6.3.4; middle panel).

Mid-depth and bottom particles deployed over the 50 m, (red) , 100 m (purple) and 200 m (green) isobaths at the bottom move to the east and then south into greater depths consistent with the central GAB summer downwelling expected (see above).

For the central GAB transect at 130.5 ^{o}E (Figure 6.3.5), the red particles nearest the coast (50 m initial wd) move to the west as expected for the wind driven flow and also, at the bottom, towards the coast - results consistent with bottom Ekman upwelling. Farther offshore, both the purple and green particles (initial wd 100 m and 200 m) move to the east again consistent with the flow of the SAC: the mid-depth (100 m) green particles are found as far as the BC over the 70 days of trajectory calculation.

For the far eastern transect at 136 ^{o}E, the surface deployed particles present a chaotic display (Figure 6.3.6) with red and purple particles moving into the Spencer Gulf and offshore, respectively. At the mid-depth (25 m and 50 m) the red and purple particles display a north-westward flow, expected for upwelling wind-driven currents, and an opposite south-eastward flow expected for wintertime winds. At depth of 100 m, the mid-depth green particles move to the south-east and again opposite to that expected for summer. At the bottom depth, the green particles cluster around the southern waters south of Kangaroo Island, while again the red and purple trajectories at the bottom are similar to those at mid-depth. In summary only the very near-shore trajectories for initial water depth of less than 50 m generally move to the north west in accordance with the expected upwelling favourable winds. Farther offshore, currents are in the opposite direction and generally to the south-east and consistent with a strong and extensive SAC.

Implications for Nutrient Supplies to the central GAB. The results also do not show any direct connection of possibly nutrient rich waters of the eastern GAB, Kangaroo Island and BC regions with the mid GAB.

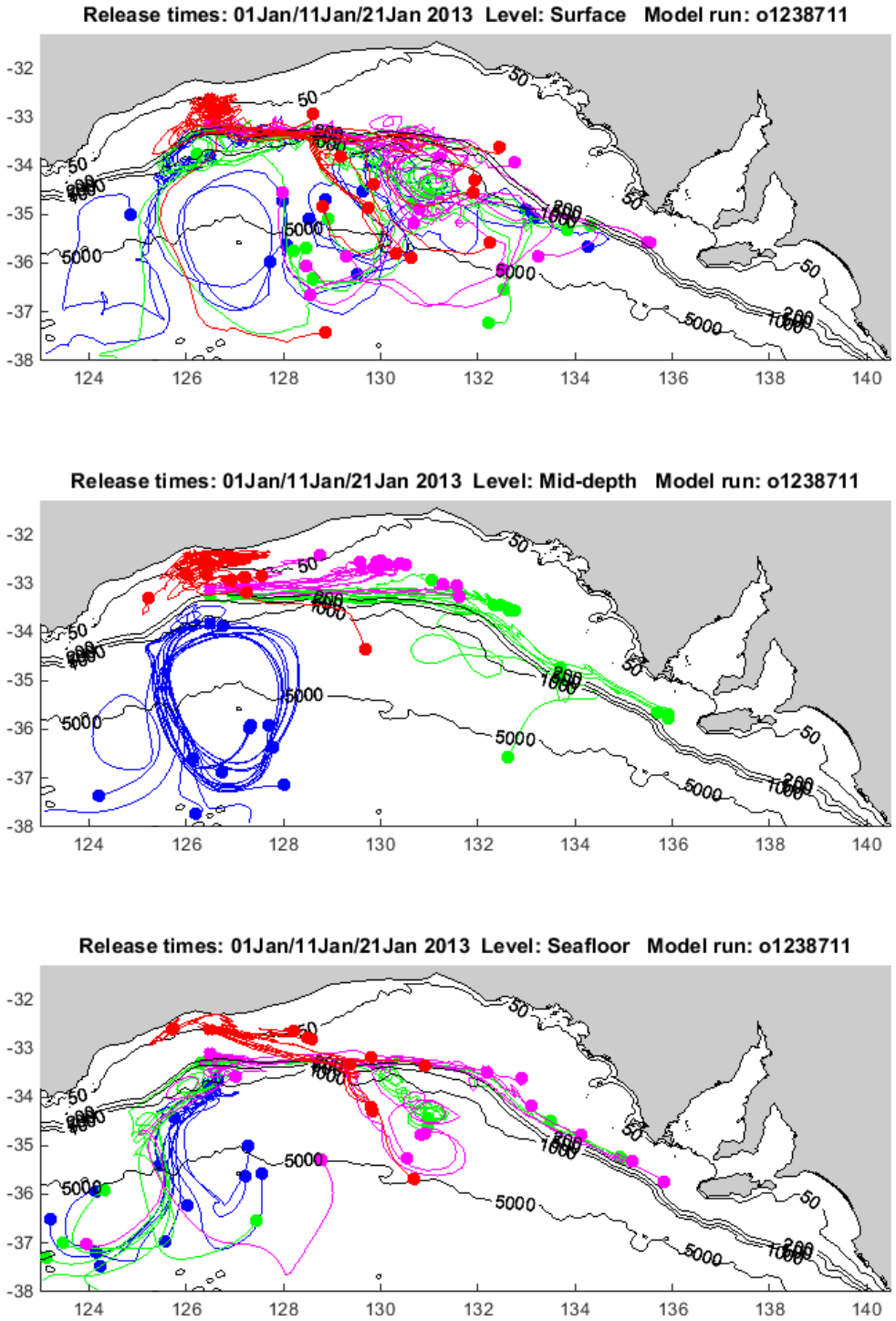

Figure 6.3.4 Plan view of float tracks for floats released at four sites along the western transect at 126.5 °E, at the surface (top panel), mid-depth (middle panel), and bottom (bottom panel), during summer 2013. The 4 sites are over the 50 m isobath in red, 100 m isobath in purple, 200 m isobath in green and 1400 m isobath in blue. Filled circles represent positions 70 days after release.

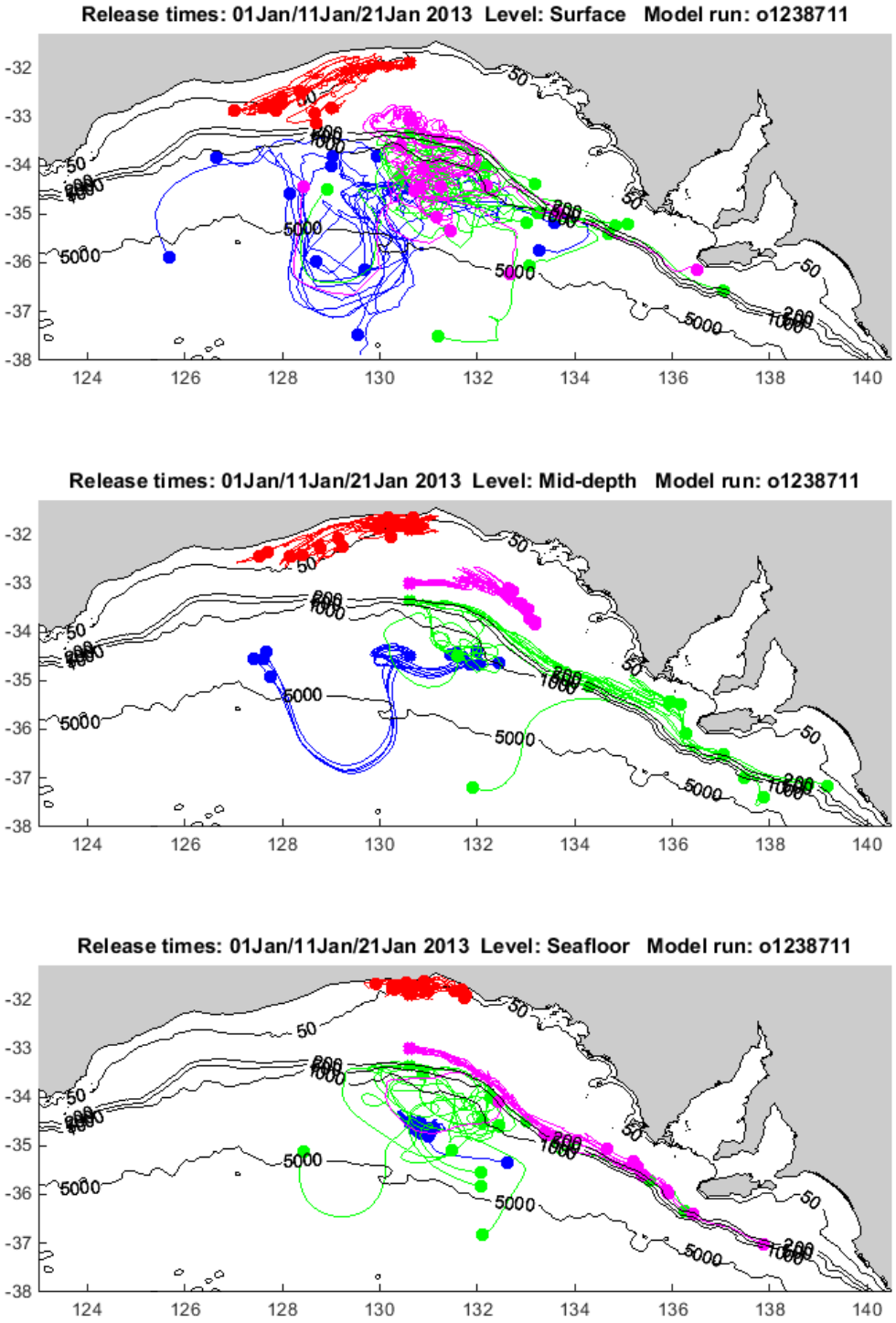

Figure 6.3.5 Plan view of float tracks for floats released at four sites along the central GAB transect at 130.5 °E, at the surface (top panel), mid-depth (middle panel), and bottom (bottom panel), during summer 2013. The 4 sites are over the 50 m isobath in red, 100 m isobath in purple, 200 m isobath in green and 1400 m isobath in blue. Filled circles represent positions 70 days after release.

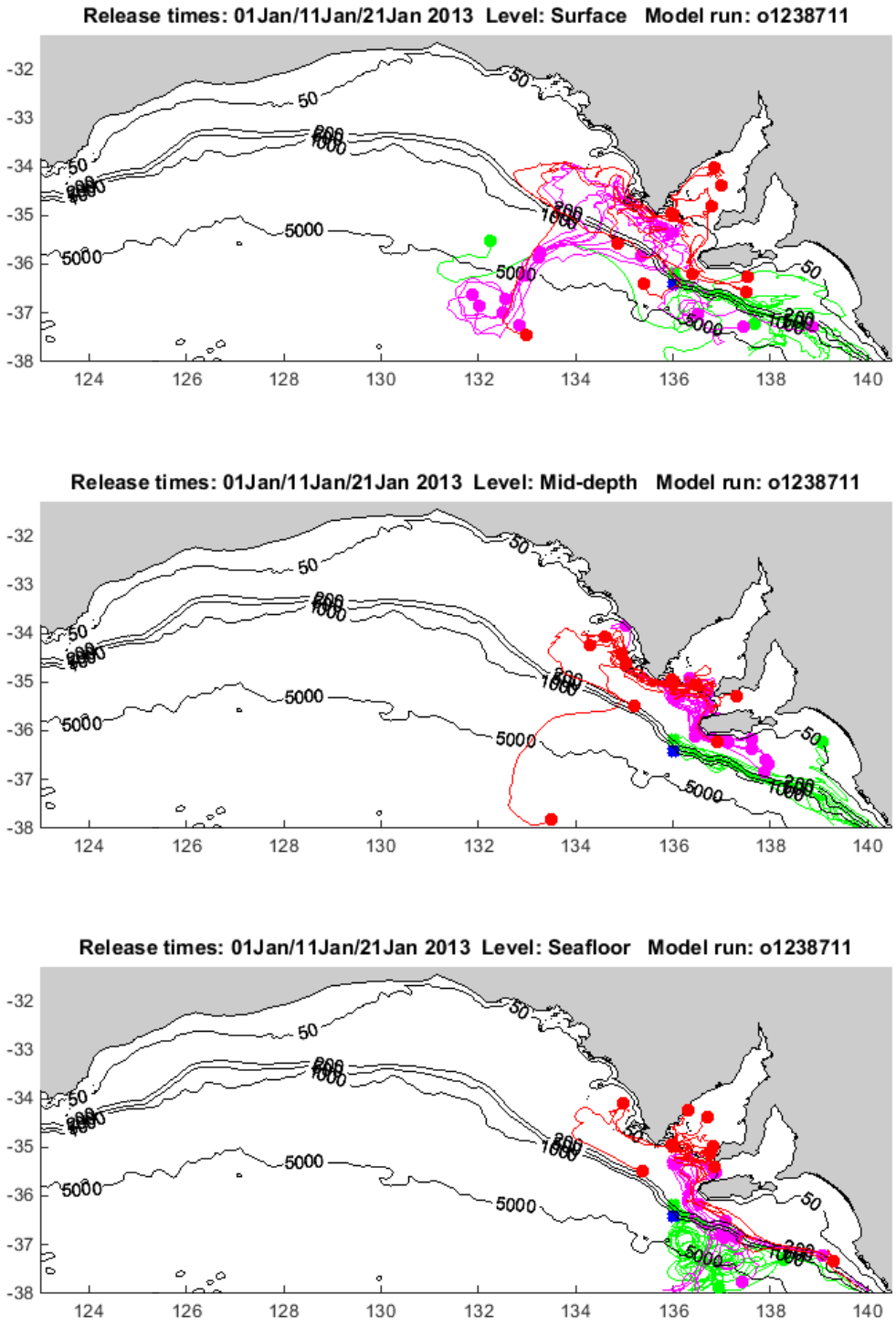

Figure 6.3.6 Plan view of float tracks for floats released at four sites along the eastern transect at 136.0 °E, at the surface (top panel), mid-depth (middle panel), and bottom (bottom panel), during summer 2013. The 4 sites are over the 50 m isobath in red, 100 m isobath in purple, 200 m isobath in green and 1400 m isobath in blue. Filled circles represent positions 70 days after release.

7. THE BRAN2016 23-YEAR PERSPECTIVE

The 2016 version of the Bluelink Re-ANalysis (BRAN2016) became available at the end of 2016, too late to be used as an input to the ROMS and SHOC modelling (which used BRAN2015), but not too late to be used as a third estimate of the physical state of the GAB.

While BRAN2015 spanned just 6 complete years (2010-2015), BRAN2016 spans 23 years (1994-2016), which is long enough for deriving robust estimates of the long-term mean, inter-annual variability and seasonal cycle, without any of these being aliased significantly by any individual event, such as a long-lived eddy.

BRAN is a global analysis. Being global, it is necessarily fairly coarse in its horizontal (0.1° for latitude and longitude) and temporal resolution (output files are daily averages). On the plus side, the very difficult problem of nesting is completely avoided; so there are no open boundaries along which spurious flows can be generated. Being an 'analysis' rather than a 'free-running' model, satellite observations inform the model as it steps forward, constraining it to resemble the true history of the ocean state over the 23-year period of the integration.

7.1 Model overview and fit to observations

Comprehensive details of the configuration and performance of BRAN2015 and BRAN2016 are not yet published, but see Oke et al.,., (2013a,b) for discussion of the previous version.

BRAN2015 and BRAN2016 both assimilate observations of SST from AVHRR and microwave sensors, satellite sea-level anomaly (SLA) from all available satellite altimeters, *in situ* temperature and salinity profiles from Argo floats, XBT, and ship-borne CTDs. Observations are assimilated sequentially, every three days, resulting in a realistic three-dimensional simulation of the ocean circulation that is constrained to (nearly) match the relatively sparse assimilated observations while also preserving the laws of geophysical fluid dynamics as much as possible. In practice, these two objectives trade off against each other but with each new version of BRAN progress towards both objectives has been made. The hydrodynamic model at the core of BRAN is the Ocean Forecasting Australia Model (OFAM), which is forced with reanalysed fields of wind stress, heat flux and precipitation minus evaporation. OFAM is not, however, forced by either tides or atmospheric pressure. So the sea level fields of BRAN are what we usually call the 'adjusted' sea level (with which geostrophic currents are in approximate balance).

Comparison of the two panels of Figure 7.1.1 shows that BRAN does not have any of the spurious eddy variability that both ROMS and SHOC exhibit in the deep ocean – the root-mean square (r.m.s.) sea level anomaly (SLA) of BRAN is very similar to that of the (gridded) altimeter SLA, with both data sets showing only a few cm of sea level variability off the continental shelf. This is hardly surprising, because the altimeter data are assimilated into BRAN, as discussed above. Tide gauge data are not assimilated, so the agreement of the r.m.s. variability along the shoreline is independent validation that the hydro-dynamical model at the core of BRAN correctly simulates the ocean's response over the shelf to wind forcing. The difference in the across-shelf structure of the variability reflects the fact that the IMOS Ocean Current gridded sea level anomaly (GSLA) product is a simple statistical mapping of two types of

sea level data; altimetry in the deep ocean and tide gauges at a few locations along the coast, but nothing over the shelf in between. The absence of tide gauges within the South Australian gulfs for example, leads to the unlikely result that the shelf signals do not propagate into the gulfs. The mapping is also blind to the existence of Kangaroo Island. Here, the BRAN sea level field is much more realistic than the simple statistical mapping, with the sea level variability skirting around Kangaroo Island, as it must do so that geostrophic flows respect the existence of land.

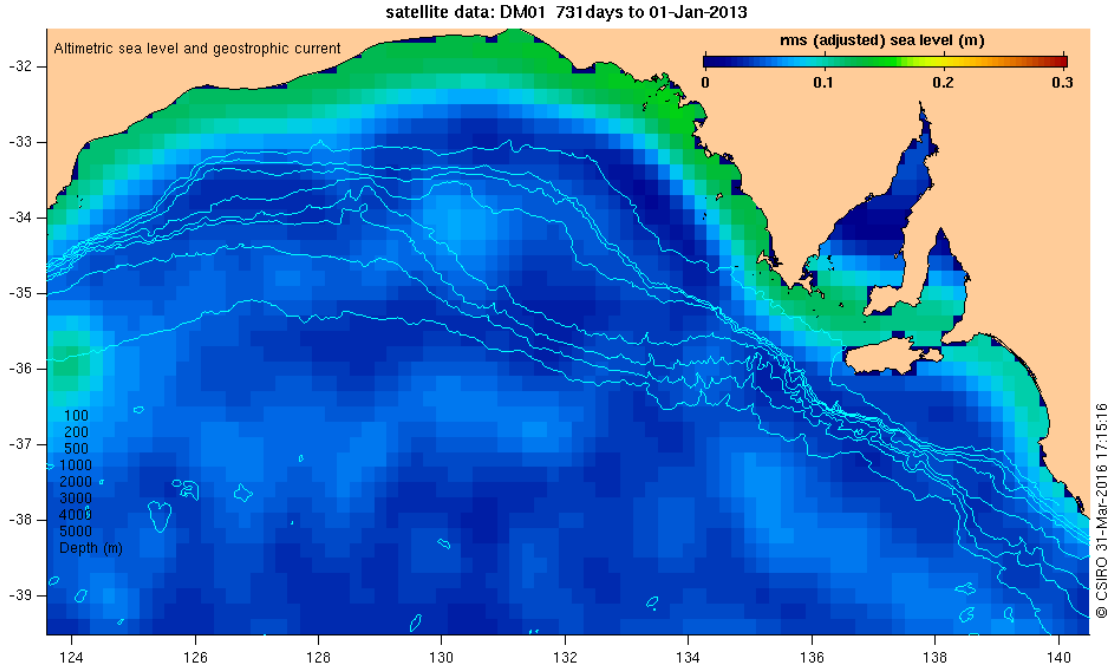

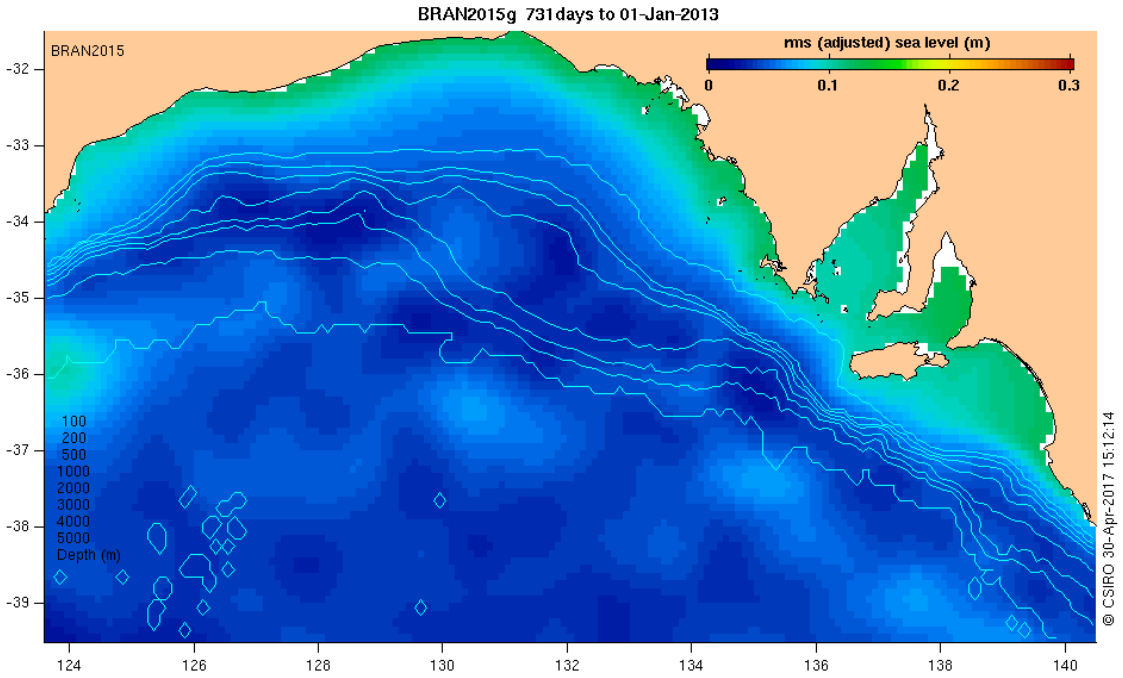

Figure 7.1.1 Root-mean-square (adjusted) Sea Level Anomaly according to gridded altimetry (upper) and BRAN2015 (lower). The analysis period for this comparison is 2 years of daily estimates in both cases. BRAN2016 (not shown) is the same.

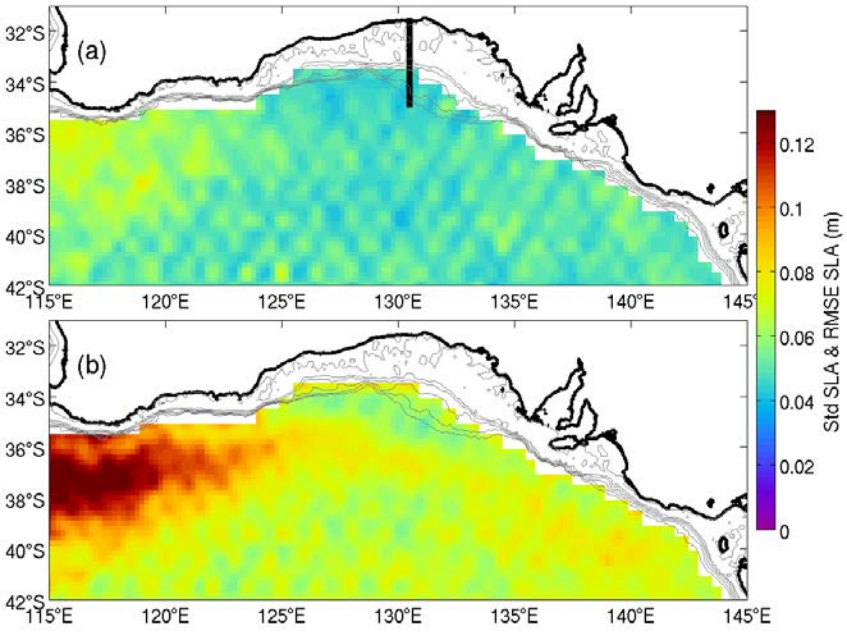

Figure 7.1.2: (a) RMS of the difference between BRAN2016 SLA and satellite altimeter along-track SLA, and (b) the standard deviation of along-track SLA observations – computed between 1994 and 2015. Contours of the model topography are also shown for context (showing the 50, 200, 500, 1000, 1500, and 2000 m isobaths). The bold line in panel (a) shows the section for which fields are presented in the analysis below.

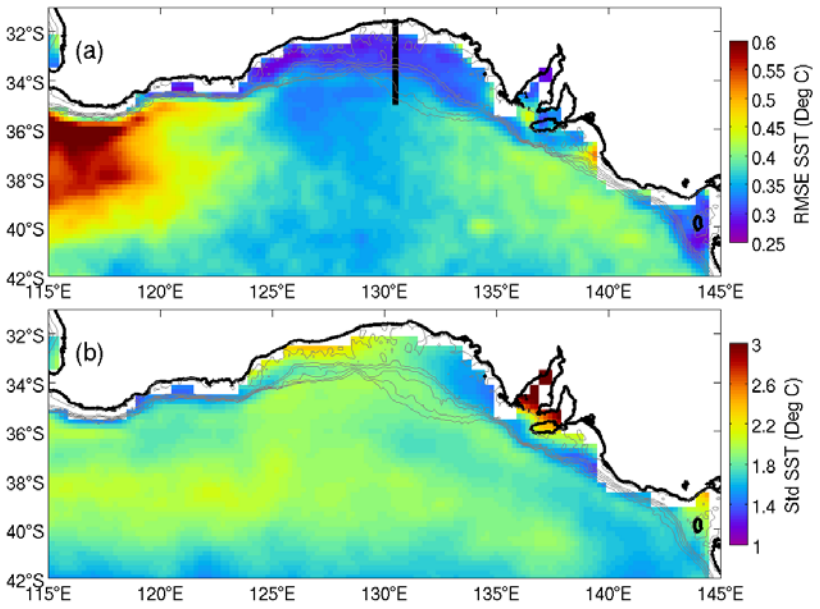

Figure 7.1.3: As for Figure 7.1.2, except for SST – comparing BRAN2016 SST and satellite SST (using data from AVHRR and microwave sensors). Note that a different colour range is used for each panel, and the colour bar minima don't start at zero.

The misfit of BRAN2016 to the along-track altimeter SLA observations (Figure 7.1.2) has a r.m.s. value ranging from 8 cm in the west where the r.m.s. of the SLA is about 15 cm, to about 5 cm in the central GAB where the r.m.s. of observed SLA is about 8 cm. Some of this misfit is due to high frequency variability at sub-daily timescale that is incompletely removed from the altimetry data during the process of accounting for atmospheric pressure effects. Altimeter range noise, orbit errors and wet-troposphere path delay errors account for another substantial fraction, leaving just a couple of cm of residual error. Thus, we conclude that while BRAN appears to be an accurate representation of sea level variability in the GAB in terms of energy level, it is also moderately accurate (with errors less than, but comparable to the signal) on a pointwise, day-for-day matchup basis, which is a more challenging task.

The re-analysed SST fields in BRAN2016 (Figure 7.1.3) are in closer agreement with the observations (compared to sea level), with model-data misfits ranging from 0.3° to 0.6° - the greater value being mainly in the far west as it is with sea level. The standard deviation of the observations is near 2° across much of the domain – much more than the model-data misfit, so it is fair to say that the model is a fairly accurate representation of surface temperature.

Compared to sea level and temperature, it is usually more difficult to accurately hind-cast point measurements of current velocity, but it appears that BRAN is also able to do this, at least for cases when relatively strong eddies occur that are well resolved by satellite altimeter observations of sea level. Figure 7.1.4 shows that the relatively strong southward flow at BPM2 in November 2011 was due to a cold-core (cyclonic) eddy just west of it.

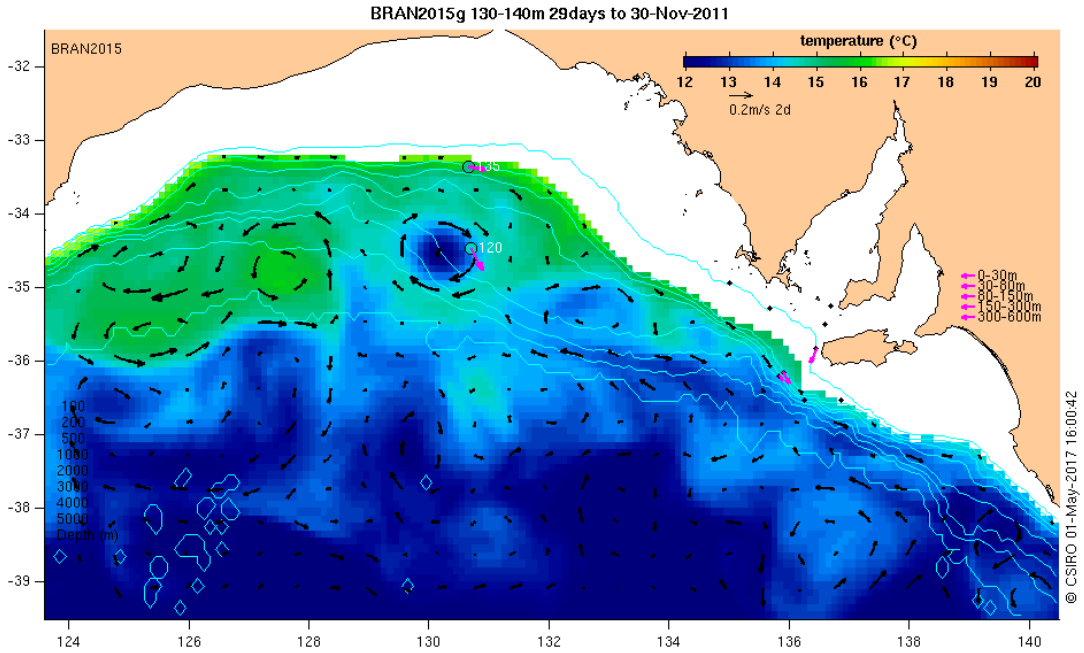

Figure 7.1.4 November 2011 mean velocity and temperature at about 130m (upper panel - this is the depth of the uppermost current meters deployed by BP). The 6-month means of BP's individual meter deployments are indicated, as are the depths of those instruments. IMOS ADCP long term means (depth-averaged appropriately) are also shown. To see the following months, click through from the [on-line copy of this Figure].

7.2 Long-term mean circulation

Averaged over several years, the LC appears in BRAN as a narrow jet along the upper portion of the continental slope, between the 1000 m and 200 m isobaths, with speeds at the surface varying along its path from 3 cm/s to half that in places (Figure 7.2.1). Inshore of the LC, the long-term mean surface velocity is weak and variable. Far offshore of the LC, outside the 5000 m isobath, the mean surface velocity is towards the ENE. In the intermediate (deep slope) region, the influence of the FC is seen with flow tending more to the west. This is also seen at 130 m (Figure 7.2.2 upper), where we also see the downwelled (anomalously warm for depth) waters of the LC. The FC is very clear at 550 m (Figure 7.2.2 lower), where it appears as a broad, slow (about 6 cm/s) flow to the west over the deep slope, skirting seaward of the Ceduna Plateau, thus avoiding the BPM2 mooring.

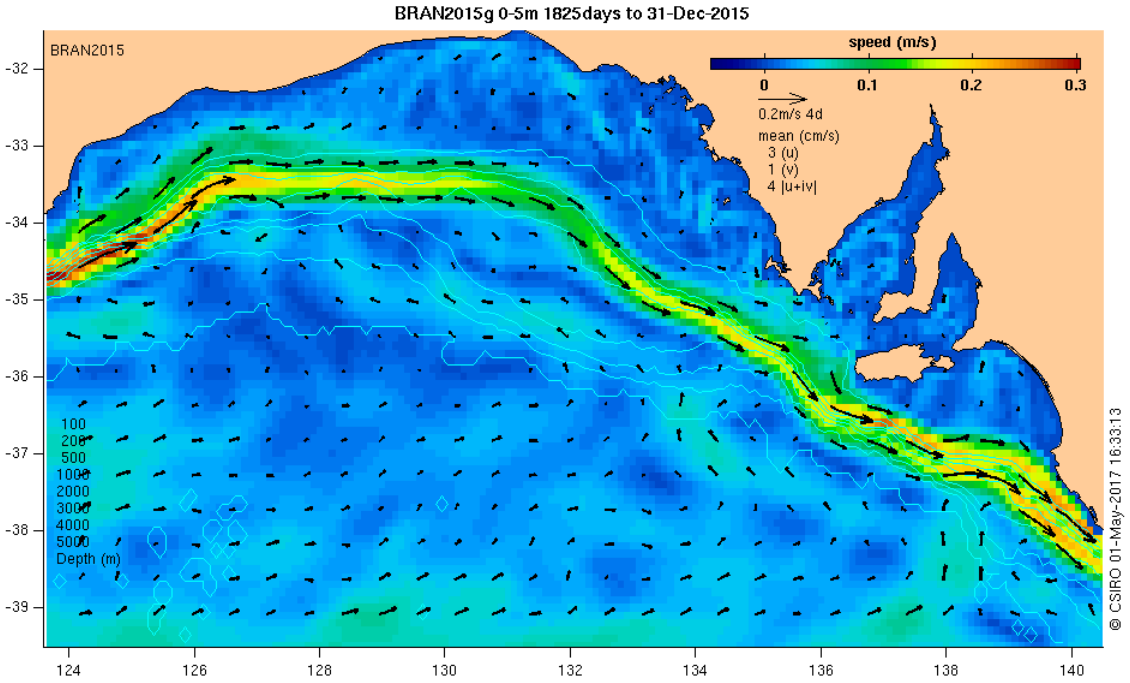

Figure 7.2.1 Near-surface, long-term mean velocity according to BRAN2015. Isobaths are as listed.

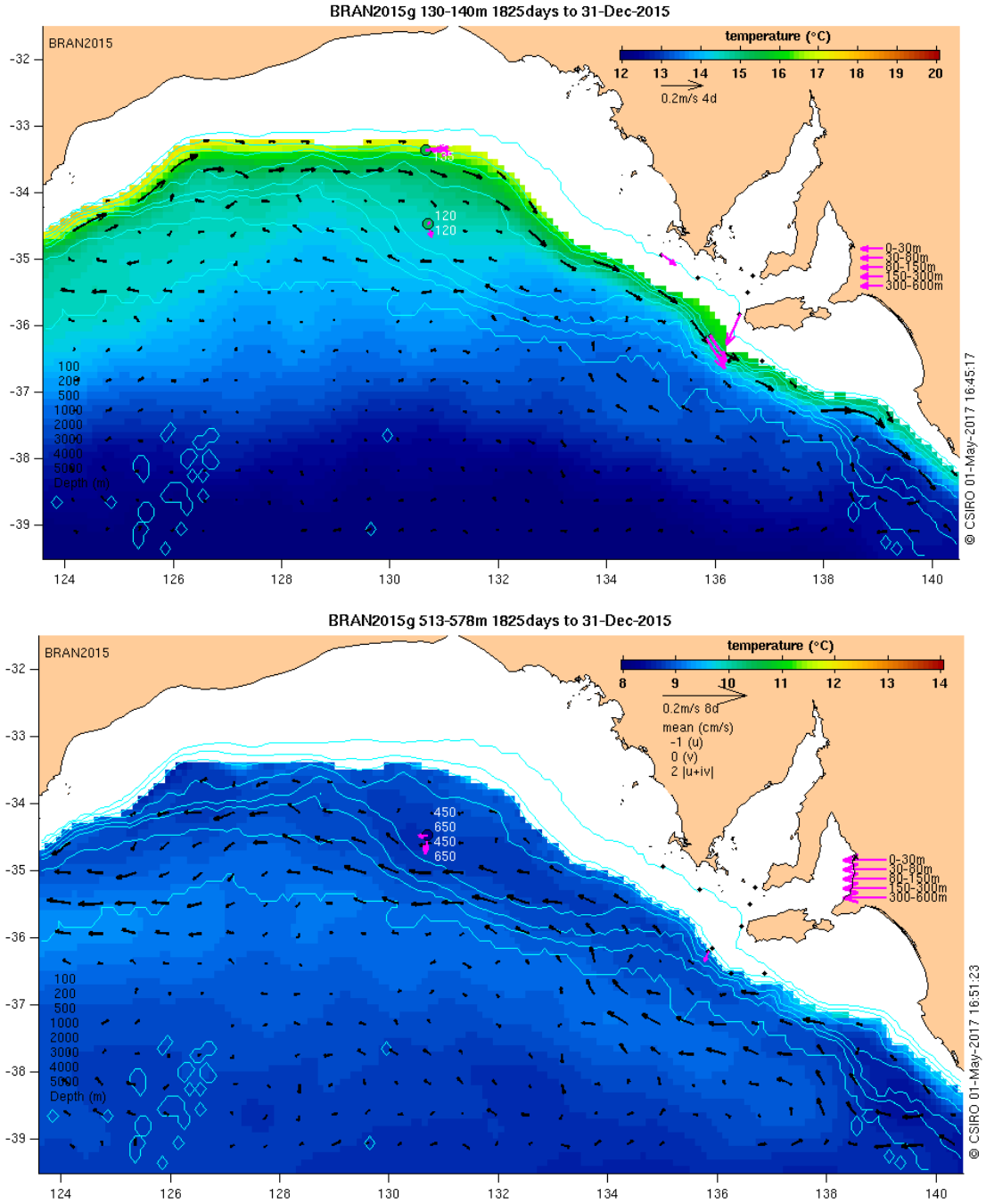

Figure 7.2.2 Long-term mean velocity and temperature at about 130m (upper panel - this is the depth of the uppermost current meters deployed by BP) and 550m (lower panel). The 6-month means of BP's individual meter deployments are indicated, as are the depths of those instruments. IMOS ADCP long term mean velocities (depth-averaged appropriately) are also shown.

The upwelled state of the deep waters associated with the FC, and downwelled state of the shallow waters associated with the LC, along with the alongshore (zonal) velocity that balances these in the long term are both evident in Figure 7.2.3. The long-term average vertical velocities (Figure 7.2.4) are close to zero.

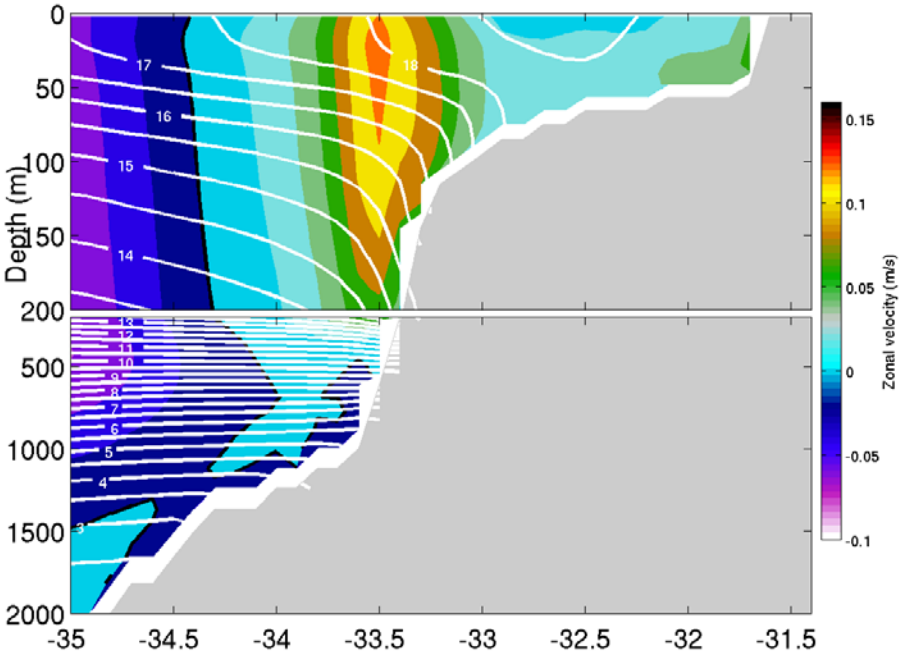

Figure 7.2.3 23-year mean zonal velocity (colour) and potential temperature (white - contour interval is 0.5ºC), from BRAN2016, at 130.5ºE.

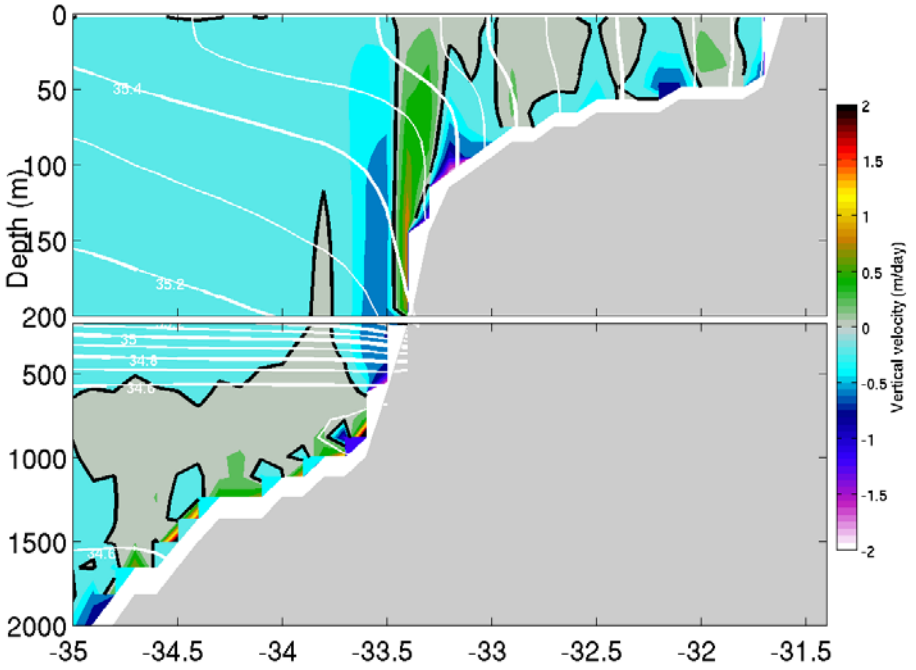

Figure 7.2.4 23-year mean vertical velocity (colour) and salinity (white - contour interval is 0.1 psu), from BRAN2016, at 130.5ºE. Note that the units of vertical velocity (positive is upward) are meters per day.

7.3 Annual and inter-annual variability of the Leeuwin Current

Of the 4 seasons, the surface speed of the LC is highest in the March-May (autumn) quarter (Figure 7.3.1 and Figure 7.3.2), according to BRAN.

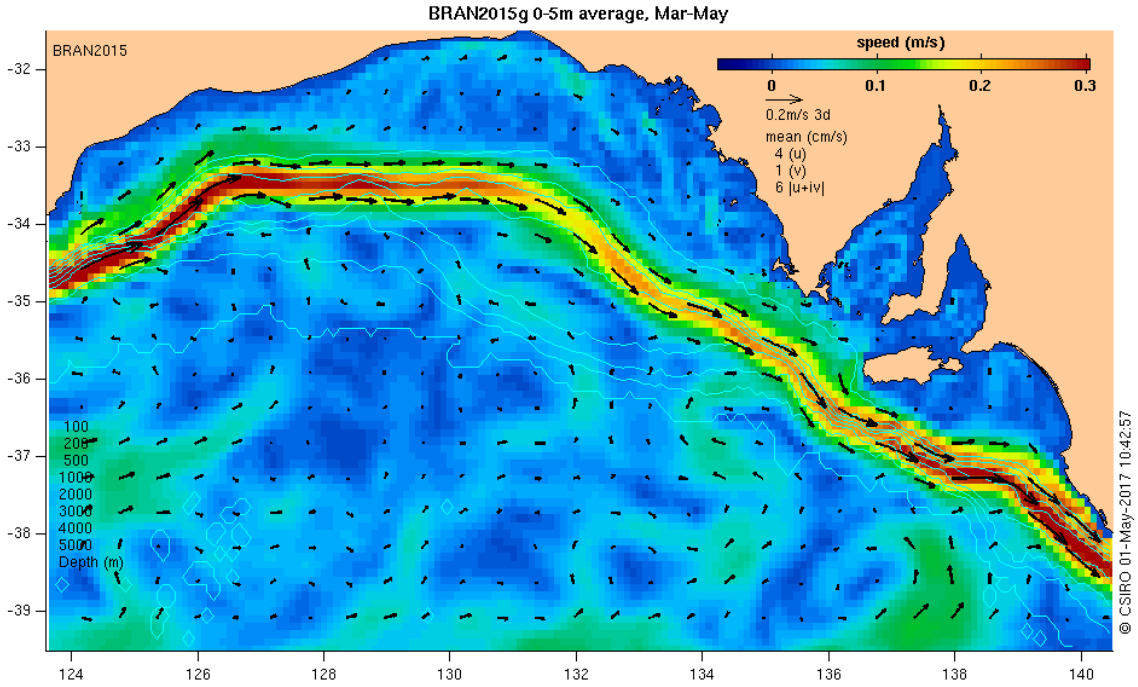

Figure 7.3.1 Five-year (autumn) mean near-surface, velocity according to BRAN. Other seasons are available [online].

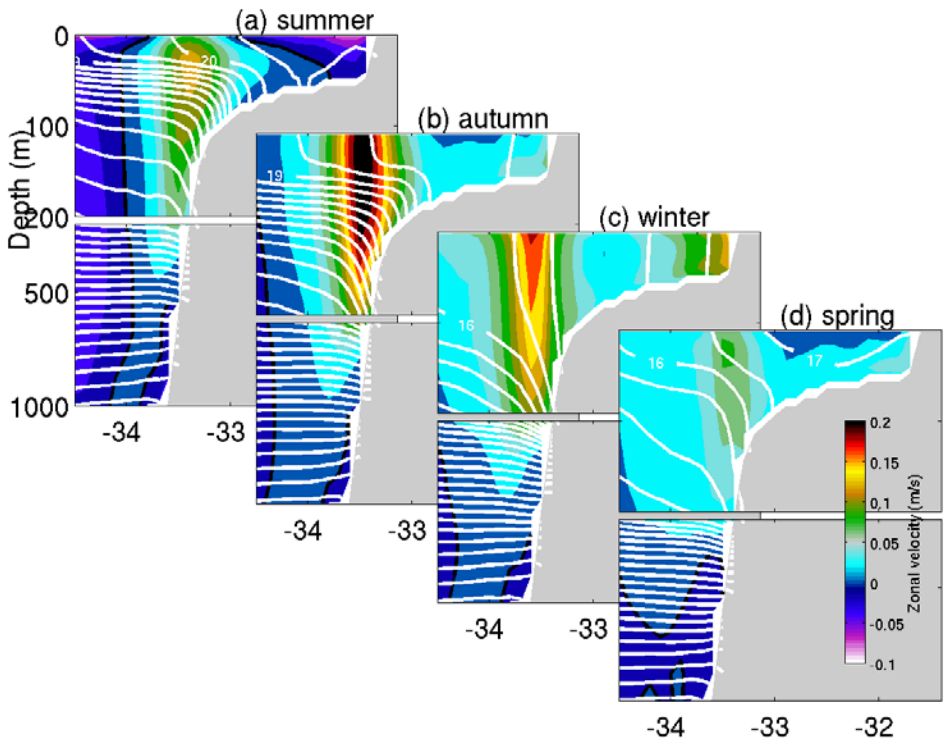

Figure 7.3.2 23-year seasonal-mean velocity and potential temperature (white contours) at 130.5°E. The zero isotach is in black.

Statistics of velocity, or integrated transport through a fixed area are easy to calculate but estimates of the volume transport of a boundary current depend a little on the exact methodology used. We have quantified the eastward volume transport of the LC by manually identifying the current's southward edge in monthly mean fields from BRAN2016. The resulting time-series of LC transport is shown in Figure 7.3.3, along with a cross-section showing the percentage of time that the LC was present at each grid point (see the inset). The time-mean (eastward) volume transport of the LC in BRAN2016 at 130.5°E is 3.1 Sv (plus/minus 0.24 Sv; *1 Sv is 10^6 m^3/s*. Feng et al.,(2003) report that the mean (southward) transport of the LC off Perth is 3 Sv at 32°S. The LC has a strong seasonal cycle, with a minimum (2 Sv) in early summer (November-January) and a maximum (5.5 Sv) in autumn (May). In some years, the transport exceeds 8 Sv, or drops to near zero (as it did in 2015). Figure 7.3.3 and Figure 7.3.4 indicate that 2012 (when the BP moorings were in place) was a typical year in terms of LC volume transport, while December 2015 (during the Investigator voyage) was highly atypical. These anomalies are discussed in Section 7.4.

Time-series of the LC SST and SST anomaly are shown in Figure 7.3.5. The seasonal cycle in temperature is clear, and more regular than that of LC transport. It is in phase with the seasons (warmest in summer) rather than the LC transport. The strong flow of the LC in May must therefore act to reduce the amplitude of the annual cycle of SST.

Another indicator of the shelf-circulation off southern Australia is the coastal sea-level, which is shown in Figure 7.3.6. A distinct seasonal cycle in this quantity is also clearly evident, lying between SST and LC transport in terms of the percentage of variability accounted for. Sea level is highest at the time of

maximum LC transport, not the time of highest temperature. Pearce and Phillips (1988) argued that sea level anomaly was an indicator of the strength of the LC, and strongest during La Nina events (when sea level was high). This correlation can be seen to also hold in the GAB to a degree: the high sea levels of 1996, 2011 and 2013 accompany strong LC transport, while the low sea level of 2015 (an El Nino year, see Figure 7.3.7) accompanies a weak LC.

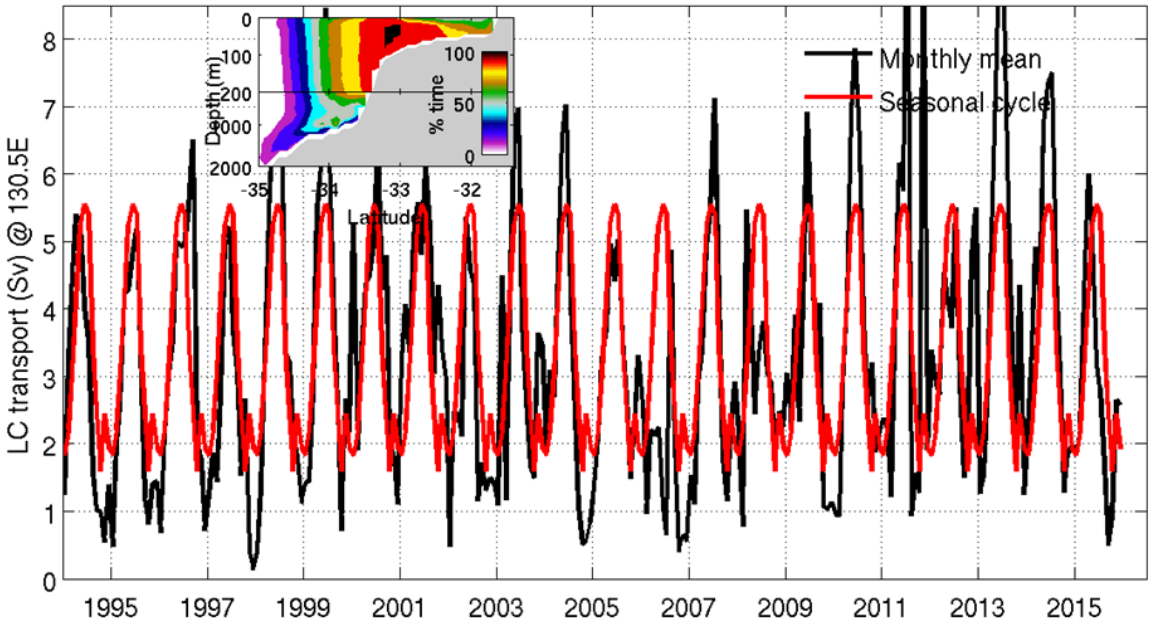

Figure 7.3.3 Time-series of the eastward transport of the LC at 130.5°E in BRAN2016. The black line shows estimates from monthly means, and the red line shows the mean seasonal cycle (based on 22 years of data, 1994-2015 inclusive). The inset shows the percentage of time that the LC was present at each grid point (100% means the LC was always present at that grid point; 50% means that the LC was present at that grid point 50% of the time, etc).

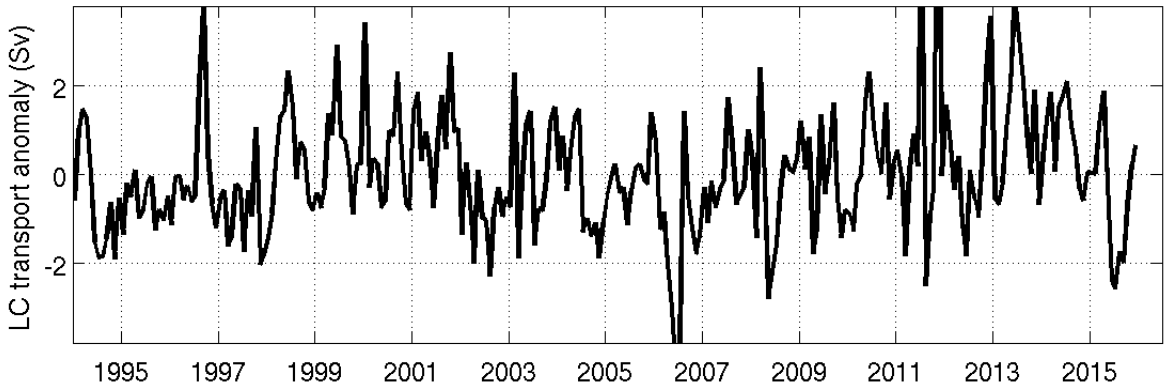

Figure 7.3.4 Times-series of the LC transport anomaly (i.e., difference from the seasonal cycle).

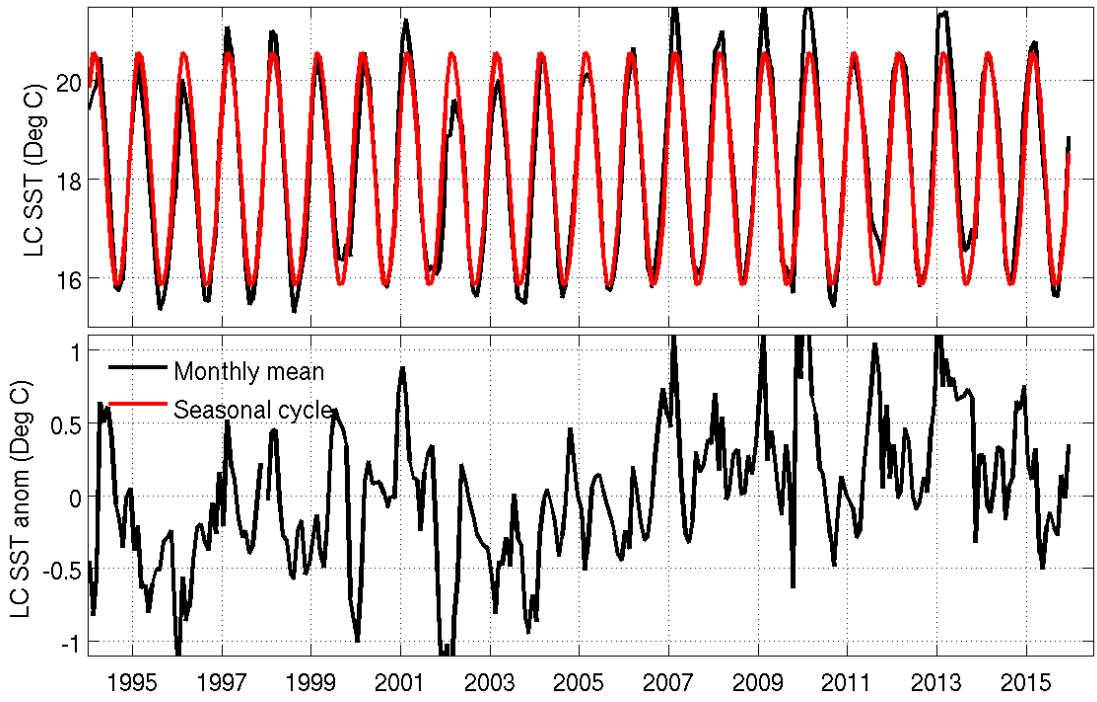

Figure 7.3.5: Time-series of the (top) monthly mean (black) and mean seasonal cycle (red) of the LC SST (i.e., the area-averaged SST immediately above the LC at 130.5ºE), and (bottom) the LC SST anomaly.

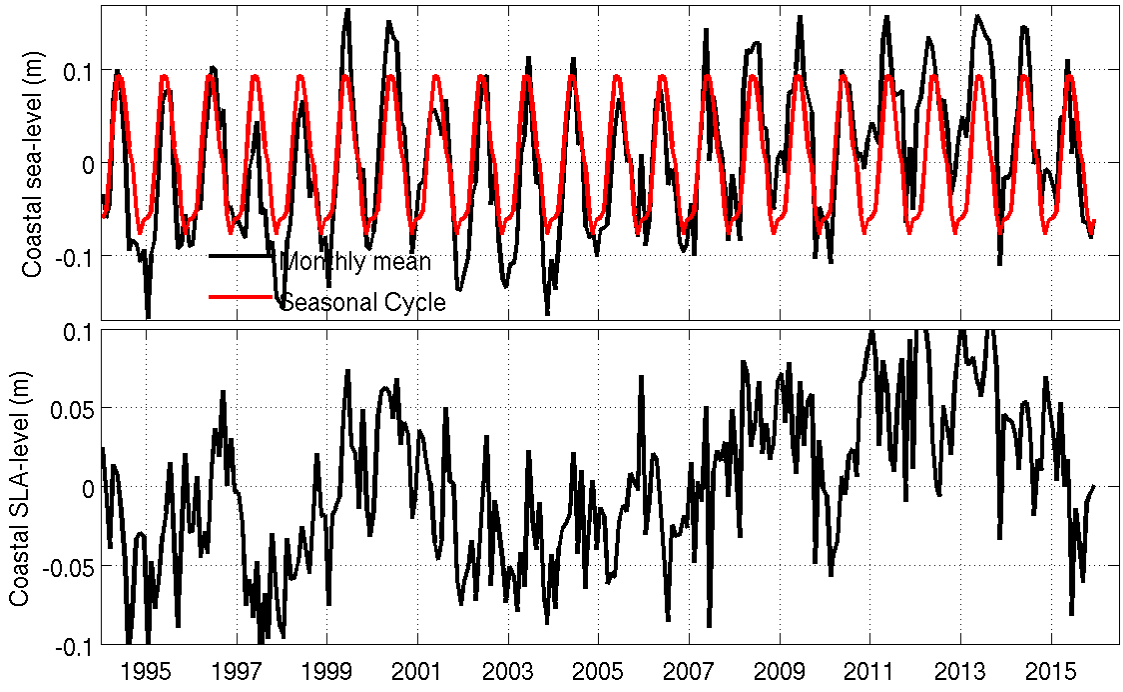

Figure 7.3.6: Time-series of - top: monthly mean (black) and seasonal cycle (red) of coastal sea-level at the head of the GAB; and bottom: coastal sea-level anomaly.

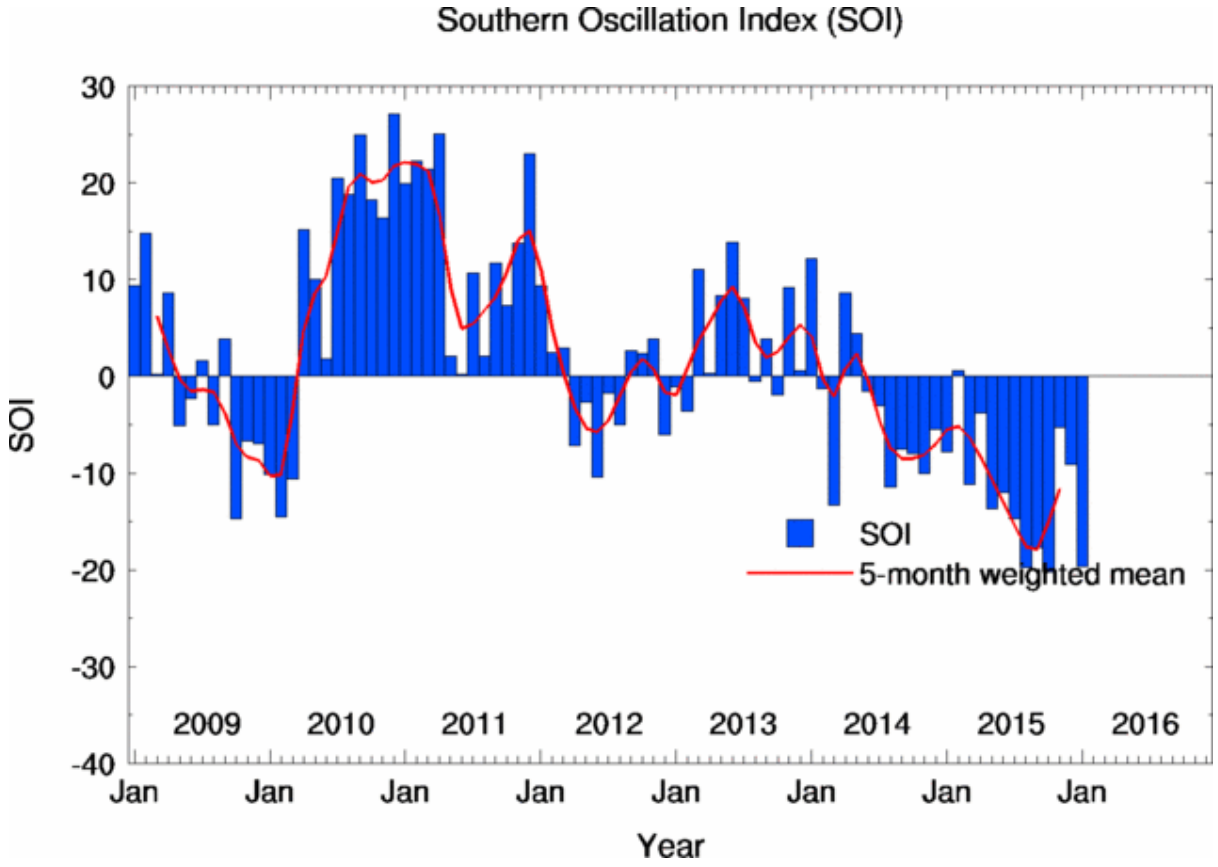

Figure 7.3.7 Southern Oscillation Index, reproduced from http://www.bom.gov.au/climate/glossary/soi.shtml

7.4 Were the 2012 and 2015 field surveys conducted during normal or anomalous conditions?

One of the motivations of this chapter of work was to put the BP moored-instrument deployment of November 2011 to December 2012 and the *R.V Investigator* voyage of December 2015 into context. Specifically, answering the questions – were these periods of field observations representative of usual conditions?

As mentioned above, 2015 was certainly not an average year, but an El Nino one, with very weak LC transport and low LC temperature, particularly during the middle of the year (before the voyage). Most of 2012, however, appears to have been fairly typical in terms of LC transport (despite sea level being very high in the middle of that year).

Section views (Figure 7.4.1) of the LC transport at the head of the Bight (130.5^{o}E) show the normal conditions for 2012 and the atypical conditions of December 2015 when the LC transport was close to zero (Figure 7.4.2).

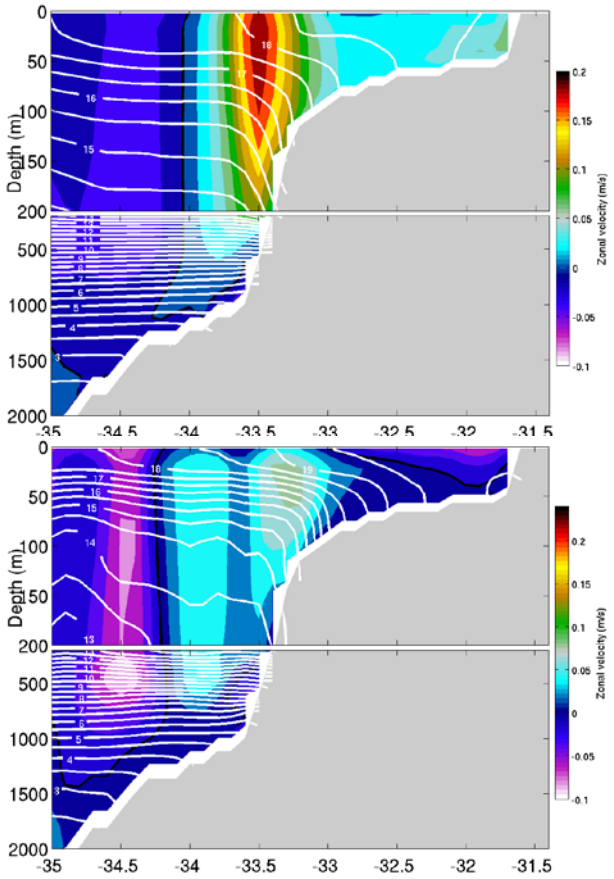

Figure 7.4.1: Time-mean conditions during two field survey intervals: November 2011 to December 2012 (upper), and December 2015 (lower). Mean zonal velocity (colour) and potential temperature (contour interval is 0.5°C) at 130.5°E.

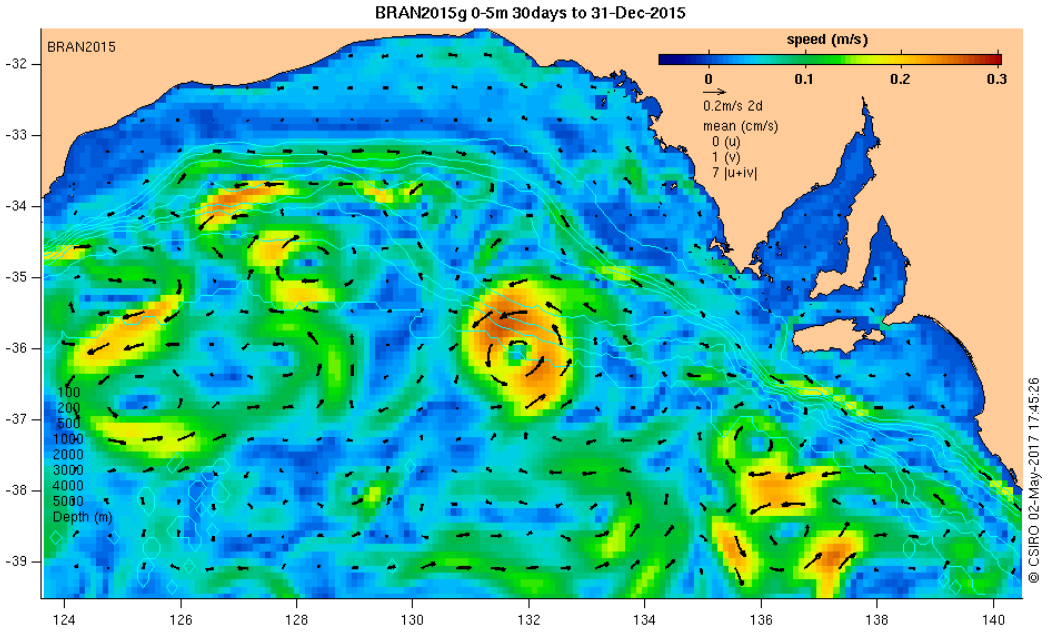

Figure 7.4.2 Surface current field averaged for December 2015 (when RV Investigator was at sea) showing a near-absence of Leeuwin Current but an energetic anticyclonic (warm core) eddy near 36°S 132°E.

8. RESEARCH AREA: SERVICE TO OTHER THEMES

8.1 Summary

Theme 1 worked with the other themes to determine what oceanographic products, analyses and advice need be undertaken and provided, so as to enhance their research outcomes. A summary of the information provided to the other themes is given below and, where possible, references given to the details in their reports.

8.2 Theme 2: Pelagic Ecosystems

8.2.1 Ocean colour acquisition and validation

Many data on the IMOS and AODN web sites are in a format called NetCDF rather than more commonly used formats such as Microsoft Excel. In general, NetCDF is not used by most people. Thus, the purpose of the report below is to enable such users and other GABRP themes to readily obtain such data and in particular, satellite derived ocean colour and SST data. The following reports were produced:

Redondo Rodriguez, A., Middleton, J. F., and R. Proctor (2015): Accessing IMOS Satellite data into csv format, from the IMOS Portal. GAB Res. Project report. – a tutorial available at imos.aodn.org.au and at http://www.misa.net.au/GAB/research_results/reports

In collaboration with Edward King (IMOS Satellite Remote Sensing Facility; imos.org.au), a detailed analysis of remote sensed and *in-situ* observations of ocean colour data has been made. Two reports have been written:

Redondo Rodriguez, A., King, E. and M. Doubell, (2015a): Validation of MODIS imagery in the Great Australian Bight, GAB Res. Project report. http://www.misa.net.au/GAB/research_results/reports

Redondo Rodriguez, A., King, E. and M. Doubell (2015b): Regional variability of MODIS imagery in the Great Australian Bight., GAB Res. Project report. http://www.misa.net.au/GAB/research_results/reports

The reports summarise the expected data availability and accuracy of three MODIS products (SST, chlorophyll-*a* and euphotic depth) and their algorithms. There was not enough *in situ* data to produce an improved algorithm, but the best algorithms for the GAB were identified in these reports, as well as the expected accuracy and limitations of the different products: submission of a research paper on these results is planned. These reports and the tutorial have been disseminated to the other themes.

8.2.2 Nutrient Pathways to the shelf edge of the central GAB.

Several sets of numerical experiments and analyses were undertaken for Theme 2 to examine possible paths of nutrient supply in the central GAB.

First, a set of general particle tracking experiments were undertaken using ROMS as outlined in Section 5 as part of those needed to establish general connectivity for the GAB. In conclusion, nutrient rich water upwelled in the eastern GAB has no direct path to the shelf edge of the central GAB. Pathways of transport were found from the western GAB which might supply nutrients, although upwelling in the far west seems to be small.

Second, a set of nutrient dispersal studies using ROMS were done for each summer season (January) of 2011, 2012, 2013 and 2014. The observed distribution of nitrate concentrations off the shelf slope (depths to 1300 m) and at the central GAB section 130.8 ^{o}E were adopted and realistic simulations undertaken to see if the known downwelling could act to mix nitrates from depths of 300 m to the shelf edge (~ 100 m). The results for the downwelling is expected to dominate with little vertical mixing of nutrients. It is noted that convective overturning is not modelled by ROMS (or most hydrodynamic models) which make the hydrostatic assumption. Thus, convective overturning may be a mechanism for nutrient supply from deep waters.

Results for these studies are presented by Theme 2, Project 2.2: Characterise spatial variability of offshore/slope plankton, and micronekton communities.

8.2.3 Analyses of tagged sea lion data:

Two analyses of tagged sea-lion CTD data was made for Theme 2 (and Project 4.2) so as to determine a) possible errors in both positional fixes and salinity observations and b) the water mass (T/S) properties of the central GAB and eastern GAB and expected oceanic transport patterns.

Results for these studies are presented by Theme 2 and Project 4.2 notably through the work: F. Bailleul, L. Richardson, P. Van Ruth, C. R. McMahon, R. G. Harcourt, J. F. Middleton, T. Ward, S. D. Goldsworthy (2017) Animal-borne instruments provide new observations of seasonal subsurface oceanographic features over the continental shelf of the Great Australian Bight. Theme 2.

8.3 Theme 3: Benthic

After discussions with the Benthic Theme, it was decided that annual averaged and maximum values of bottom stress magnitude would be the most appropriate oceanographic parameter to influence the benthos. To this end bottom stress from ROMS was averaged over a two year model simulation (2013-2014) and the mean and maxima stored. These were used as one of a suite of environmental covariates in the analysis of infaunal and epifaunal data in Theme 3, to determine what variables were influencing patterns of infaunal and epifaunal community structure.

8.4 Theme 4: Iconic Species

Project 4.2 aimed to determine areas of ecological significance for iconic species and apex predators or mean preferred foraging regions and associated physical drivers. The investigators plan to use Time Spent by Sector (TPS) analyses to identify such areas. The information was provided included summer and winter averages of the surface and bottom model outputs (velocity, temperature, mean water depth *etc*) and on the ROMS model grid of 4 X 4 km. These digital output were provided to Theme 4 to help determine any physical drivers of ecosystem/apex predator activity.

8.5 Theme 5: Petroleum geology and asphaltite and tar ball origins

Tar balls behave as surface drifters and are influenced by both Stokes and wind drift. Asphaltites are neutrally buoyant and less effected by Stokes and wind drift. To assist in understanding the possible origins of these petroleum products three sets of particle tracking studies were undertaken and the information provided to Theme 5. These were:

The general connectivity studies conducted using ROMS and detailed in Section 5 above. These were forward tracking studies of neutrally buoyant particle: a proxy for asphaltites.

A second set of ROMS studies with the (16) origins of particles being known or suspected deep water hydrocarbon seepage sites provided by Theme 7. The deep water results are strongly influenced by the unrealistic eddy fields and at best only indicative.

Backward tracking studies of tar balls were conducted by CSIRO using the global BRAN model and Wavewatch III estimates of surface Stokes drift from Theme 1 Project 1.2: waves.

Results for these studies are presented by Theme 5.

8.6 Theme 7.1: Integration and modelling.

It was agreed that 12 hr to 3 day averages of the model outputs for the four years 2011 to 2014 would be needed by Theme 7.

These were provided in 2016 and have been utilised to generate forcing files for the ecosystem models. The forcing fields were calculated by taking exchanges between boxes form the current flows in the hydrodynamic models. Consistent environmental conditions for each layer of each ecosystem model box (cell) was also calculated by sampling the hydrodynamic model output and taking an average of the hydrodynamic grid cells sitting within the ecosystem model box. This output was then cycled repeatedly to make up the full set of hydrodynamic forcing for each run of the ecosystem models.

Results for these studies are presented by Theme 7.

9. DISCUSSION AND CONCLUSIONS

To understand the circulation within the Great Australian Bight (GAB), three distinct hydrodynamic models were used; two shelf-focused models for the four year period 2011 to 2014 (ROMS and SHOC) and one deep-sea focused model (BRAN) for the 23-year period 1994-2016. Good to very good agreement between shelf model hind-casts and data were found for the shelves and at depths less than 200-300 m or so: farther offshore, the shelf models were unable to replicate important observed features of the meso-scale eddy fields.

However, during both winter and summer, the model results were as expected from previous studies summarised by Middleton and Bye (2007). Notably, the results here were obtained at higher resolution and with more realistic forcing and initial fields of stratification.

The GAB is characterised by a deep ocean FC, nearshore CC and shelf edge LC and SAC. These current systems have typical magnitudes of 5 – 25 cm/s that are relatively small compared to the other major current systems around the Australian continent (e.g., East Australian Current). Nonetheless, over a season, such currents can transport particulate matter and marine biota over distances of 390 km to 2000 km. Shelf and shelf edge currents within the GAB are also generally seasonal in nature (in keeping with the atmospheric forcing), with the notable exception of the eastward SAC. The existence of the SAC during summer has been ascribed to sea level gradients (Middleton and Platov, 2003) that arise from the "collision" of Sverdrup transports in the central GAB and at the shelf edge. However, its existence off Kangaroo Island suggests that other mechanisms such as thermohaline forcing may be important; the differences in temperature (and density) between the shelf and deep ocean may lead to pressure forces that drive the SAC and other aspects of the GAB shelf circulation. The importance of such forcing compared to that of winds remains a knowledge gap to be addressed in future studies.

Downwelling was found to occur all year round in the central GAB; in winter driven by atmospheric cooling and evaporation while in summer, driven by the "collision" of Sverdrup transports in the central GAB. This downwelling is important to nutrient paths which for the first time have been identified for the GAB based on the analysis here and the related studies by Middleton et al (2014), Middleton and de Oliviera (2017), de Oliviera and Middleton (2017), and Richardson (2015).

For summer, the upwelling in the eastern GAB is enhanced by the existence of submarine valleys and headlands (de Oliviera and Middleton 2017) which draws nutrient rich water (e.g., nitrates) from depths of 150 m or more along the Bonney Coast and Kangaroo Island regions: this water is transported to the west coast of the Eyre Peninsula. In the far western GAB, SST observations and theory indicate wind-forced upwelling to be largely shut down (Middleton and de Oliviera, 2017). In the central GAB the year-round downwelling would seem likely to preclude upwelling, although other mechanisms such as double diffusion and convective overturning may be important.

During winter, atmospheric cooling and evaporation create cold dense water that ultimately is expelled off the shelf and into the 200 - 250 m deep waters of the shelf break. This water may contain high levels of detritus, sediments and ammonia. In analogy with Spencer Gulf (Middleton et al., 2013) we speculate that ammonia in this detritus might be re-mineralised into atmospheric nitrogen and nitrates.

The above indicates that wind-forced upwelling occurs on a seasonal basis. More precisely it is associated with summertime south-easterly wind events that can act for 5-10 days and occur 4-5 times

during each summer. Similarly, during winter the passage of intense low pressure systems can cool coastal water and drive very strong shelf currents that may trigger offshore flows of cold, dense coastal waters.

In conclusion, the modelling and data analyses conducted have revealed the GAB and environs to host quite complex and unique current systems and mechanisms for cross-shelf exchange. As shown these have implications for nutrient paths which underpin the ecosystem of the region.

10. REFERENCES

Akhir, M (2009) *Physical processes along the southern continental shelf and slope of Western Australia.* PhD Thesis, University of Western Australia.

Black, A. (1857). *Black's general Atlas of the World (new edition), embracing all the recent discoveries and containing introductory chapters on the physical geography of the Earth, descriptions of the various countries of the world and a complete index of 65,000 names*. Adam and Charles Black, North Bridge, Edinburgh.

Cirano, M., Middleton, J. F. (2004). The Mean Wintertime Circulation along Australia's Southern Shelves: a numerical study. *J. Phys. Oceanogr.,* 34(3), 668-684.

Cresswell, G., and J. L. Peterson (1993). The Leeuwin Current of Western Australia. *Aust. J. Mar. Freshw. Res.,* 44, 285-303.

Cresswell, G.R. and D. A. Griffin (2004). The Leeuwin Current, eddies, and sub-Antarctic waters off south-western Australia. *Marine and Freshwater Research,* 55, 267-276.

Feng, M., G. Meyers, A. Pearce and S. Wijffels (2003) Annual and interannual variations of the Leeuwin Current at 32°S, *J. Geophys. Res.,* 108, 3355, doi:10.1029/2002JC001763, C11.

Gersbach, G. H., C.B. Pattiaratchi, G. N. Ivey and G. Cresswell (1999). Upwelling on the south-west coast of Australia – source of the Capes Current? *Continental Shelf Research,* 19(3), 363-400.

Godfrey, J. S., Vaudrey, D. J., Hahn, S. D. (1986). Observations of the shelf-edge current south of Australia. *J. Phys. Oceanogr.,* 16, 668-679.

Harcourt, R. R. 2013: A Second-Moment Closure Model of Langmuir Turbulence. *J. Phys. Oceanogr*., 43, 673–697. doi: http://dx.doi.org/10.1175/JPO-D-12-0105.1

Herzfeld, M. and M. Tomczak (1999). Bottom driven upwelling generated by eastern intensification in closed and semi-closed basins. *Aust. J. Mar. and Freshw. Res.,* 50, 613-627.

Herzfeld, M. and J. R. Andrewartha (2012). A simple, stable and accurate Dirichlet open boundary condition for ocean model downscaling. *Ocean Modelling,* 43-44, 1-21.

Hobday A.J., J. Hartog, C. Spillman and O. Alves (2011). Seasonal forecasting of tuna habitat for dynamic spatial management. *Canadian Journal of Fisheries and Aquatic Sciences 68*, 1-14.

Kaempf, J., M. Doubell, D. Griffin, R. L. Matthews and T. M. Ward (2004): Evidence of a large seasonal coastal upwelling system along the southern shelf of Australia. *Geophysical Research Letters* 31: L09310, doi:10.1029/2003GL019221.

Kondo, J. (1975) Air-sea bulk transfer coefficients in diabatic conditions. *Boundary-Layer Meteorology,* 9, 91-112.

Lennon, G. W., D.G. Bowers, R. A. Nunes, B.D. Scott, M. Ali, M., J. Boyle, C. Wenju, M. Herzfeld, G. Johansson, S. Nield, P. Petrusevics, P., P. Stephenson, A. A. Suskin and S. E. A. Wijffels, (1987). Gravity currents and the release of salt from an inverse estuary. *Nature,* 327, 695-697.

Mason E., J. Molemaker, A.F. Shchepetkin, F. Colas, J.C. McWilliams, P. Sangrà, (2010). Procedures for offline grid nesting in regional ocean models, *Ocean Modelling,* 35, 1-15.

Mellor, G. L., and T. Yamada (1994). Development of a turbulence closure model for geophysical fluid problems. *Rev. Geophysics., 20,* 851-875.

Middleton, J. F. and M. Cirano (2002). A Boundary Current along Australia's Southern Shelves: the Flinders Current. *J. Geophys. Res.* 107(C9), doi:10.1029.

Middleton, J. F. and G. Platov (2003). The Mean Summertime Circulation along Australia's Southern Shelves: a numerical study. *J. Phys. Oceanogr.,* 33(3), 2270-2287.

Middleton, J. F., and J.T Bye, (2007). The Physical Oceanography of Australia's Southern Shelves: a review. Progress in Oceanography, Volume 75, Issue 1, October 2007, Pages 1-41.

Middleton J. F., C. Arthur, P. van Ruth, T. Ward, J. McClean, M. Maltrud, P. Gill, A. Levings, and S. Middleton, (2007). El Nino effects and upwelling along Australia's southern shelves. *J. Phys. Oceanogr.,* 37, 2458 – 2477.

Middleton, J. F., R. McGarvey, A. Linnane, S. M. Middleton, C. E .P. Teixeira, P. Hawthorne (2012). Using observations of bottom temperature to calibrate the output of an ocean model, *Journal of Marine Systems.* 91 (2012) 34–40

Middleton, J. F, Doubell, M., James, C., Luick, J. and van Ruth, P. (2013). PIRSA Initiative II: carrying capacity of Spencer Gulf: hydrodynamic and biogeochemical measurement modelling and performance monitoring. Final Report for the Fisheries Research and Development Corporation. South Australian Research and Development Institute (Aquatic Sciences), Adelaide. SARDI Publication No. F2013/000311-1. SARDI Research Report Series No. 705. 97pp.Is now published at:

http://pir.sa.gov.au/research/publications/research_report_series/research_report_series_2013

Middleton, J. F. N. P. James, C. James, Y. Bone. (2014). Cross-shelf sea water exchange controls the distribution of temperature, salinity and neritic carbonate sediments in the Great Australian Bight. *J. Geophys. Res., (Oceans),* 10.1002/2013JC009420, 1-11.

Middleton, J. F. and H. B. de Oliveira (2017). Upwelling along the shelves of the Greater Australian Bight - Part II: set-up, geographical origins, the viscous limit and role of Coastal Trapped Waves. *J. Geophys. Res.,* submitted

Mihanovic, H., C. Pattiaratchi and F. Verspecht (2016). Diurnal Sea Breezes Force near-Inertial Waves along Rottnest Continental Shelf, Southwestern Australia. *J. Phys. Oceanogr.,* November, V46, 3487 – 3508.

Oke, P. R., P. Sakov, M. L. Cahill, J. R. Dunn, R. Fiedler, D. A. Griffin, J. V. Mansbridge, K. R. Ridgway and A. Schiller, (2013a). Towards a dynamically balanced eddy-resolving ocean reanalysis: BRAN3, *Ocean Modelling*, 67, 52-70,10.1016/j.ocemod.2013.03.008.

Oke, P. R., D. A. Griffin, A. Schiller, R. J. Matear, R. Fiedler, J. V. Mansbridge, A. Lenton, M. Cahill, M. A. Chamberlain and K. Ridgway (2013b). Evaluation of a near-global eddy-resolving ocean model, *Geoscientific Model Development*, **6**, 591-615, doi:10.5194/gmd-6-591-2013.

Orlanski, I., (1976). A simple boundary condition for unbounded hyperbolic flows. *J. Comp. Sci*., 21(3), 251-269.

Petrusevics, P., J.A.T. Bye, V. Fahlbusch, J. Hammat, D.R. Tippins and E. van Wijk. (2009). High salinity water outflow from a mega inverse estuary – the Great Australian Bight. *Cont. Shelf. Res.,* 29, 371-380.

Pearce N. and H. Phillips (1988). ENSO Events, the Leeuwin Current, and larval recruitment of the western Rock Lobster. *J. Cons. Int. l'Exp. Mer.* 45, 12-21.

Rogers, P., T. Ward, P. van Ruth, A. Williams. Contributing authors (alphabetically): Barry Bruce, Sean Connell, David Currie, Campbell Davies, Karen Evans, Bronwyn Gillanders, Simon Goldsworthy, David Griffin, Nick Hardman-Mountford, Alex Ivey, Rudy Kloser, John Middleton, Anthony Richardson, Andrew Ross, Jason Tanner and Jock Young (2013). *Physical processes, biodiversity and ecology of the Great Australian Bight region: a literature review.* Prepared for the Great Australian Bight Ecosystem Project, CSIRO, Australia, 198 pp.

Richardson, L., (2015). *Water mass connectivity and mixing along the southern margin of Australia: hydrographic and stable isotope analyses.* PhD thesis, A.N.U, April 2015.

Ridgway, K. R., J. R. Dunn and J. L. Wilkin (2002). Ocean interpolation by four-dimensional least squares - Application to the waters around Australasia. *J. Atmos. Oceanic Technol*., 9, 1357-1375.

Schodlok, M. P. and M. Tomczak (1997a.) The circulation south of Australia derived from an inverse model. *Geophys. Res. Letters,* 24, 2781-2784.

Schodlok, M. P. and M. Tomczak (1997b). Deep sections through the South Australian Basin and across the Australian-Antarctic Discordance. *Geophys. Res. Letters,* 24, 2781-2784.

Smagorinsky, J. (1963). General circulation experiments with the primitive equations. *Mon. Wea. Rev*., 91/3, 99-164.

van Ruth, P. D., G. G. Ganf and T. M. Ward (2010a). Hot-spots of primary productivity: AN alternative interpretation to conventional upwelling models. *Estuarine, Coastal and Shelf Science* 90: 142-158.

van Ruth, P. D., G. G. Ganf and T. M. Ward (2010b). The influence of mixing on primary productivity: A unique application of classical critical depth theory. *Progress in Oceanography* 85: 224-235

Ward, T.W., L. McLeay, F. Wetjens, F. Dimmlich, P. J. Rogers, S. McClatchie, R. Matthews, J. Kaempf, J. and P. van Ruth (2006). Pelagic ecology of a northern boundary current system: effects of upwelling on the production and distribution of sardine (Sardinops sagax), anchovy (Engraulis australis) and southern bluefin tuna (Thunnus maccoyii) in the Great Australian Bight, *Fish. Oceanogr.* 15:3, 191–207.

Zhang et al., 2016. A near-global eddy-resolving OGCM for climate studies. Geosci. Model Dev. Discuss., doi:10.5194/gmd-2016-17, 2016 http://www.geosci-model-dev-discuss.net/gmd-2016-17/gmd-2016-17.pdf

11. APPENDIX 1: DESCRIPTION OF OCEANOGRAPHIC DATA USED

An outline of the mooring data is given first followed by a Table listing all data sources adopted.

11.1 Mooring data

The BP current measurements were conducted using RPS CM04 current meters. The CM04 is a vector-averaging current meter which operates on an acoustic phase shift principle. Continuously sensed velocity components are internally rotated to a north-south, east-west coordinate system using orientation information from an internal compass. The resultant velocity components are then averaged over a specified period prior to recording onto a solid state memory unit.

The SAIMOS current profile measurements were conducted using a Teledyne RDI Workhorse Acoustic Doppler Current Profiler (ADCP) which measures current velocity profile and water temperature. The current profile is measured at preselected intervals (bins) through the water column using a range-gating technique. The ADCP comprises four 300 kHz acoustic transducers angled at 20° to the vertical, an internal compass and two tilt sensors.

The BP temperatures were recorded by the current meters as well as a surface Star-Oddi temperature recorder at the top of each mooring. The SAIMOS temperatures were recorded by Seabird CTDs.

Table 11.1.1 Sites of mooring data used in this report.

	BP1	**BP2**	**NRSKAI**	**SAM5CB**	**SAM7DS**
Location	33° 21’ 57” S, 130° 39’ 15” E	34° 28.5’ S, 130° 42’ E	35° 50’ 24” S, 136° 26’ 24” E	34° 55’ 42” S, 135° 0’ 40” E	36° 10’ 24” S, 135° 50’ 11’ E
Water depth (m)	200	1425	109	99	550
Start/End	2 Nov 2011 / 12 Dec 2012	2 Nov 2011 / 12 Dec 2012	2011/2012 with gaps	2011/2012 with gaps	2011/2012 with gaps

The nominal sensor pressures (depths) at which currents and temperatures are used in this report are shown in Table 11.1.2 to Table 11.1.6: one db equals one meter in depth.

Table 11.1.2 BP1 (shelf) mooring summary table

Mooring BP1 depth below surface (db)	Data type
13	Temperature
15	Currents & Temperature
77	Currents & Temperature
135	Currents & Temperature
197	Currents & Temperature

Table 11.1.3 BP2 (slope) mooring summary table.

Mooring BP2 depth below surface (db)	Data type
81	Temperature
120	Currents & Temperature
200	Currents & Temperature
300	Currents & Temperature
450	Currents & Temperature
650	Currents & Temperature
850	Currents & Temperature
1100	Currents & Temperature
1350	Currents & Temperature
1420	Currents & Temperature

Table 11.1.4 SAIMOS mooring NRSKAI summary table.

Mooring NRSKAI depth below surface (db)	Data type
37	Temperature/salinity
104	Temperature/salinity
6.2, 10.2, 14.2 …90.2	ADCP Currents

Table 11.1.5 SAIMOS mooring SAM5CB summary table.

Mooring SAM5CB depth below surface (db)	Data type
95	Temperature/salinity
6.2, 10.2, 14.2, …82.2	ADCP Currents

Table 11.1.6 SAIMOS mooring SAM7DS summary table.

Mooring SAM7DS depth below surface (db)	Data type
522	Temperature
25, 41, 57, …473	ADCP Currents

11.2 Table of data sources

Description	Link	Location	First Date	Last Date	Data Type
Sea surface temperature from NOAA AVHRR HRPT	http://rs-data1-mel.csiro.au/thredds/catalog/imos-srs/sst/catalog.html	IMOS AODN	Mar 21 1992	Ongoing	SST
NASA MODIS (on Terra and Aqua) estimates of Chl-*a*	http://rs-data1-mel.csiro.au/thredds/catalog/imos-srs/oc/catalog.html	IMOS AODN	Jul 4 2002	Ongoing	Chl-*a*
Argo temperature and salinity profiles	http://thredds.aodn.org.au/thredds/catalog/IMOS/Argo/catalog.html	IMOS AODN	Oct 1 1999	Ongoing	CTD
Surface velocity and temperature from Global Lagrangian Drifters	http://www.aoml.noaa.gov/phod/dac/dacdata.php	Various		Ongoing	Surface Current and Temperature
IMOS Ocean Current	http://oceancurrent.imos.org.au/	IMOS	Jan 1 2004	Ongoing	Currents, SST, Ocean Colour
IMOS Mooring Data (ANMN)	http://thredds.aodn.org.au/thredds/catalog/IMOS/ANMN/SA/catalog.html	IMOS AODN	Oct 21 2008	Ongoing	Current Profiles, CTD+Biological
IMOS Mooring Data (NRS)	http://thredds.aodn.org.au/thredds/catalog/IMOS/ANMN/NRS/NRSKAI/catalog.html	IMOS AODN	Aug 12 2008	Ongoing	Current Profiles, 2-level CTD+Biological, Temperature Profile
IMOS HF Radar Data (ACORN)	http://thredds.aodn.org.au/thredds/catalog/IMOS/ACORN/catalog.html	IMOS AODN	Dec 2 2009	Ongoing	Currents, Waves, Wind Direction
IMOS CTD Profiles (ANMN)	T:\DATA\SAIMOS\Processed_CTD_IMOS	SARDI	Feb 12 2008	Ongoing	CTD+Biological Profiles
IMOS CTD Profiles (NRS)	T:\DATA\SAIMOS\Processed_CTD_IMOS	SARDI	Feb 12 2008	Ongoing	CTD+Biological Profiles
IMOS Glider (ANFOG)	http://thredds.aodn.org.au/thredds/catalog/IMOS/ANFOG/catalog.html	IMOS AODN	Jul 16 2008	Sep 29 2014	CTD+Biological Profiles
Marine Mammal Based CTD	T:\DATA\Sea Lion Data	SARDI	Mar 26 2007	Jul 1 2010	CTD+Biological

(Sea lions)					Profiles
SARDI Sardine Cruise CTD Profiles	T:\DATA\SARDINE_DATA	SARDI	Feb 18 1999	Ongoing	CTD+Biological Profiles
CARS Atlas source Data	T:\DATA\CARS\2010_Source	SARDI	Oct 4 1826	Apr 24 2010	CTD
Flinders Ports NTC Sea level Data	http://www.bom.gov.au/oceanography/projects/abslmp/data/index.shtml	SARDI	June 1 1992	Ongoing	Sealevel
SeaSoar Profiles and CTD casts	T:\DATA\SeaSoar Data	SARDI	Feb 3 1998	Mar 2 2001	CTD
BP-MET-01	T:\DATA\BP_GAB\BP-MET-01	SARDI/CSIRO	Nov 2 2011	Dec 12 2012	Temperature, Depth, Current Meters, Water Level
BP-MET-02	T:\DATA\BP_GAB\BP-MET-02	SARDI/CSIRO	Nov 3 2011	Dec 12 2012	Temperature, Depth, Current Meters, ADCP
BP-MET-03	T:\DATA\BP_GAB\BP-MET-03	SARDI/CSIRO	Nov 11 2012	Feb 13 2013	Met Data
BP-MET-04	T:\DATA\BP_GAB\BP-MET-04	SARDI/CSIRO	Dec 12 2012	Apr 11 2014	Met Data, temperature, Directional Waves
BoM Cape du Couedic WaveRider	T:\DATA\WAVES\WaveRider	SARDI	Nov 20 2000	Feb 14 2012	Waves
Bathymetry from NOAA ETOPO1	https://www.ngdc.noaa.gov/mgg/global/global.html	NOAA	N/A	N/A	Bathymetry
Bathymetry from Geosciences Australia	http://www.ga.gov.au/scientific-topics/marine/bathymetry	GA	N/A	N/A	Bathymetry

Table 11.2.1 The data listed under T:\ are held by SARDI under its linux system T drive

12. APPENDIX 2: HYDRODYNAMIC MODEL PARAMETERS

As noted, two versions of both the ROMS and SHOC models were developed. The first versions (V1) were initially developed and through extensive model/data comparisons, improved through a number of modifications resulting in a second version (V2) reported on above. The model parameters adopted for each version are summarized in the following two tables.

Table 11.2.1 Model parameters in the V1 (initial) ROMS and SHOC models. The acronyms, abbreviations and references used are indicated below.

Numerical component	**ROMS V1**	**SHOC V1**
Simulation ID number(s)	o1199327	Run38
Simulation interval	January 2011 – December 2012	Jan 2011 – Jan 2013
Name of grid	SAM	GAB3
Size of grid	163 x 350 horizontal 15 vertical	160 x 240 horizontal 55 vertical – 0.5m at surface
Horizontal grid cell size	0.04° (approx. 4 km)	3 – 11 km (5.4km average)
Horizontal coordinate system	Uniform	Orthogonal curvilinear
Vertical coordinate system	Terrain-following stretched	Horizontal levels, with wetting and drying of surface cells
Bottom drag formulation	Quadratic (2.25×10^{-3})	Quadratic (variable roughness)
Vertical mixing parameterisation	Mellor-Yamada (1994) 2.5	Harcourt(2013,2015)
Horizontal eddy viscosity coefficient	5 m^2/s	Smagorinsky (1963): (c=0.05)
Horizontal mixing coefficient for temperature and salt	2 m^2/s	Smagorinsky(1963): (c=0.05)
Bathymetric data set	Geosciences Australia 2009 0.005°. Smoothed	Geosciences Australia 2009 0.005°. Unsmoothed.
Initial conditions (T, S, u, v, U, V)	BRAN2015 (CSIRO global model)	OFAM JRA55 (CSIRO global model)
Open boundary nesting: T & S source Width of nudging layer Time scale at boundary Time scale at interior	 BRAN2015/10 days 0.4° (~40 km) 1/3 days 1/30 days	 OFAM JRA55 0 n/a n/a

Open boundary condition: source Variable/Type Variable/Type Variable/Type	 BRAN 2015 Sea level / Chapman U & V / Mason et al.,. (2010) u & v / Orlanski (1976) (modified)	Herzfeld & Andrewartha (2012) OFAM JRA55 Sea level unconstrained u,v Dirichlet U,V integrals of u,v
Surface heat flux correction data source/time scale	NCSS (SST)/monthly (adjusts heat flux so model tends towards observations)	None
Surface momentum and heat fluxes	ECMWF	ACCESS-R
Surface pressure forcing	No	Yes
Bulk formulation for surface fluxes Y/N	No	Yes (Kondo 1975)
Global tidal model	TPXO 8.1	CSR

Table 11.2.2 Model parameters in the V2 (final) ROMS and SHOC models. The acronyms, abbreviations and references used are indicated below.

Numerical component	**ROMS V2**	**SHOC V2**
Simulation ID number(s)	o1236173/o1239579	Run67
Simulation interval	January 2011 – December 2014	Jan 2011 – Jan 2012
Name of grid	SAM	GAB5
Size of grid	163 x 350 horizontal 30 vertical	430 x 199 horizontal 55 vertical – 0.5m at surface
Horizontal grid cell size	0.04° (approx. 4 km)	3.85 km average
Horizontal coordinate system	Uniform	Geographic rectangular (false pole)
Vertical coordinate system	Terrain-following stretched	Horizontal levels, with wetting and drying of surface cells
Bottom drag formulation	Quadratic (2.25×10^{-3})	Quadratic (variable roughness)
Vertical mixing parameterisation	Mellor-Yamada (1994) 2.5	Harcourt(2013)
Horizontal eddy viscosity coefficient	5 m^2/s	150 m^2s^{-1} + Smagorinsky (1963): (c=0.1)

Horizontal mixing coefficient for temperature and salt	2 m^2/s	Smagorinsky (1963): (c=0.1)
Bathymetric data set	Geosciences Australia 2009 0.005°. Minimal smoothing	Geosciences Australia 2009 0.005°. Unsmoothed.
Initial conditions (T, S, u, v, U, V)	BRAN2015 (CSIRO global model)	BRAN2015 (CSIRO global model)
Open boundary nesting: T & S source Width of nudging layer Time scale at boundary Time scale at interior	 BRAN2015/10 days 0.4° (~40 km) 1/3 days 1/30 days	 BRAN2015 0 n/a n/a
Open boundary condition: source Variable/Type Variable/Type Variable/Type	 BRAN 2015 Sea level / U & V / Schchepetkin u & v / Orlanski (modified)	Herzfeld & Andrewartha (2012) BRAN2015 Sea level unconstrained u,v Dirichlet U,V integrals of u,v
Surface heat flux correction data source/time scale	NCSS (SST)/monthly (adjusts heat flux so model tends towards observations)	None
Surface momentum and heat fluxes	ECMWF	ACCESS-R
Surface pressure forcing	No	Yes
Bulk formulation for surface fluxes Y/N	No	Yes (Kondo 1975)
Global tidal model	TPXO 8.1	CSR

13. APPENDIX 3: EDDY FIELD EVALUATION

13.1 Description

An evaluation is here made of the validity or otherwise of the meso-scale eddies found in deep water and in both the V2 ROMS and SHOC models. This is done by comparing the mean sea level and standard deviations of the models with altimeter+tidegauge derived observations of sea level: source - IMOS Ocean Current. The accuracy of the altimetry is in the vicinity of 1-2 cm. This is what enables it to correctly estimate eddies when the models cannot. See, for example, the alignment of the altimeter-based estimates of near-surface current with the BP M2 observations of [Nov 2011].

In summary, it is found that the deep-water ROMS and SHOC model eddy fields are generally too intense compared to the observations.

For ROMS, the mean and standard deviation was calculated over a three-year interval (2012 - 2014) with tidal effects included (but small) and the inverse barometer contribution excluded.

For the altimeter product over the same period, two types of sea level data are available: GSL (Gridded Sea Level, or sea surface height above geoid) and GSLA (Gridded Sea Level Anomaly). GSL was used for finding the means, and GSLA was used for finding standard deviations. The difference is that GSL has a model (OFAM) estimate of the long-term mean included, GSLA has it set to zero. Sea level minus the tides and inverse barometer (IB) response, rather than total sea level, is mapped.

To facilitate comparisons, the spatial mean (an areal mean of the temporal mean sea level) was subtracted from both the ROMS and the GSL mean prior to plotting. Note, the mean sea level fields presented all contain an arbitrary constant.

Mean sea level results for the winter months of 2012-2014 period are shown in Figure 13.2.1 from the altimeter data (top panel) and ROMS (lower panel).

13.2 Analysis

The winter altimeter data shows coastal values of about 10 cm that become negative (~ -10 cm) in the deep ocean with several weak ~ 5 cm high pressure (green) on blue) “eddies” near the 5000 m isobath. The ROMS winter means have a similar structure near the coast but exhibit a large blue (low pressure trough) of up to 20-30 cm. This trough is associated with that found for the depth-averaged velocity. The comparison with the altimeter data shows that the trough is almost certainly unrealistic.

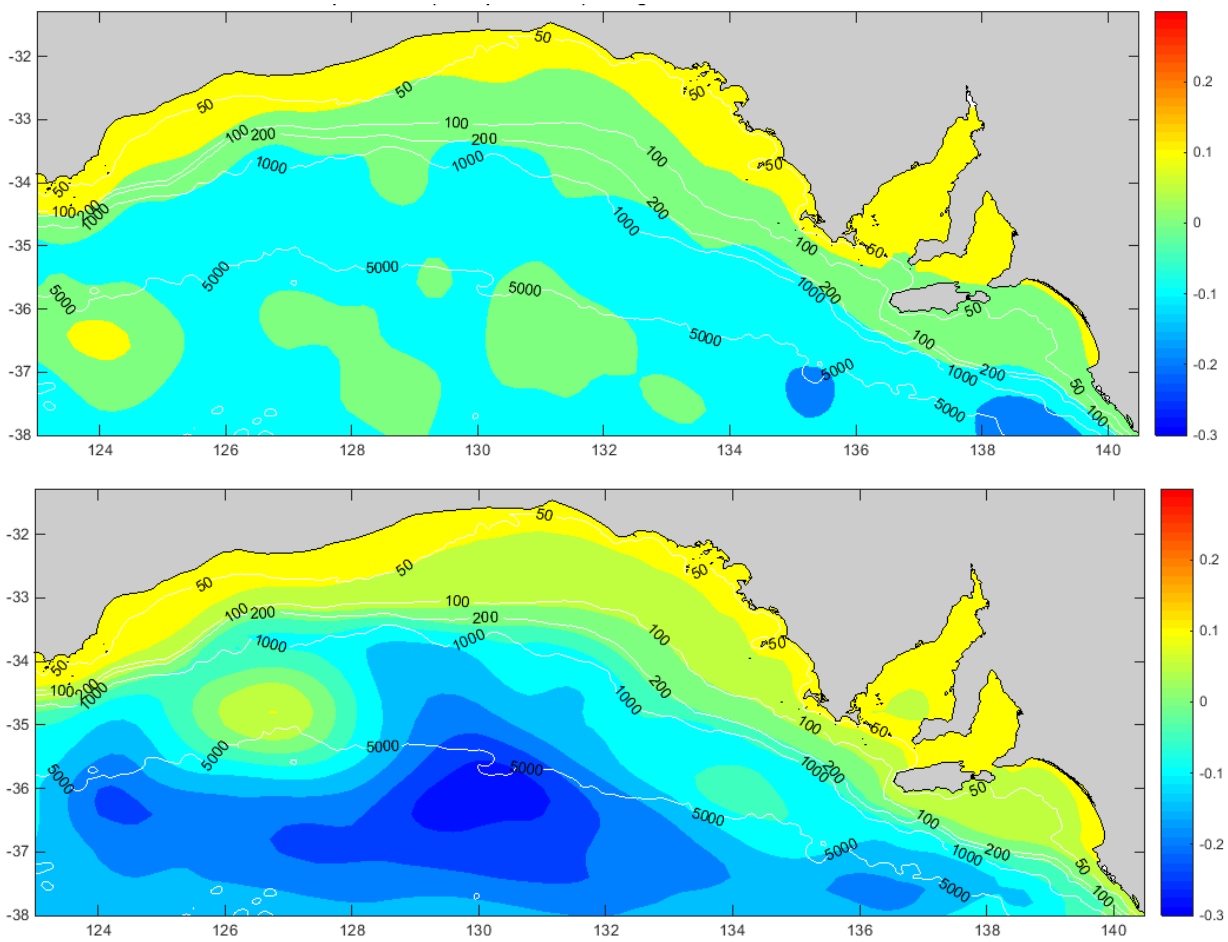

Figure 13.2.1 The mean sea level fields for the winter months of 2012-2014: upper panel altimeter data and lower panel ROMS. Units meters. Labelled contours here and below are isobath depths in meters.

ROMs results for the standard deviation σ of sea level are presented for winter in Figure 13.2.2. For the sea level data, σ is near 10 cm near the coast (probably due to the passage of high/low pressure systems), while for ROMS it is a little larger (~ 15 cm). However, the altimeter data indicates deep ocean variability of only 2-5 cm and much smaller than that for ROMS where σ can range from 5-30 cm indicating an unrealistically intense eddy field. The eddies for SHOC V2 (Run 67) are more realistic than ROMS in the west but less so for the continental slope region offshore from the SA Gulfs.

Similarly unrealistic eddy fields were also found for the summer months of 2012-2014 for ROMS and also for SHOC. In conclusion, the altimeter results indicate that the ROMS and SHOC offshore eddies are unrealistically intense. The cause of this is unknown as various (published) open boundary conditions for the ROMS and SHOC models have been tried that elsewhere are claimed to be of some validity.

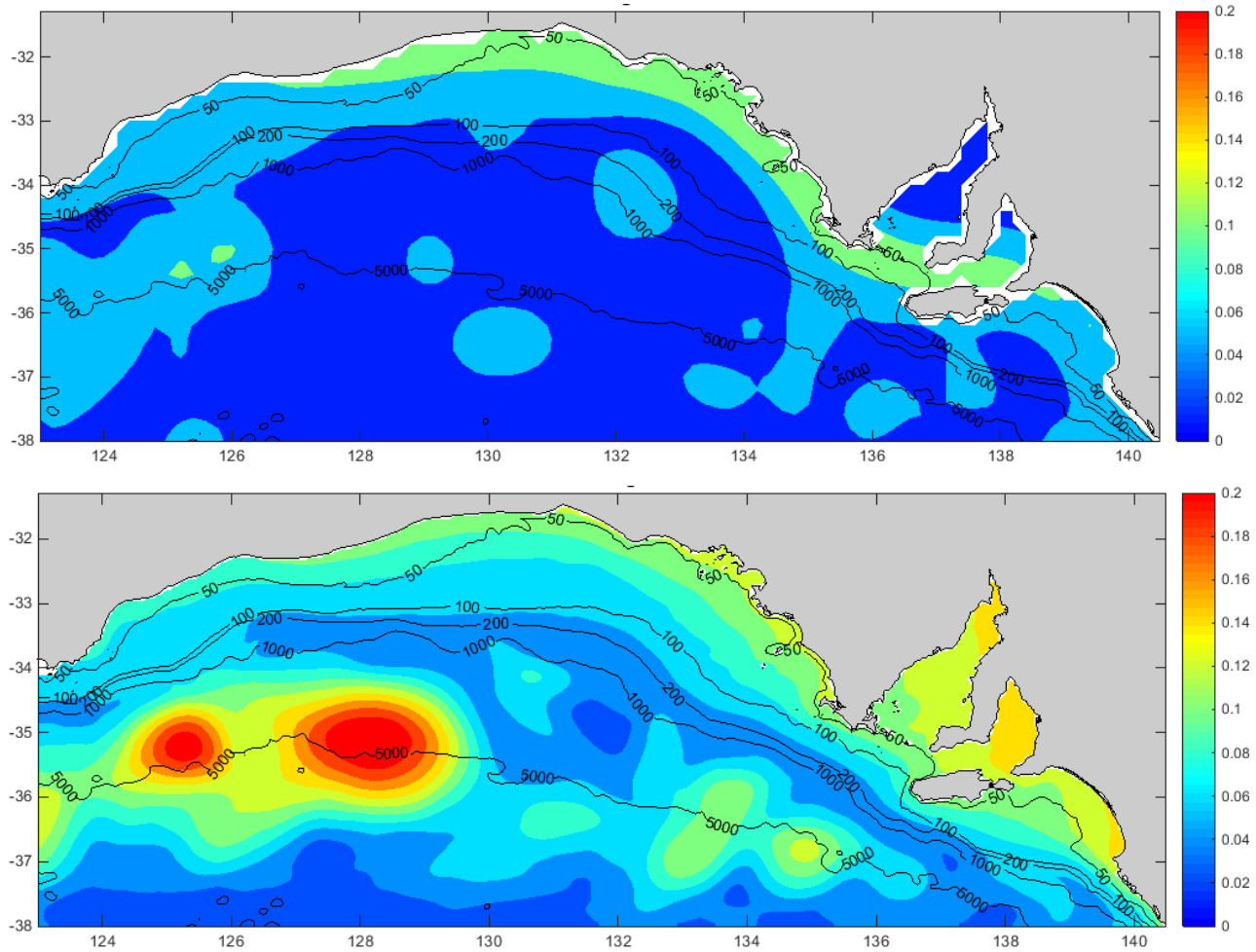

Figure 13.2.2 The standard deviation of the sea level fields for winter months of 2012-2014: upper panel altimeter data, lower panel ROMS. Units meters. Labelled contours here are isobath depths in meters.

14. APPENDIX 4: DATA MANAGEMENT

14.1 Raw dataset created

Two IMOS Glider Missions run by IMOS.

14.2 Data processing and derived datasets

Data processed by IMOS.

14.3 Data curation and archive

IMOS Glider data available at:
http://thredds.aodn.org.au/thredds/catalog/IMOS/ANFOG/seaglider/GAB20160311/catalog.html

14.4 Data access, use agreements and licensing - N.A.

14.5 Publication of datasets - as above

15. APPENDIX 5: PROJECT PUBLICATIONS

15.1 Papers/GAB Reports

Redondo Rodriguez, A., Middleton, J. F., and R. Proctor (2015): Accessing IMOS Satellite data into csv format, from the IMOS Portal. GAB Res. Project report. – a tutorial available at imos.aodn.org.au and at http://www.misa.net.au/GAB/research_results/reports

Redondo Rodriguez, A., King, E. and M. Doubell, (2015a): Validation of MODIS imagery in the Great Australian Bight, GAB Res. Project report.
http://www.misa.net.au/GAB/research_results/reports

Redondo Rodriguez, A., King, E. and M. Doubell (2015b): Regional variability of MODIS imagery in the Great Australian Bight., GAB Res. Project report.
http://www.misa.net.au/GAB/research_results/reports

15.2 Presentations

Middleton, J. F., Australian Coastal Modelling and Observations Workshop held in Canberra (7th-8th October 2014).

Middleton J.F. and Griffin, D. Annual Integrated Marine Observing System (IMOS) planning meeting (February 18th 2015).

Middleton J.F. and Griffin, D., Oceanography of the GAB. Australian Coastal Ocean Modelling and Observations., Canberra, 11th October 2016.

15.3 Related Research undertaken during the GAB RP:

Middleton, J. F. N. P. James, C. James, Y Bone. (2014). Cross-shelf sea water exchange controls the distribution of temperature, salinity and neritic carbonate sediments in the Great Australian Bight. J. Geophys. Res., (Oceans), 10.1002/2013JC009420, 1-11.

de Oliveira, H. B. and J. F. Middleton 2017. Upwelling along the shelves of the Greater Australian Bight – Part I: the role of submarine headlands and valleys. *J. Geophys. Res.,* to be submitted.

Middleton, J. F. and H. B. de Oliveira (2017) Upwelling along the shelves of the Greater Australian Bight - Part II: set-up, geographical origins, the viscous limit and role of Coastal Trapped Waves. . *J. Geophys. Res.,* to be submitted

Richardson, L., 2015. Water mass connectivity and mixing along the southern margin of Australia: hydrographic and stable isotope analyses. PhD thesis, A.N.U, April 2015.

Middleton J. F., et al., (2016-2017) eSA-Marine: Phase I: the first step towards an operational now-cast/forecast model ocean prediction system for Southern Australia. FRDC 2016/005.


bp


CSIRO


SOUTH AUSTRALIA
Government
of South Australia
Primary Industries
and Regions SA


SARDI
SOUTH AUSTRALIAN
RESEARCH AND
DEVELOPMENT
INSTITUTE


SUB CRUCE LUMEN
THE UNIVERSITY
of ADELAIDE


Flinders
UNIVERSITY